

Filter Position Optimisation in Transmission System using Homotopy Analysis Method

Morten Vadstrup, Troels Jakobsen
Energy Technology, EPSH4-1032, May 31, 2019

Master's Thesis





Board of Studies of Energy
Aalborg University
<http://www.aau.dk>

AALBORG UNIVERSITY

STUDENT REPORT

Title:

Filter Position Optimisation in Transmission System using Homotopy Analysis Method

Theme:

Master's Thesis

Project Period:

Spring Semester 2019

Project Group:

EPSH4-1032

Participants:

Morten Vadstrup
Troels Jakobsen

Supervisor:

Filipe Miguel Faria da Silva

Co-Supervisor:

Chengxi Liu

Page Numbers: 137**Appendix:**

A, B, C, D, E and F

Date of Completion:

May 31, 2019

Synopsis:

This report presents a new method for identifying the most impactful filter positions in transmission systems, without directly specifying filter values. The method is based on the homotopy analysis method, which is applied to the frequency scan method, as a voltage power series is created. Using the first order coefficient of the voltage power series the most impactful filter positions for a specific resonance point can be identified. The first order coefficient homotopy method only needs the admittance matrix of the power system and a matrix specifying a given filter position. The method is applied to a large example system, and satisfactorily predicted the most impactful filter positions for different resonance peaks. The method should be used as an early screening of the power system in planning studies, as it does not provide the final voltages in the system, after an actual filter is implemented, due to the method not relying on actual filter values.

The content of this report is freely available, but publication (with reference) may only be pursued due to agreement with the author.

Preface

This master's thesis was made by group EPSH4-1032 during the 4th semester of the Master of Science programme, Electrical Power Systems and High Voltage, at the Department of Energy Technology, Aalborg University, in a four month period from the 4th of February 2019 to the 31st of May 2019. The project was made under the supervision of Filipe Miguel Faria da Silva and co-supervision of Chengxi Liu. The authors would like to thank Christian Flytkjær Jensen and Chris Skovgaard Hansen from Energinet for providing help, suggestions and feedback during the work on this master thesis from a practical point of view.

Reading Guide

Throughout this report, source notes will be appearing in brackets. The source notes have been noted using the IEEE referencing method, meaning that the notes in the text will be stating a reference number. The reference number refers to the complete source list in the end of the report, where books are listed with author, title, year, publisher and ISBN, and web pages are put with author, title, URL and date. Each chapter is introduced by a short paragraph written in italic form, explaining the overall content of the chapter.

Figures, equations, appendices and tables are numbered in order of the chapter of their appearance. For example, the third figure in Chapter 4, will be numbered 4.3, the same applies for equations and tables. Every figure and table is provided with a caption, explaining its content. The notation for matrices is a bold symbol e.g. **V**.

Some of the figures in the report are touched up versions of figures found in different literature. When such a figure appears it will be noted in the caption of the figure what literature inspired the remade figure.

Aalborg University, May 31, 2019

Morten Vadstrup

Troels Jakobsen

Nomenclature List

Special Symbols and Denotations

Symbol	Description	Derived unit	Unit
A	Area	Metre squared	m^2
a	Convergence control parameter	-	-
B	Flux density	Tesla	T
C	Capacitance	Farad	F
c	Scaling Factor	-	-
f	Frequency	Hertz	Hz
G	Conductance	Siemens	S
h	Harmonic order	-	-
I	Current	Ampere	A
J	Jacobian	-	-
j	Complex number operator	-	-
k	Scaling constant	-	-
L	Inductance	Henry	H
l	Length of line	Meters	m
m	Order	-	-
P	Active power	Watt	W
Q	Reactive power	Volt-ampere reactive	var
q	Quality factor	-	-
R	Resistance	Ohm	Ω
r	Radius	Meters	m
S	Rated apparent power	Volt-ampere	VA
U	Nominal voltage	Volt	V
V	Voltage	Volt	V
v	Velocity of propagation	Meters per second	m/s
X	Reactance	Ohm	Ω
Y	Admittance	Siemens	S
y_{fil}	Filter admittance	Siemens	S
Z	Impedance	Ohm	Ω
γ	Propagation constant	-	-
λ	Wavelength	Meters	m
ω	Angular velocity	Radians per second	rad/s
ρ	Resistivity	Ohm metre	$\Omega \cdot m$
θ	Angle	Degrees	$^\circ$

Acronyms

Acronym	Abbreviation of:
DC	Direct current
DK1	Western Danish transmission system
EHV	Extra high voltage
FD	Frequency dependent
HV	High voltage
HVDC	High voltage direct current
IEC	International Electrotechnical Commission
LCC	Line commutated converter
LV	Low voltage
MV	Medium voltage
OHL	Overhead line
pu	Per-unit
PE	Power electronic
RMS	Root mean squared
RUS	Reinvesterings- Udbygnings- og Sanerings-
ST	Single-tuned
TSO	Transmission system operator
UGC	Underground cable
WPP	Wind power plant
XLPE	Cross-linked polyethylene

Executive Summary

There is a global trend in power systems towards de-carbonisation of the electricity production by integration of wind and solar plants as a substitute to conventional power plants. These are typically connected to the grid via power electronics, which are sources of harmonic emission. The Danish power system has several HVDC connections, already implemented or in the planning process, which are also sources of harmonic emission. The replacement of overhead lines with cables has lowered the frequencies of resonance point in the power system. The resonance points acts as amplification for harmonic emission which can lead to harmonic distortion in the power system. Filters are often used as mitigation to limit the affect of harmonics in the system. This is typically solved on a case-by-case basis, by the use of passive filters, at the locations where excessive amounts of harmonic content is observed. Another philosophy for the placement of filters would be to identify the positions in the system, where a filter has the overall largest impact on the overall system. The idea of this global filter placement is that potentially less filters are needed to address the harmonic issues in the system. In order to investigate the idea of global filter placement it is found that new methods should be investigated, in order to find the optimal filter positions and provide a better intuitive understanding of the harmonic behaviour of the power system. This has let to the goal set by the authors to answer the following:

To which extent can a new semi-analytical method be utilised to examine the impact of filter implementation in the power system, in order to further the idea of global filter placement?

Based on the state of the art it was chosen to work in the frequency domain with focus on the frequency scan method, due to it typically being used for harmonic studies. The method developed in this project, to examine the impact of filters, is a homotopy analysis method based on the frequency scan method. By setting the voltage of a specific point in the system as a power series, and calculating the coefficients, the homotopy analysis method can provide the final voltage after a filter is implemented. In order to find the most impactful filter positions without specifying a specific filter, the first order coefficient of the power series is used.

The first order coefficient homotopy method only needs the admittance matrix of the system and a matrix specifying the filter location which is to be tested for. The method is able to indicate which filter positions are the most impactful on specific resonance points. For most cases, involving resonance peaks, the absolute value of the first order coefficient is accurate. In the case of resonance peaks and resonance valleys the real values of the first order coefficient can indicate whether a filter in a specific location will introduce a damping or an amplification of the given resonance point. The imaginary values of the first order coefficient can be used to get a relative indication, between different filter

positions, in terms of how much a resonance point will shift in frequency, after the implementation of an actual filter. The first order coefficient homotopy method can not provide the final harmonic voltage distortions in the system, after an actual filter is implemented, as the voltages will be determined by the values of the actual filter. Therefore the method should be used early in planning studies to identify the optimal filter locations.

The first order coefficient homotopy method was applied to a small example system and correctly predicted the most impactful filter positions, when compared to a filter implementation with an actual C-type filter. Further application of the method on a large example system, which resembles the structure of the Danish 400 kV western transmission system, showed that the method accurately predicted the impact of difference filter positions, and could be used to gain an understanding of which parts of the power system affected specific resonance points.

Changes to the power system can affect the impact of the filter positions. This is most evident at filter locations directly impacted by the change in the system, but is also seen for filter positions not directly impacted by the change in the system.

One important aspect that the method brought to attention is that the most impactful filter position is not necessarily at the position where the harmonic current injection is. If another filter position can effectively remove or severely dampen the resonance condition, causing the harmonic issues, the filter position will be more effective, compared to placing a filter at the emission source which does not remove the resonance condition.

The first order coefficient homotopy method is still in its early stages of development and therefore has a lot of potential in terms of how it can be efficiently used, and be applied to other power system components.

Contents

Preface	v
Executive Summary	ix
1 Introduction	1
1.1 The Danish Experience	1
2 State of the Art	7
2.1 Harmonics	7
2.2 Mitigation	13
2.3 Component Modelling for Harmonic Analysis	17
2.4 Propagation	27
3 Problem Statement	31
3.1 Problem Definition	32
3.1.1 Project Limitations	33
4 Analysis of Resonance Points in Small System	37
4.1 Impact of Different Line Lengths	38
4.2 Impact of Different Filter Positions	43
4.3 Summary of Chapter	49
5 Methods for Assessing Optimum Filter Location	51
5.1 Brute Force Method	52
5.2 Homotopy Method	53
5.2.1 Calculation of Power Series Coefficients	56
5.2.2 Power Series Convergence	60
5.2.3 Usability of the Homotopy Method	63
5.2.4 First Order Coefficient Homotopy Method	63

5.2.5	Test of First Order Coefficient Homotopy Method on Small System	65
6	First Order Coefficient Homotopy Method Applied to Large System	73
6.1	Description of Large System	73
6.2	Movement of Resonance Peaks during EDR-IDU Line Implementation . . .	75
6.3	Results of First Order Coefficient Homotopy Method	76
7	Discussion	85
7.1	Results from Chapter 5 and 6	85
7.2	Usability in Connection to Optimisation Methods	87
7.3	Effect of a Continues Changing Power System	88
7.4	Data Management of Results	90
7.5	Implementation with PowerFactory	90
7.6	Unbalanced Power System	91
7.7	Summary of Discussion	91
8	Conclusion	95
9	Further Work	97
	Bibliography	101
A	Sensitivity Analysis of C-type Filter Parameters	103
B	Cable Data used in the Small System	113
C	Radial Independent Resonance in the Small System	115
D	Additional Results from Chapter 5	119
E	First Order Coefficient Homotopy Method using Real and Imaginary Parts	123
F	Additional Results for Large System	129

Chapter 1

Introduction

This chapter first presents a historical outlook on the issue of harmonic distortion followed by the Danish experience concerning the increased power quality issues, in relation to harmonics, that has been seen in the Danish transmission system in recent years.

A global trend in power systems is the transition towards de-carbonisation of the electricity production through large-scale integration of renewable energy sources, which is gradually replacing the conventional power plants [1]. The connection of renewable energy sources are typically achieved through power electronics (PEs), which are sources of harmonic emission [1]. Another trend increasing the harmonic emission to the transmission system is the increased utilisation of flexible AC transmission system devices, HVDC systems and PE converters, used for demand purposes, such as electric vehicles and domestic appliances.

Traditionally the transmission line type utilised in transmission systems has been the overhead line (OHL), while underground cables (UGCs) and submarine cables have only been used sparingly when needed. The invention of cables using cross-linked polyethylene (XLPE) as dielectric in the 1960s has enabled the use of UGCs in high voltage (HV) and extra high voltage (EHV) transmission systems [2]. UGCs have significantly larger capacitance compared to OHLs, but also lower inductance. The use of UGCs, as well as submarine cables, lowers the frequencies of resonance points, due to the increase in capacitance outweighing the decrease in inductance. This increases the risk of having undesirable resonance phenomena, as the resonance points are moved to frequencies with higher harmonic emissions. When the frequency of a harmonic emission current matches a resonance frequency in the power system the harmonic voltage distortion is amplified. [2].

1.1 The Danish Experience

Role of the TSO

In Denmark Energinet is the TSO responsible for the transmission system and therefore also responsible for the coordination of overall power quality at the transmission level in Denmark [3]. To maintain acceptable power quality Energinet issues emission limits for new connectees. Energinet has adopted the indicative planning levels of the International Electrotechnical Commission (IEC), in terms of the technical report IEC 61000-3-6, which

specifies the allowable harmonic content for different harmonics at specified voltage levels [3].

Cablings in the Danish Transmission System

The Danish transmission system consists of a 400 kV level and a 150/132 kV level, which have different shares of OHLs and UGCs. For some connections of WPPs 220 kV lines are used. Table 1.1 shows the tracé-km of AC OHLs and UGCs in the Danish transmission system. Tracé-km accounts for the length of the OHL towers which means that in case of an OHL double circuit on the same tower the length is not counted for each individual circuit. In case of cables tracé-km accounts for each circuit. The total length of AC OHLs and UGCs would be around 6000 km if the individual length of each OHL circuit on the same tower was accounted for. [4]

Voltage level [kV]	Overhead line [km]	Cable [km]	Total [km]
132	753	476	1228
150	1216	605	1822
220	40	84	124
400	946	114	1061
Total	2956	1279	4235

Table 1.1: Tracé-km of AC OHLs and UGCs in the Danish transmission system in 2017 [4].

The large share of UGCs on the 150/132 kV level in the Danish transmission system is largely due to an agreement made in 2008, which dictated that all new 150/132 kV connections should be UGCs. Furthermore all the existing 150/132 kV OHLs should be converted to UGCs over a 30 year period [3], [5]. From 2009 to 2017 the share of UGCs in the Danish transmission system increased from 20 % to 35 % [4].

Currently the political agreements for the transmission system in Denmark, primarily from a political agreement in 2016, give the following guidelines for new and existing OHLs and UGCs [4]:

- New 400 kV lines are established as overhead lines, with the option for certain sections to be laid as underground cables. Furthermore there is an option to convert existing 150/132 kV overhead lines, in the vicinity of the new 400 kV overhead lines, to underground cables in order to compensate for the new overhead lines.
- Existing 150/132 kV overhead lines are by default kept as overhead lines with the option for cabling of certain sections, such as specific nature and urban areas.

- New 150/132 kV connections are established as underground cables.

Even though the agreement from 2016 initially will cause less established connections to be laid as cables the option for compensating new 400 kV OHLs with cabling of existing 150/132 kV OHLs will potentially continue the increase in UGCs at the 150/132 kV level. Energinet's RUS-plan 2017 presents a number of new projects in the Danish 150/132 kV part of the transmission system, where UGCs are to be used according to the political agreements [4].

Denmark already have a number of offshore wind power plants (WPPs) and several new WPPs are projected in the future [6], [7]. The connection between the offshore WPPs and the main grid has so far been done through UGCs in the voltage range between 132 kV and 220 kV. The connections to the WPPs are radial connections with varying length, depending on where the WPPs are connected to the transmission system and the location of the WPPs. Whether future WPPs will utilise UGCs at the 400 kV level is not known, however Energinet considers it an option, in the RUS-plan, which has to be investigated in the planning process for the connections of the new WPPs [4].

Harmonic Issues

In recent years projects in the Danish transmission grid have resulted in increased harmonic distortion, which was not expected nor found in the planning stages of the projects [3], [8], [9].

One of the projects which resulted in an unexpected increase in harmonic amplification was the connection of two parallel 400 kV UGCs of 8 km each, which partially replaced OHLs [3]. Harmonic issues were not investigated in the planning stage due to the belief that such issues would not arise in meshed systems. Immediately after the connection of the UGCs a significant increase in harmonic voltages of the 11th and 13th harmonic orders were observed in two substations, with one being 90 km away from the UGC installation and the other being 80 km away in another direction. In one of the substations the planning levels for the 11th harmonic order was exceeded. Later it was found that the amplification of the 11th and 13th harmonic orders was due to the new cables shifting the system resonances to lower frequencies.

This highlights the problem with designing limits for harmonic emission for new connectees, as even though the harmonic distortion is within the limits at the time of connection, changes in the transmission system can affect this. The changes can subsequently move the resonance points in the transmission system, and cause increased amplification of background harmonics, which increases the harmonic distortion in the grid, potentially exceeding the limits. This is a problem for the TSO as it is not possible to go back to the connectees and demand them to lower the emission below the earlier agreed emission

level, and the TSO thus has to handle the increased harmonic distortion themselves.

The Danish experience, which is also seen in most other transmission systems worldwide, is that the characteristic 5th, 7th, 11th and 13th harmonic orders are the most critical. In Denmark these harmonics are approximately at 50-60 % of IEC planning levels [3].

The problem with an increased share of UGCs on the 400 kV level was highlighted in relation to the planning of the Danish West Coast line from the German border to Endrup and from Endrup to Idomlund. The line is to be built in order to facilitate the use of the new 1400 MW HVDC connection, Viking Link, between Denmark and United Kingdom, which is to be connected in the 400 kV substation Revsing, and future renewable energy sources connected in West Jutland [3]. Originally the agreement between Energinet and the Danish government was that the 170 km of lines was to be built primarily as OHLs, with a maximum of 10 % of the line length being UGCs.

The choice of primarily building the transmission lines as OHLs caused large debate and concern in the local communities where the new OHLs are to be placed. This debate caused the Danish Minister of Energy, Utilities and Climate to commission Energinet to study the applicability of extended use of 400 kV UGCs, as an alternative to the proposed 400 kV OHL solution originally agreed upon. This study materialised in the Energinet report "Technical issues related to new transmission lines in Denmark" released to the public in October 2018 [3]. The conclusion in the Energinet report was that the total share of of the 400 kV UGCs in the Danish West Coast line could be increased from 10 % to 15 %. The limiting factor to how large a share of UGCs that could be implemented was the harmonic issues related to the use of UGCs instead of OHLs. The simulations conducted in the Energinet report show that not only the substations where the cables would be connected, would have a significant amplification of background harmonics, but also other substations in the transmission system would have increased distortion of certain harmonics. This was found to be due to the large shift of the resonance points in the system, due to the usage of UGCs. It was also highlighted that the use of passive filters at the substations where the cables were to be connected could potentially cause increased amplification of harmonics at other substations in the system, a phenomenon that Energinet calls anti-resonance. [3]

As a compensation for installing the new 400 kV OHLs, 243 km of OHLs on the 150 kV level will be taken down and replaced by UGCs in the areas where the 400 kV OHLs are to be placed [10]. At this point it is not clear how this will impact the harmonic distortion levels of the overall system.

Harmonic distortion issues with UGCs in radial networks, for the connection of off-shore WPPs, have been highlighted in [8], [9] and [11], which are all discussing issues seen at the Anholt WPP in Denmark. The harmonic distortion issues at the Anholt WPP because of amplification of the background harmonic content from the main transmission

grid, which has caused high harmonic distortion at the WPP point of connection and at the island of Anholt, which is radially connected to the WPP point of connection through an underwater cable.

Chapter 2

State of the Art

This chapter presents the state of the art regarding harmonics and the mitigation of harmonics, with special focus on the C-type filter. Furthermore the modelling of passive power system components, such as line types and transformers for harmonic studies are shown. Lastly methods for analysing harmonic distortion issues are presented.

2.1 Harmonics

Power quality of a power system is associated with the voltage of any point in the system. This involves the frequency, magnitude, waveform and symmetry between the three phases. Good power quality can be defined as a steady voltage with frequency close to the nominal frequency, and a smooth voltage waveform which resembles a sine wave [12]. There are many power quality problems, with harmonics being a major one due to the development of the power system in terms of a larger amount of UGCs, converter-based generation and loads, with the last two being harmonic sources [13].

Orders

Normally it is assumed that each individual harmonic order contains only one unique sequence component, namely their natural sequences. This means that the 1st harmonic order is predominantly a positive sequence harmonic order, the 2nd harmonic order is predominantly a negative sequence harmonic order and the 3rd harmonic order is predominantly a zero sequence harmonic order, with the orders continuing as shown in Table 2.1

Harmonic Order	Natural Sequence Component
1	+
2	-
3	0
4	+
5	-
6	0

Table 2.1: Harmonic orders and their respective natural sequences component.

In [8] it was seen that the assumption of a harmonic order having its natural sequence being dominant is not always true. In a specific case the 11th harmonic order, which is expected to be a negative sequence dominant harmonic order also contained a non-negligible positive sequence component. The 3rd harmonic order was seen to contain all three sequence components and as such the assumption that individual harmonic order contain only one unique sequence component will lead to errors [8]. The reason for this unbalance of sequence components in the harmonic orders was due to inter-sequence couplings, caused by the asymmetrical structure of the power system [8].

Sources

The rise in converter-based generation and loads has increased the amount of harmonics sources in the power system. General for harmonic sources is that they are non-linear loads. This means that when a sinusoidal voltage is applied to the load it does not results in a sinusoidal flow of current, thus their operation generate harmonics. Harmonic sources can be divided into two categories: Steady state and temporary harmonics.

A temporary harmonic could be the energisation of a transformer. The flux density when energising a transformer can reach peak levels of up to $2B_{max}$ or $B_r + 2B_{max}$ depending on the residual flux density in the core of the transformer when it was switched off, which can have values between $+B_r$ or $-B_r$ [14]. This can cause the transformer to go into saturation, which will lead to an increase in magnetising currents above its nominal value. The inrush current will contain both odd and even harmonics. The energisation of a transformer is a temporary harmonic source, due to the energisation of the transformer being a rare occurrence. Due to damping from surrounding components the harmonics generated by the transformer energisation are damped after some seconds [11]. A HVDC converter is considered a constant harmonic source, as during operation it constantly produces harmonics.

A classical example of a steady state harmonic is an electrical arcing device, such as an electric arc furnace, which has a highly non-linear voltage-current characteristics [14]. The harmonics of the electric arc furnace are also not definitely predicted as it depends on the feed material and there is a vast difference between the harmonics produced between the melting and refining stages [13].

In this report only steady state harmonics will be taken into account as they are constant sources of harmonics and will therefore almost always impact the power system. Some more examples of steady state harmonics sources include adjustable speed drive systems, home appliances, static var compensators, HVDC converters, electrical vehicle charging systems and fluorescent lighting. The HVDC converters and static var compensators are connected directly to the transmission system while the rest is connected at the

distribution level and can propagate up to the transmission system. What most of these have in common is that they are PE devices, as their operation rely on semiconductors.

Effects

Harmonics can cause the voltage and current waveforms to be distorted, which can have negative effects on the power system and its components. The main effects of voltage and current harmonics within the power system are [14]:

- *"The possibility of amplification of harmonic levels resulting from series and parallel resonances."*
- *"A reduction in the efficiency of the generation, transmission and utilisation of electric energy."*
- *"Ageing of the insulation of electrical plant components with consequent shortening of their useful life."*
- *"Malfunctioning of system or plant components."*

Resonances

Resonances in a power system is the interaction of the inductive and capacitive reactances in regards to the frequency, as they are both frequency dependent. The inductive reactances increases while capacitive reactances decreases with frequency. Dependent on the value of the inductance and capacitance the two reactances will become equal at specific frequencies, but with opposite sign. The effect of this on the impedance depends on the system, as it can be divided into series and parallel resonances.

The simplest series resonance circuit is given in Figure 2.1 (a) and consist of an inductor and a capacitor in series. For the circuit shown in this section they are assumed to be lossless, however in a real circuit there would be resistance, which will limit the impedance at the resonance points.

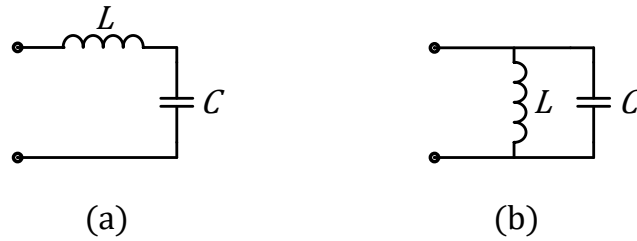


Figure 2.1: (a) series resonance circuit. (b) parallel resonance circuit

The reactance of an inductor and a capacitor is given in Equation 2.1 and 2.2 respectively.

$$X_L = 2\pi fL \quad (2.1)$$

$$X_C = \frac{1}{2\pi fC} \quad (2.2)$$

The resonance frequency in an AC circuit occurs when the two reactances become equal, but with opposite sign and thus cancel each other out as $X_L = X_C$. This causes the impedance of the system to be very low at the resonance frequency, as only the resistance of the system is left. The resonance frequency for a series resonance circuit is given in Equation 2.3.

$$f = \frac{1}{2\pi\sqrt{LC}} \quad (2.3)$$

The simplest parallel resonance circuit is given in Figure 2.1 (b) and consist of an inductor and a capacitor in parallel. Equation 2.3 can also be used to obtain the resonance frequency of a parallel circuit. However due to the inductor and capacitor being in parallel, the resonance has a very large impedance magnitude.

The most dominant harmonics in the power system are the characteristic harmonic orders, being the 5th, 7th, 11th and 13th, which are due to the large share of 6th and 12th pulse converters in the system and rectifiers for industrial usage. Therefore if resonance peaks or valleys are close to these frequencies, the harmonics can be magnified significantly.

Efficiency and Lifetime Reduction

The flow of harmonic currents in the power system cause additional power losses due to the increased RMS value of the current waveform. The increase in losses causes additional heating for power system components resulting in a higher operating temperature. If

the increase in operating temperature rises too far above the rated temperature of the components, their lifetime can be reduced and lead to economic losses [11].

Skin effect and proximity effect are two frequency dependent factors affecting the resistance of components. The effect of skin and proximity effect increases with frequency, therefore these effects will have a larger impact on harmonics at higher frequencies. The skin and proximity effect causes an increase in current density on the conductor surface that increases with frequency. The impact is an increase in the effective resistance of the conductor due to a reduction in the effective cross-sectional area and slightly on the internal inductance, as it will decrease due to the non-homogeneous current in the conductor. [1].

For rotating machines harmonic voltages or currents will give additional losses in the stator windings, rotor circuits, and stator and rotor laminations, which will lead to higher operating temperature and reduced lifetime. The harmonic current can also lead to pulsating torques which can significantly increase the wear and tear of the machines [14].

Harmonic voltages increases the hysteresis and eddy current losses in the laminations of transformers and stresses the insulation. There can be resonances between the transformer and capacitive components of the power system such as cables which will amplify the harmonics. Additional problems include vibrations and the possibility for delta-connected windings to be overloaded by circulating zero-sequence currents [14].

System Component Malfunctioning

The presence of harmonics in the voltage or current waveform can cause protection devices to degrade their operation characteristics as the waveforms can be overly distorted, with especially zero crossings being prone to errors [14]. Harmonics can also affect HVDC line-commutated converters (LCCs) and lead to reduced power transfer, or even commutation failures if the voltage waveforms are too distorted. PE loads could also have problems operating properly, as the distorted waveform could affect the phase-locked loop of the PE controllers.

Limits

The Danish TSO Energinet follows the indicative planning levels of the IEC 61000-3-6 standard for establishing the limits of harmonic voltage distortion in the transmission system [15]. In the standard the distinction between voltage levels is done according to the line-to-line RMS voltage level as follows [15]:

- Low voltage (LV) $V_n \leq 1 \text{ kV}$
- Medium voltage (MV) $1 \text{ kV} < V_n \leq 35 \text{ kV}$
- High voltage (HV) $35 \text{ kV} < V_n \leq 230 \text{ kV}$
- Extra high voltage (EHV) $230 \text{ kV} < V_n$

The definition of the planning level in IEC 61000-3-6 is stated as follows:

"Level of a particular disturbance in a particular environment, adopted as a reference value for the limits to be set for the emissions from the installations in a particular system, in order to co-ordinate those limits with all the limits adopted for equipment and installations intended to be connected to the power supply system."

The planning levels in IEC 61000-3-6 are indicative which means that in the end the TSO determines the planning levels, however the given IEC planning levels can be used as an internal quality objective [11], [15]. Many equipment manufacturers use the IEC standards and therefore it is very difficult for TSOs to apply their own limits, as this will potentially affect the already installed equipment and affect the equipment manufacturers for future equipment design.

The indicative planning levels according to IEC 61000-3-6, for harmonics on the HV/EHV voltage level, are shown in Table 2.2, where h is the harmonic order [15].

Odd harmonics non-multiple of 3		Odd harmonics multiple of 3		Even harmonics	
Harmonic order h	Harmonic voltage %	Harmonic order h	Harmonic voltage %	Harmonic order h	Harmonic voltage %
5	2	3	2	2	1.4
7	2	9	1	4	0.8
11	1.5	15	0.3	6	0.4
13	1.5	21	0.2	8	0.4
$17 \leq h \leq 49$	$1.2 \cdot \frac{17}{h}$	$21 < h \leq 45$	0.2	$10 \leq h \leq 50$	$0.19 \cdot \frac{10}{h} + 0.16$

Table 2.2: IEC 61000-3-6 indicative planning levels for harmonic voltages in the HV/EHV transmission system [15]. Planning levels are given as percentage of the fundamental voltage.

The indicative planning levels according to IEC 61000-3-6 for the total harmonic voltage distortion in the HV/EHV transmission system is 3 %.

The indicative planning levels differentiate between long-term and short-term effects of the harmonics. Long-term effects are mainly affecting the system components such as cables, transformers and motors thermally, which is caused by harmonics that are sustained for 10 minutes or more. The indicative planning levels presented in Table 2.2 are for long term effects. Very short-term effects are effects sustained for 3 s or less and relates to

disturbance of electronic devices. For very short-term effects the planning levels shown in Table 2.2 must be multiplied by the factor k_{hvs} given in Equation 2.4.

$$k_{hvs} = 1.3 + \frac{0.7}{45} \cdot (h - 5) \quad (2.4)$$

The following indices can be used to compare the actual harmonic levels with the planning levels [15].

- *"The 95 % weekly value of V_{hsh} (RMS value of individual harmonics over "short" 10 min periods) should not exceed the planning level."*
- *"The greatest 99 % probability daily value of V_{hvs} (RMS value of individual harmonic components over "very short" 3 s periods) should not exceed the planning level times the multiplying factor k_{hvs} given in Equation 2.4"*

2.2 Mitigation

Harmonic mitigation can be approached in different ways. Firstly the harmonic sources can be designed to avoid emitting certain harmonics, an example being the use of phase shifted transformers eliminating the 5th and 7th harmonic orders for a twelve-pulse HVDC-LCC [14]. Specific switching patterns in PEs can also exclude certain harmonics from being emitted. External harmonic mitigation is achieved through the use of filters, which can be either active or passive.

Active Filters

Generally active filters mitigate harmonic emission by injecting harmonic current into the system, which is equal to the harmonic current emission in magnitude but opposite in polarity, thus correcting the waveform to a sinusoid [13]. High-power active filters for HV transmission systems are not cost-effective due to the limited availability of high-switching-frequency devices with high-voltage and high-power ratings [16]. Because of the non-usefulness of active filters for HV it is chosen to not investigate active filters further in this report.

Passive Filters

Typically a passive filter is a shunt filter which provides a low-impedance path for certain harmonics, thus enabling the harmonic emission to flow into the filter path and not into the system [13]. Different filter types will give different impedance characteristics, with

some types, such as tuned filters, being used to mitigate specific harmonics and other types, such as damped filters, being used to mitigate several harmonics around a specific tuning frequency [13].

Tuned filters, which encompasses single-tuned, double-tuned and triple-tuned filters, are sharply tuned to their harmonic frequencies, which allows for optimum attenuation of the tuned harmonics. The disadvantage of the tuned filter types is de-tuning effects such as frequency variations in the power system, manufacturing tolerances of the filter components and ambient temperature variations [17]. De-tuning effects happen when the above mentioned variations causes the actual tuning frequency of the sharply tuned filter to be slightly above or below the planned tuning frequency, which decreases the effectiveness of the filter. Tuned filters also have the disadvantage that they often result in parallel resonances between the filter and system admittances at a harmonic order below the lowest tuned harmonic order of the filter or in between tuned filter frequencies [14].

Damped filters are characterised by providing a low impedance path for a wide spectrum of harmonics [14]. Due to a flatter impedance characteristic around the tuning frequency damped filters are less susceptible to de-tuning effects compared to tuned filters. A disadvantage of damped filters is that in order to achieve the same performance of tuned filters the damped filters need to be designed for higher fundamental VA ratings [14]. Another disadvantage of damped filters is the increased resistive losses in the filter at fundamental frequency compared to tuned filters [14]. The primary filter that will be focused on in this report is the C-type filter, which is a damped filter. This is due to [3], which is a report from the Danish TSO Energinet where the harmonic distortion impacts from new UGCs at the transmission level is investigated, which states the following:

"As filters are known to impact system resonances and anti-resonance can cause problems at other frequencies than the tuning frequency only damping type (C-type) filter with a low quality factor are utilised".

From the Energinet report [3] it was found that in some simulation scenarios C-type filters still caused anti-resonance at other harmonic orders. The following section will describe the characteristics of the C-type filter in further detail.

C-type filters

Figure 2.2 shows the schematic of the C-type filter. The significant feature of the C-type filter is the components C and L that are chosen to be resonant at the fundamental frequency, thus creating a path that by-passes the resistor at the fundamental frequency, which results in lower fundamental frequency losses compared to other damped filters. Thus at the fundamental frequency the impedance is largely determined by C_1 . At fre-

quencies above the fundamental, harmonic current flows through R thus achieving the desired damping [17]. As the C - L branch is essentially a tuned filter itself de-tuning effects can happen, which causes the resistor rating to be higher than in an ideal scenario [17].

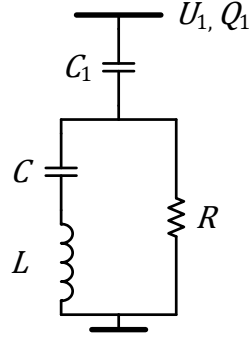


Figure 2.2: C-type filter. Figure inspired by [18]

The C-type filter component values can be calculated by determining the nominal voltage U_1 , the tuning frequency f_0 , the quality factor q and the reactive power capacity at fundamental frequency Q_1 .

If it is assumed that the dielectric losses in the capacitors and the resistance in the inductor can be neglected, the impedance of the C-type filter can be calculated as seen in Equation 2.5 [18].

$$Z(\omega) = \left(\frac{1}{R} + \frac{1}{j\omega L - j(\omega C)^{-1}} \right)^{-1} + \frac{1}{j\omega C_1} \quad (2.5)$$

At fundamental frequency C_1 provides all of the reactive power capacity Q_1 and also determines the impedance at the fundamental frequency $Z(\omega_F)$, where ω_F is the fundamental frequency angular velocity. Thus Equation 2.6 can be set up and C_1 can be obtained [18].

$$Z(\omega_F) = -\frac{j}{\omega_F C_1} = -j \frac{U_1^2}{Q_1} \iff C_1 = Q_1 \cdot U_1^{-2} \cdot \omega_F^{-1} \quad (2.6)$$

The component values of C and L can be calculated from Equation 2.7 and 2.8 respectively, where h_0 is the harmonic order the filter is tuned to.

$$C = \frac{(h_0^2 - 1)Q_1}{\omega_F U_1^2} \quad (2.7)$$

$$L = \frac{U_1^2}{(h_0^2 - 1)\omega_F Q_1} \quad (2.8)$$

The value of R can be obtained from Equation 2.9, which also shows the impact of R on the quality factor q . The quality factor determines how sharp the impedance characteristic is around the tuned frequency. In the C-type filter this is due to R being in parallel with the C-L branch and thus the larger R becomes the more the C-L branch gets to dominate the impedance profile. Generally tuned filters have large quality factor and damped filters have low quality factor, as damped filters are used to attenuate more harmonic orders [14].

$$q = \frac{R}{\omega_0 L} \iff R = q \cdot \omega_0 L \quad (2.9)$$

Figure 2.3 shows the impedance magnitude characteristics of a single-tuned (ST) and a C-type filter tuned to the same frequency. The ST filter's characteristic is obtained from a ST filter in the Danish transmission system which is tuned to the 5th harmonic [19], but for illustration purposes it is tuned to 3rd harmonic in the figure, while the original Q_1 and q is kept. The C-type filter in Figure 2.3 is not necessarily an existing filter in the Danish transmission system, but the values chosen are the same as is used in [3] and lies within the ranges described in [18] for existing C-type filters, which is $Q_1 = 38 - 130$ Mvar and $q = 1 - 2.3$. It can also be seen that the C-type filter provides attenuation for a wide range of harmonics, especially for harmonic orders higher than the tuned frequency, due to its low quality factor. In the zoom in of the figure it can be seen that the ST filter has a sharper impedance characteristic at the tuned frequency compared to the C-type filter, due to the larger quality factor.

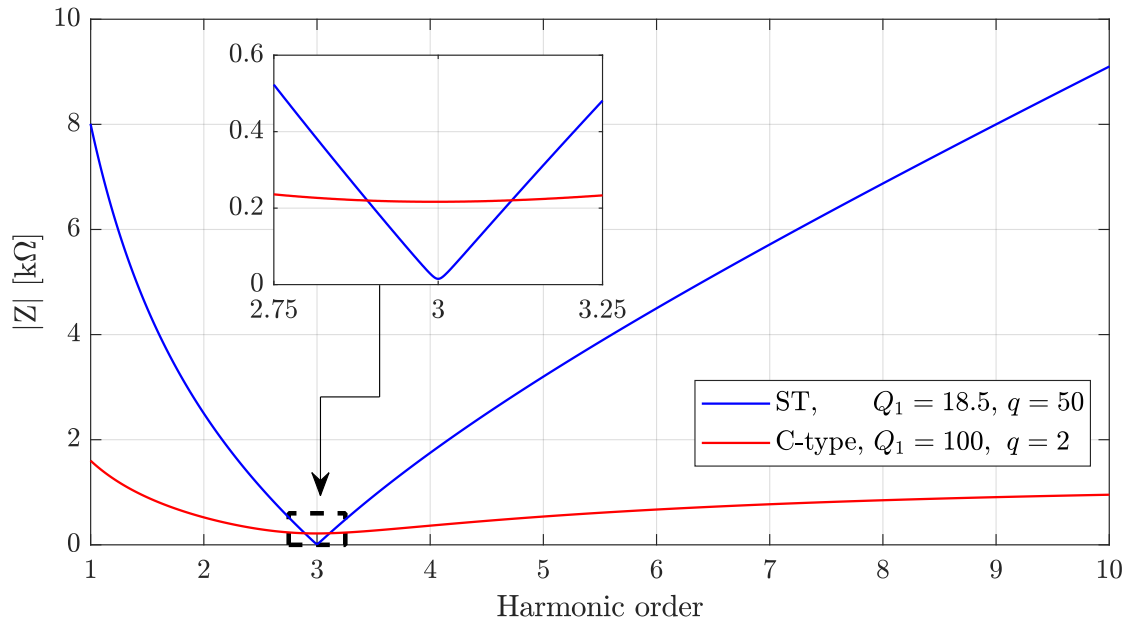


Figure 2.3: Typical ST and C-type filter impedance magnitude characteristics, tuned to the 3rd harmonic order.

In Appendix A a sensitivity analysis on the parameters of a C-type filter is conducted in order to see what parameters affects the filtering and losses of the C-type filter, if the winding resistance of the inductor is not neglected, with the results of the analysis listed below:

- A lower q of the C-type filter results in a flatter impedance profile, which means that the harmonic orders above the tuning frequency are attenuated more.
- A larger value of Q_1 gives better attenuation at all harmonic orders.
- The most important parameter in terms of the fundamental frequency losses is the quality factor of the inductor. It should be mentioned that other assumptions, such as no losses in the capacitor and variations in the fundamental frequency were not examined.
- Q_1 determines the reactive power injection into the system. Unless the filter is placed at substations with HVDC-LCC connections, shunt reactors are likely to be needed to absorb the generated reactive power.

2.3 Component Modelling for Harmonic Analysis

The importance of precise modelling of power system components during harmonics studies is significant as a small difference in the location of the resonance points can mean a large difference in the impedance magnitude at specific frequencies. The modelling also affects the damping in the system and if not modelled correctly can lead to optimistic results or overdimensioning of compensation devices. Simplified studies can be used to predict resonance points, however if the resonance points are close to dominant multiples of the fundamental frequency, further analysis has to be made. The use of simplified models can sometimes be necessary, not to make the calculations faster, but because of the values or dimensions of the parameters and components are not always available during the planning stage and generic models and parameters have to be used instead [1].

Transmission Line Models

Common transmission line models such as the nominal-PI model and the equivalent-PI model, offer different levels of accuracy when compared to a geometry based model, which is the most accurate modelling. A nominal-PI model, which is also known as a lumped model, considers the series impedance lumped together in the middle with the shunt admittance split on both sides of the series impedance, as seen in Figure 2.4. A

nominal-PI model will give one resonance point, as will be shown later, and is thus only accurate for the first resonance of short length lines [14].

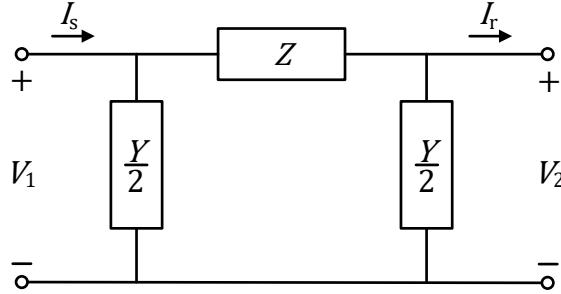


Figure 2.4: Schematic of nominal-PI model.

The equivalent-PI model distributes the electrical parameters along the line which is developed through the solution of the second order differential equations describing wave propagation along transmission lines [14]. The schematic of an equivalent-PI circuit is similar to the nominal-PI however the inputs for Z and Y are corrected. There are different versions of the equations used to correct Y . The equations for correcting Y shown later accounts for the division by 2 in the shunt elements, so the circuit for the equivalent-PI model becomes as seen in Figure 2.5.

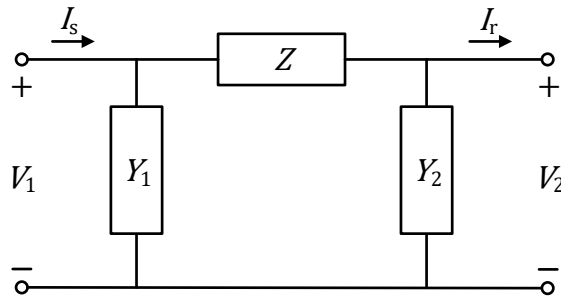


Figure 2.5: Schematic of equivalent-PI model.

The parameters Z , Y_1 and Y_2 in Figure 2.5 are given in Equation 2.10 and 2.11 respectively.

$$Z = Z_0 \sinh(\gamma l) \quad (2.10)$$

$$Y_1 = Y_2 = \frac{1}{Z_0} \tanh\left(\frac{\gamma l}{2}\right) \quad (2.11)$$

Where Z_0 is the characteristic impedance of the line and given in Equation 2.12.

$$Z_0 = \sqrt{\frac{Z'}{Y'}} \quad (2.12)$$

With $Z' = R + j2\pi fL$ and $Y' = G + j2\pi fC$ being the series impedance and shunt admittance respectively. γ is the propagation constant and is given in Equation 2.13.

$$\gamma = \sqrt{Z'Y'} \quad (2.13)$$

Figure 2.6 shows an impedance profile of the equivalent-PI series and shunt resistance and reactance for the cable in Appendix B, with the cable set to 25 km. Skin effect is implemented to the resistance according to [14]. An OHL will have similar behaviour, however at other frequencies as the relationship between the capacitance and inductance is different for the OHL compared to the cable. The shunt resistance and reactance are obtained by inverting the shunt admittance [14]. In the legend *se* denotes series and *sh* denotes shunt.

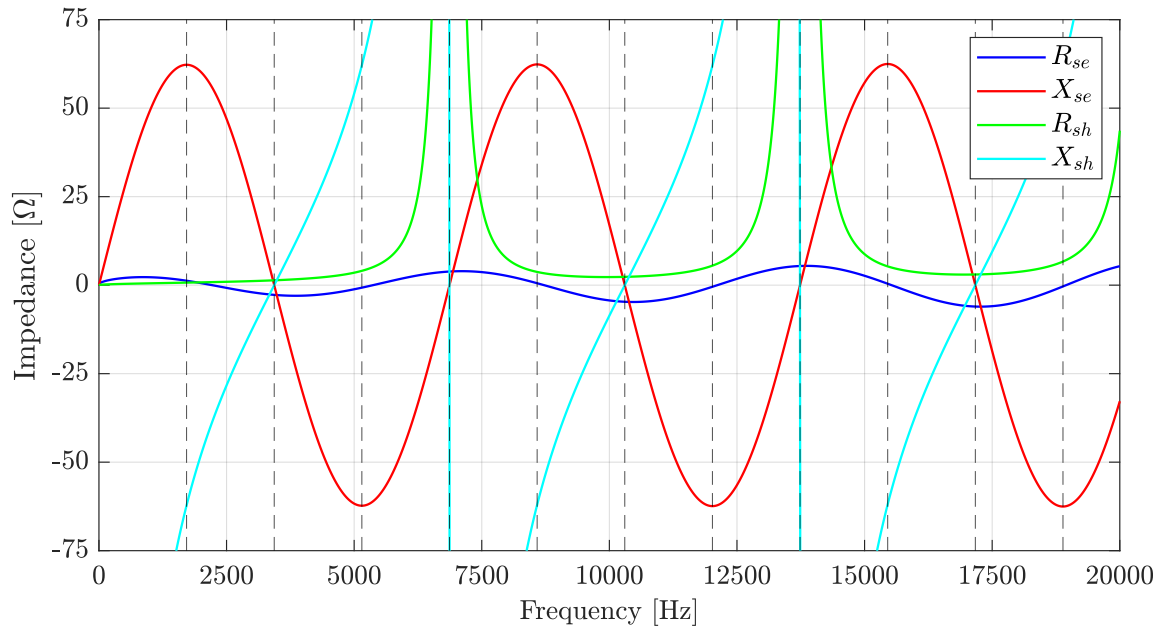


Figure 2.6: Frequency scan of equivalent-PI series and shunt elements for the cable in Appendix B. The cable length is set to 25 km. The vertical dashed lines marks the resonance points for the cable.

The wavelength at 50 Hz, λ_{50} , of the shown line is 3434 km, as calculated from Equation 2.14, where v is the velocity of propagation and f is the frequency.

$$\lambda = \frac{v}{f} \quad (2.14)$$

v can be obtained from Equation 2.15, which for this cable is calculated to $v = 1.72 \cdot 10^8$ m/s.

$$v = \frac{1}{\sqrt{LC}} \quad (2.15)$$

The natural occurring resonance points of a line occurs at intervals of one quarter of the wavelength of the line at the fundamental frequency [14]. Thus the frequency of the resonance points can be calculated from Equation 2.16, where l is the length of the line and n specifies which resonance point the frequency is being calculated for with $n = 1$ being the first resonance point and so forth.

$$f_{res} = \frac{\lambda_{50}}{4l} \cdot f_{50} \cdot n \quad (2.16)$$

In Figure 2.6 the vertical black dashed lines indicate the frequency of each resonance point within the shown frequency range, which match up with the calculated values from Equation 2.16. The first resonance point is seen to occur when the series reactance is at its maximum value, which also corresponds with the shunt reactance having the same value but with opposite sign. For an open-circuited line this corresponds to a series resonance which has a low purely resistive impedance magnitude. At the half wavelength frequency a parallel resonance occurs and although both the series and shunt reactances are small the open-circuited line has a large impedance.

The series resistance alternates and increases in magnitude as the frequency increases due to skin effect. Unlike the nominal-PI model, which normally considers the shunt resistance to be zero, the equivalent-PI model has a large shunt resistance as the wavelength frequency is approached [14].

The nominal-PI and equivalent-PI models use electrical parameters calculated at power frequency and these parameters are thus not frequency dependent. The resistance can be made frequency dependent by accounting for the skin effect of the conductor. The proximity effect is also a frequency dependent parameter which affects the resistance. The equations for calculating a geometry based frequency dependent model of a transmission line are not shown due to being out of the scope for the purpose of the project, however a MATLAB script with the equations, which are presented in [2], is used in order to compare the different ways of modelling a transmission line. The geometry based model uses Bessel equations and accounts for frequency dependency of the electrical parameters, including skin effect. The transmission line, which is modelled, is the cable described in Appendix B and the comparison between the described models can be seen in Figure 2.7. The cable is shown when it is short-circuited to an ideal voltage source in one end of the cable, while the measurements are made from the other end.

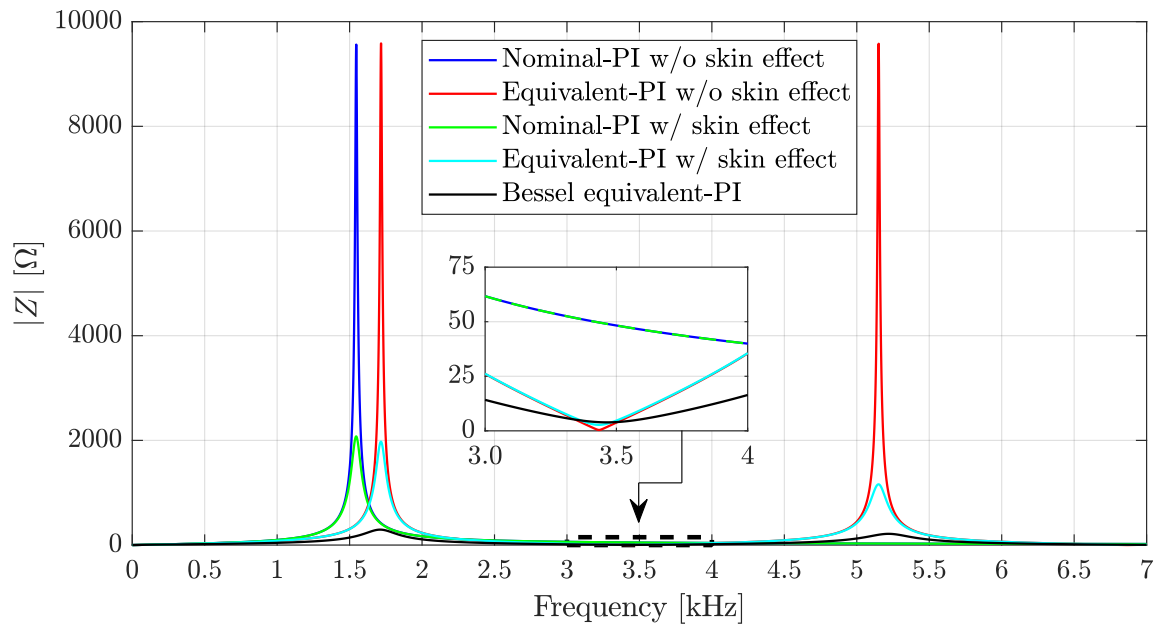


Figure 2.7: Comparison between nominal-PI, equivalent-PI and Bessel equivalent-PI with and without skin effect.

It is clear that the geometry based model has significantly lower impedance magnitudes at the resonance peaks and higher impedance magnitude at the resonance valleys. As predicted the nominal-PI model only has one resonance point which resonance frequency is lower than that of the equivalent-PI. There is a small difference between the resonance frequency of the resonance points for the equivalent-PI and geometry based model. The skin effect leads to a significantly lower impedance magnitude at the resonance peaks for both the nominal-PI and equivalent-PI models.

Overhead Lines

When modelling OHLs for harmonic studies the equivalent-PI model should be used, as the equivalent-PI model takes the parameters of the line as distributed parameters and accounts for long line effects [1]. The nominal-PI model can be used as an alternative technique to represent short lines of $240/h$ km, with h being the harmonics order investigated, and can be made usable for long lines if cascading nominal-PI sections is used, as more sections will make the model approach the distributed model. This is however not done in practice [1].

The length of the OHL has a significant impact on the frequency and magnitude of resonance points, and thus the number of harmonic resonance points within the frequency range of interest. An increase in length will give a lower resonance frequency for the

positive- and zero sequence. During the planning stage the length of an OHL can vary, as the path between two points in the system can not always be a straight line, and the path will have to adapt to account for areas being preserved, such as farms or nature.

A multi-phase model, as seen in Figure 2.8, should be used to account for the geometric layout of OHLs, as most layouts are asymmetrical. The asymmetrical nature of OHLs give different mutual impedances between phases and different resonance frequencies for each phase. This can result in a large unbalance in the voltages and currents at certain harmonic frequencies [1].

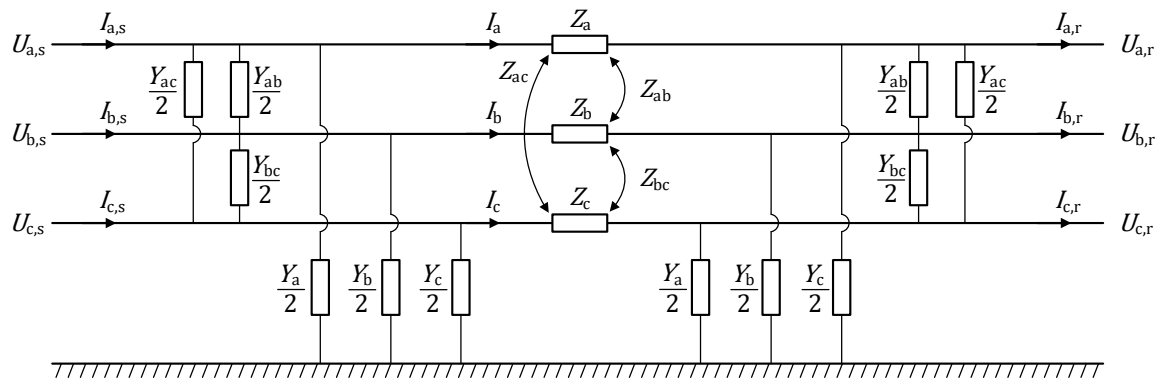


Figure 2.8: The impedance and admittance for a three-phase transmission line.

The layout of the line can also change when going from one tower to another. This could be the case when two lines on different towers are transferred to a single tower. Modelling of double circuits and line transposition, if present, should also be represented as it affects the mutual impedance.

The frequency dependency of the line parameters should be taken into account. The skin effect and earth return path is the most affected by the frequency dependency, with the later affecting the zero sequence currents and since all of the Danish 400 kV transmission system is grounded, the zero sequence will have an impact. Neglecting skin effect will lead to an underestimation of circuit damping at resonance frequencies and will also result in a slight error for the resonance frequencies, as it will give a slight upward shift in the resonance frequency due to the non-homogeneous current in the conductor [1].

For OHLs with large cross-sectional areas, stranded conductors are normally used due to limit skin effect, however most commercial software can not model stranded conductors, and therefore corrections have to be made to the resistivity [20]. The corrections comes from the cross-sectional area of stranded conductors in data-sheets not being equal to πr^2 , with r being the radius of the conductor. Equation 2.17 shows the correction to the resistivity with ρ' being the corrected resistivity, ρ being the material resistivity and

A being the cross-sectional area of the conductor.

$$\rho' = \rho \frac{\pi r^2}{A} \quad (2.17)$$

When dealing with harmonic studies where the zero sequence is of importance the earth resistivity should be considered. It is however very difficult to precisely model the earth resistivity without making significant simplifications, as the ground conditions are affected by weather, which can change on a day to day basis. The composition of the earth can also vary significantly along the circuit both in longitude and in depth. To model this correctly the model would need to be split into sections, each with their own respective earth resistivity. Normally in a study involving many transmission lines of considerable length an average earth resistivity for the whole area is used, however this can introduce substantial errors [1].

Cables

When modelling cables the equivalent-PI model should be used for cables above 2-5 km, however for shorter cables the lumped model can be used, with the number of PI sections dictating the number of resonance points. With the computational power available the distributed model is recommended as the first choice in [1]. Frequency dependent (FD) models such as the FD phase model can be used to model the cable or OHL, however this increases the simulation time significantly and the increase in accuracy of this model would require that the data is also precise or the extra accuracy of the FD phase model would be neglected.

The length of the cable has, as was also applicable for the OHL, a significant impact on the frequency and magnitude of the resonance points, which is due to the same reasons mentioned for the OHL.

The radius of the conductor will affect at which frequencies the resonances occur in the positive sequence, but hardly the zero sequence as this mostly depends on the sheath of the cable, and the radius of the conductor does not affect this. The cable capacitance is increased with a larger conductor radius while the inductance is decreased, which to some extent counteract each other, and therefore the overall downward shift in resonance frequency is affected less, than if only the capacitance was increased alone. The magnitude of the positive sequence is not affected by an increase in the conductor radius, however the magnitude for the zero-sequence impedance is slightly affected as more damping is introduced when the conductor radius is increased [1]. There can be uncertainties in the thickness of the cable layers provided by the manufacturer. Also the choice of conductor material can be up to the manufacturer, thus there can be a large

difference in the radius of the conductor depending on the material of the conductor, such as aluminium or copper for example.

The use of stranded conductors for OHLs, is the same for cables, and therefore corrections to the resistivity of the material has to be made, which was given in Equation 2.17.

The thickness of the insulation for the cable will affect the frequency and magnitude of the resonance points for the positive sequence as a decrease in insulation thickness increases the capacitance of the cable and shift the resonance frequency downwards. In [1] it was shown that only the zero sequence impedance magnitude was affected when changing the insulation thickness as a larger insulation thickness gave a larger impedance magnitude.

As with OHLs the frequency dependency of the line parameters and stranded conductors should be taken into account for cables. The cable formation layout will have a significant impact on the positive sequence as it affect the frequency of resonance points and their magnitudes. The most common formations for cables are trefoil, flat and touching trefoil, with the flat formation having the largest asymmetry, causing it to have more resonance peaks in the frequency range [1]. For the touching trefoil the resonance peaks are shifted to higher frequencies due to the mutual inductance being increased as the distance between the cables is lower. The larger mutual inductance causes the positive sequence inductance to decrease. The zero sequence impedance is not affected by the cable formation.

The configuration of the cable sheath bonding will affect the positive sequence impedance as it introduces a non-continuous impedance along the cable [1]. The use of cross-bonding will give higher magnitudes and lower resonance frequencies compared to a both-end bonded cable. This is due to the positive-sequence inductance being larger in a cross-bonded cable compared to an equivalent both-end bonded cable, whereas the series resistance is larger for the both-end bonded cable [21]. The larger inductance comes from the cross-bonded cable having a lower circulating current in the sheath and the lower circulating current induces a weaker magnetic field, resulting in a larger positive sequence inductance [21]. The conductor positive-sequence shunt admittance is equal for both bonding configurations and does therefore not have an effect on the resonance frequencies [1], [21]. The zero sequence impedance is only slightly affected as only a limited amount of current should flow to the ground at the grounding points [1].

For cross-bonded cables the number of major sections affects the frequency, magnitude and the number of resonance peaks, in the positive sequence, within the chosen frequency range. The more of the actual major sections that are modelled the more precise the model will be. If only the first or second resonance points are of importance, less major

sections can be used as these will still be accurate, however the accuracy depends on how many major sections there is in the actual cable. The zero sequence is not affected by the amount of major sections modelled, as only a limited amount of current is flowing to the ground [1].

Submarine cable losses will impact the damping of the system models, but are difficult to model. This is due to that most commercial software models the armour of the cable as a hollow cylinder, while some cables' armour consist of steel wires [11]. The use of steel wires change the magnetic behaviour significantly, due to the permeability of steel being high, and the distribution of the steel wires therefore affect the mutual impedance. It can therefore be difficult to get the right dimensions and thus the right modelling of the losses. These challenges that the cable armour introduces is out of the scope of this project.

For multi-core or closely laid cables proximity effect should be considered, as it will affect the damping, which gives a reduction in the magnitude of the resonance peaks. It is however difficult to model it precisely as correction factors is often not accurately at resonance frequencies [1]. When very accurate models is needed a method such as Method of Moments Surface admittance Operator can be used, but it is not commonly available in commercial software [1]. This is however out of the scope of this project.

A summary of the parameters and their impact when modelling OHLs and cables is given in Table 2.3.

Parameter	Line Type		Impact	Res. Frequencies		Res. Magnitude	
	OHL	UGC		Pos. Seq.	Zero Seq.	Pos. Seq.	Zero Seq.
Length	X	X	Significant	X	X	X	X
Model Type	X	X	Significant	X	-	-	-
Multi-phase Geometric	X	X	Significant	X	-	X	-
Frequency Dependency	X	X	Significant	X	X	X	X
Stranded Conductor	X	X	Minor	X	-	X	-
Earth Resistivity	X	-	Moderate	-	X	-	X
Conductor Radius	X	X	Minor	X	X	-	X
Insulation Tickness	-	X	Moderate	X	-	X	X
Sheat Bonding	-	X	Significant	X	-	X	-

Table 2.3: Summary of the parameters and their impact when modelling OHLs and cables. Resonance is denoted "Res", positive is denoted "Pos" and sequence is denoted "Seq".

Power Transformers

Power transformers have an inductive behaviour for the frequency range of interest and can with cables, which are predominantly capacitive elements, create parallel or series resonances. Therefore the modelling of transformers will impact the location of resonance points and their magnitudes, when performing harmonic studies.

In [1] five models to represent power transformers in harmonic analysis are given and tested for three different transformers. The models tested were models which data could easily be obtained from transformer data sheet or from the Factory Acceptance Test report, which is preferred, however some models did require some additional factors, where default values are used. Three out of five models had the common assumption that the transformer leakage inductance is constant for the range of frequencies of interest. For the two other models, one assumed a constant leakage inductance for high voltage transformers. The second model had a L-f characteristic, however for the frequency range of interest of this project it can also be assumed constant. Therefore the frequencies at which the resonance peaks occur are unchanged from model to model [1].

The difference between the transformer models comes from the modelling of the resistance and thus the magnitudes of the peaks. The higher the resonance frequency is the further apart the different transformer models will be from each other. The different types of models will give different amounts of damping and can lead to an underestimation or overestimation of damping. [1] tested the five different transformers models for three power transformers, where measurements were available. The test showed that no single transformer model could be used to represent the three different transformers. In another test in [1] the transformer models are tested in a full system model of the Irish transmission grid. This was done to see how the transformer behaved in a system, instead of as a single component. It could be concluded that the different transformer models gave similar results, except at the parallel resonance points and at nodes where the harmonic impedance is dominated by the transformer [1]. It was also found that the further away the node of interest is from the transformer the less impact the selection of the transformer model has. The transformer winding connection should also be represented to take into account the phase shifting effect on harmonics currents. If high accuracy is needed [1] recommends to obtain frequency dependent characteristics for the resistance and reactance from the transformer manufacturer.

2.4 Propagation

The purpose of harmonic propagation studies is to analyse how the harmonic currents or voltages distribute into the power system from the harmonic source [13]. The goal is to determine the magnitude of distortion at each frequency, the distribution of harmonic voltages in the system and if resonances occur at characteristic harmonic orders [11]. This can then be used for harmonic filter design and study effects such as derating of transformers and overloading of system components [13].

There are several approaches for conducting harmonic propagation studies, due to the practical limitations of modelling each component in a large power system, as each approach has different accuracy and also depends on the components in the power system of interest, as some are non-linear, and therefore too simplistic methods can give erroneous results [13].

Studies for calculating harmonics and the effects of non-linear loads can involve measurements, where appropriate instruments are required to get accurately current and voltage waveforms. These studies can be done in a non-invasive manner where the waveforms are measured under normal operation or in an invasive manner where HVDC converters are used to inject harmonic currents into the power system [13]. Studies involving computer simulation can also be used and does as such not require measurements or interactions with the power system. The harmonic studies in this report are based on

computer simulation studies.

Harmonic propagation computer simulations are normally conducted in either the frequency or the time domain. The later is used in some special applications and is getting more common, while the former has been the most commonly used.

Frequency Domain

The frequency domain includes direct and iterative methods, with most practical harmonic studies using the direct method. The iterative method is used in the case where the harmonic injections are considered to be dependent on the harmonic voltage [1]. A common frequency domain study is a frequency sweep, where the magnitude of the system impedance is given at each frequency, which can be used to determine resonance points in the system seen from different busbars, with different injections. Frequency domain analysis can be very efficient and reliable for steady-state solutions, given the simple representation of harmonics and the short calculation time. However the models used in the frequency domain for devices such as converters and of non-linear behaviour, like transformer saturation, may be oversimplified [1].

One of the frequency domain direct methods is the frequency scan, which is the same as the frequency sweep mentioned earlier. This method is based on the nodal admittance matrix, which form at a given frequency is given in Equation 2.18. It should be noted that a bold symbol represents a matrix.

$$\mathbf{Y}_f = \begin{bmatrix} Y_{1,1} & -Y_{1,i} & -Y_{1,j} & \cdot & -Y_{1,n} \\ -Y_{i,1} & Y_{i,i} & -Y_{i,j} & \cdot & -Y_{i,n} \\ -Y_{j,1} & -Y_{j,i} & Y_{j,j} & \cdot & -Y_{j,n} \\ \cdot & \cdot & \cdot & \cdot & \cdot \\ -Y_{n,1} & -Y_{n,i} & -Y_{n,j} & \cdot & Y_{n,n} \end{bmatrix} \quad (2.18)$$

The diagonal elements are the self-admittances and the off-diagonal elements are the mutual-admittances.

To get each frequency of interest the admittance matrix has to be generated for each individual frequency, as the matrix at one frequency can not be applied at other frequencies [13]. The matrix is build from component models of transformers, transmission lines and other passive components in the power system. The impact of ideal voltage sources and current sources on the admittance matrix is seen as a very large and very small admittance respectively. This is due to the voltage source acting as a short-circuit and the current source as an open-circuit. The components thus have to be accurately modelled in the frequency range of interest to get an accurate admittance matrix [14]. The frequency

scan is made by repeated applications of Equation 2.19.

$$\mathbf{I}_f = \mathbf{Y}_f \mathbf{V}_f \quad (2.19)$$

Where the matrix \mathbf{I}_f given in Equation 2.20 represents the harmonic current source in each busbar.

$$\mathbf{I}_f = \begin{bmatrix} I_{1,1} & 0 & 0 & \cdot & 0 \\ 0 & I_{i,i} & 0 & \cdot & 0 \\ 0 & 0 & I_{j,j} & \cdot & 0 \\ \cdot & \cdot & \cdot & \cdot & \cdot \\ 0 & 0 & 0 & \cdot & I_{n,n} \end{bmatrix} \quad (2.20)$$

A 1 pu, or 1 A, current injection is applied in each busbar where the current injections can be either positive, negative or zero sequence, which will result in the positive, negative or zero sequence driving point and transfer impedances [1]. This would however require that the admittance matrix is to be formed based on sequence networks, such that a positive current injection is given to a positive sequence network. If the method is used with only positive sequence it can give erroneous results for systems including arc furnaces or PE converters [22]. The couplings between sequences can be implemented to improve accuracy, with couplings between the positive and negative sequence having the largest impact [11]. The system harmonic voltages can then be calculated by direct solution of Equation 2.21.

$$\mathbf{V}_f = \mathbf{Y}_f^{-1} \mathbf{I}_f \quad (2.21)$$

When expanding Equation 2.21, Equation 2.22 is obtained.

$$\begin{bmatrix} V_{1,1} & V_{1,i} & V_{1,j} & \cdot & V_{1,n} \\ V_{i,1} & V_{i,i} & V_{i,j} & \cdot & V_{i,n} \\ V_{j,1} & V_{j,i} & V_{j,j} & \cdot & V_{j,n} \\ \cdot & \cdot & \cdot & \cdot & \cdot \\ V_{n,1} & V_{n,i} & V_{n,j} & \cdot & V_{n,n} \end{bmatrix} = \begin{bmatrix} Y_{1,1} & -Y_{1,i} & -Y_{1,j} & \cdot & -Y_{1,n} \\ -Y_{i,1} & Y_{i,i} & -Y_{i,j} & \cdot & -Y_{i,n} \\ -Y_{j,1} & -Y_{j,i} & Y_{j,j} & \cdot & -Y_{j,n} \\ \cdot & \cdot & \cdot & \cdot & \cdot \\ -Y_{n,1} & -Y_{n,i} & -Y_{n,j} & \cdot & Y_{n,n} \end{bmatrix}^{-1} \begin{bmatrix} I_{1,1} & 0 & 0 & \cdot & 0 \\ 0 & I_{i,i} & 0 & \cdot & 0 \\ 0 & 0 & I_{j,j} & \cdot & 0 \\ \cdot & \cdot & \cdot & \cdot & \cdot \\ 0 & 0 & 0 & \cdot & I_{n,n} \end{bmatrix} \quad (2.22)$$

The system harmonic voltages given by Equation 2.21 will when varying the frequency give a series of driving point and transfer impedances and each can be plotted to give indications of the resonance conditions [13]. An impedance peak in the plot imply a parallel resonance while an impedance valley imply a series resonance [1]. The frequency scan ignores system non-linearity and as such the admittance matrix dependency on system voltages and currents is not considered and is therefore one of the limitations of the method [1].

When a 1 pu or 1 A current injection is applied the impedance matrix of the system equals the voltage matrix, as seen in Equation 2.23.

$$\mathbf{Z}_f = \mathbf{V}_f = \mathbf{Y}_f^{-1} \quad (2.23)$$

In Equation 2.22 the voltage given in $V_{1,1}$ corresponds to observing the voltage in Bus 1 while a current injection is given in Bus 1. From Equation 2.23 a notation for this can then be given by $Z_{i,j}$, where i is the busbar that the impedance is observed from and j is the busbar where a current injection is applied. Therefore the notation $Z_{1,1}$ indicates that the impedance is observed from Bus 1 with a current injection in Bus 1.

One of the iterative methods in the frequency domain is the Harmonic Power Flow Method, which takes into account the voltage-dependent nature of power components. Using Newton-type algorithms it solves the voltage and current harmonic equations simultaneously. The method gives explicitly representations of the balance, unbalance, linear, non-linear and time-varying components, harmonics and harmonic cross-couplings effects [22]. The solution is however based on a linearisation process around a specific operating point. The linearisation process results in a Norton harmonic equivalent where the aforementioned effects are explicitly represented. The computational effect of this method increases in direct proportion to the size of the system and the number of harmonic orders represented [22].

Time Domain

Time domain studies uses the same methods as is used for transient studies. In this domain differential equations is solved to build up a model, for harmonic propagation, which could avoid some of the approximations that is inherent in the frequency domain approach [13]. The output of the time domain for the harmonic propagation is the time varying waveforms for the voltages and currents and the harmonic distortions can be directly calculated by the use of Fast Fourier Transform to convert the time domain into the frequency domain [13]. Harmonic propagation studies in time domain are very accurate, therefore the part of the system to be analysed has to be modelled very detailed. This makes time domain studies very computational heavy and as such simplifications are often made to the surrounding part of the system with lumped RLC branches connected at interconnection busbars to represent the driving point and transfer impedance at the selected busbars [13].

In [1] the frequency domain is deemed adequate and highly recommended for applications such as impedance scans to evaluate potential resonance issues, network harmonic impedance envelopes and filter design. As these are the key objectives of the report the frequency scan is chosen as the method to be used in the report.

Chapter 3

Problem Statement

This chapter presents the problem statement and the problem definition of the report. Furthermore, limitations to the project are listed together with an explanation of why the limitation is made and the impact of the limitation.

There is a global trend in power systems toward de-carbonisation of the electricity production by integration of renewable energy sources as a substitute to conventional power plants. The connection of renewable energy sources is typically achieved through power electronics which are sources of harmonic emission. Exceptions are hydro and nuclear which utilise classical generator technology. The Danish power system has several high voltage direct current connections which also add to the harmonic emission. Furthermore the replacement of overhead lines with cables to transfer energy has lowered the frequencies of resonance points in the power system. The resonance points acts as amplification for harmonic emission both in terms of voltage and current. Harmonic distortion in the power system can reduce the efficiency and lifetime of components and possibly cause maloperation, therefore limits have been introduced in order to keep the harmonic distortion within acceptable ranges, according to standards, such as IEC 61000-3-6. In order for the harmonic distortion to exceed the acceptable ranges typically two things need to happen. The first thing is that there needs to be a harmonic emission, such as harmonic current injection from high voltage direct current line-commutated converters, and the second thing is that there needs to be a resonance condition, such as a resonance peak in the impedance envelope observed from a specific location in the given system.

If there are locations in the power system where the harmonic distortion is too high or has been amplified by resonance points mitigation, such as filters, is needed. This is typically solved on a case-by-case basis by the use of passive filters. A problem with this approach is that changes in the power system can cause new locations to be in the need of filtering and the original filters can become redundant as the resonance points have changed. Typically filtering will be made at the connection of large emission sources, such as high voltage direct current line-commutated converters, in order to limit the emission at the source. As more power electronic devices are connected to the power system it becomes increasingly difficult to identify the sources of emission.

Another issue related to the installation of filters is the creation of anti-resonances, as the installation of filters in one location in order to lower the harmonic distortion locally, can cause a rise to the harmonic distortion in other locations, due to the shift of resonance points caused by the filter implementation.

Typically harmonic studies on cables has only been done on radial systems as problems had not been prevalent in meshed systems. However the replacement of overhead lines to underground cables in a meshed system has been seen to cause a rise in harmonic distortion in locations far away from the location of the cable.

This report will aim to investigate methods to further the idea of placing filters from a global point of view, the idea being that filters should be placed where they mitigate the most seen from an overall system view, instead of a singular busbar view. The thought behind this is that potentially fewer filters are needed to be installed, as the power system continues to change, if a number of filter locations are found to be able to mitigate harmonic issues not only at the filter locations busbars but also at other busbars throughout the system.

Using the classical frequency scan method to graphically investigate the system-wide impact of a filter is a possibility, however for large systems this becomes unmanageable. It is possible to couple the frequency scan approach with a brute force optimisation method, in order to find the best filter location through running a large number of test cases with different filter positions, however this becomes computationally heavy and does not provide any inherent understanding of the power system being investigated. In order to investigate the idea of global filter placement, it is therefore found that a new semi-analytical mathematical method for observing a filter's impact on the power system should be investigated. The goal of the method being presented in this report is that it not only can be used as a means to investigate the idea of global filter placement, but also provide a better understanding of the harmonic behaviour of the power system.

This has led to the problem definition which is:

3.1 Problem Definition

To which extent can a new semi-analytical method be utilised to examine the impact of filter implementation in the power system, in order to further the idea of global filter placement?

As an extension to the problem definition a set of sub-questions have been formed:

- *How does passive filters impact the resonance points locally and globally?*
- *How does the continued change of the power system impact the effectiveness of filters?*
- *How can the method be used to track and avoid potential issues with anti-resonances created by the implementation of filters?*

3.1.1 Project Limitations

The following list presents the project limitations and an explanation for why the individual limitation has been made. Furthermore a description of the impact of the limitation, is presented. The limitation is marked as (•), the explanation is marked as (–) and the impact is marked as (*):

- *The method are using the frequency scan method as a starting point.*
 - *Due to the frequency scan method's easy implementation into calculation software such as MATLAB, it is chosen as the starting point. Methods such as harmonic power flow and time domain are therefore not investigated. Due to the difficulty in locating the harmonic emission sources and their angles the frequency scan can be used to give an understanding of where potential resonance phenomena can occur.*
 - * *There are limitations within the frequency scan method itself, including the modelling of non-linearities in devices. However as stated in [1] the frequency scan method, will be adequate for steady-state operation and the non-linear devices will typically operate in their linear region in most scenarios except for high frequencies.*
- *The frequency range of interest is between 50-1000 Hz.*
 - *This range is the most critical for the transmission system. However in some of the chapters wider frequency ranges are used in order to capture resonances, especially when the test system is not a representation of a real existing system.*
 - * *Having a maximum frequency up to 1000 Hz will exclude the resonances created specifically at higher frequencies, an example being transformer stray capacitances, which are not typically modelled for harmonic studies [1]. However as the characteristic harmonic orders, which are the 5th, 7th, 11th and 13th, are the most critical for the power system, there is no specific interest in modelling the system accurately for a larger frequency range.*
- *Lines are modelled as equivalent-PI based on power frequency parameters.*
 - *In order to keep down the complexity of the implementation in MATLAB, power frequency parameters are used. Later the complexity of the line modelling can be increased, to account for geometrical data. At this point in the developing of the method accurate modelling of the system components is not the main priority.*
 - * *For modelling of lines Bessel equations are most accurate, and therefore the frequency and magnitudes of the resonance points will not be accurate using power frequency parameters.*

- *The modelling of power electronics is out of the scope of the project.*
 - *As the method is being developed the system is being kept simple, and it is found that accurately modelling the power electronics connected to the system is something that can be added later if the method is found to be useful. Accurate modelling of power electronics is very complex and typically it can be difficult to acquire the needed data for precise modelling.*
 - * *Converters and other power electronic related devices connected to the power system affect both the emission to the system and the impedance of the system. Therefore for highly detailed harmonic studies power electronics should be modelled [1]. Using highly detailed models during the development of the method would mostly increase the complexity and it would bring no benefit in the early stage of development.*
- *Skin effect is not modelled.*
 - *In order to keep the test systems simple it is decided to not model skin effect. For harmonic studies on real systems skin effect should definitely be modelled, however as the focus is on developing and investigating the usefulness of the method accurate modelling of the system components is not the main priority.*
 - * *Excluding the modelling of skin effect will neglect a large portion of the damping in the power system. The damping is especially impactful at higher frequencies as the impact increases with frequency, and thus the resonances at higher frequencies will be more severe compared to if the skin effect was modelled. The addition of skin effect in the method would be easy to implement as only the admittance matrix is affected.*
- *Passive filters of the C-type will be the main focus when applying filters to the power systems.*
 - *Per dialogue with the Danish TSO it is decided to focus on C-type filters only, due to the C-type filter's ability to dampen several harmonic orders at once because of its dampened characteristics [3].*
 - * *The examined method's effectiveness for other filter types will potentially remain uncertain. The characteristics of ST filters, although commonly used directly at emission sources, does not lend themselves particularly well to the idea of global filter placement, as only one resonance can be mitigated by the ST filter.*
- *Unless otherwise noted the positive sequence will be the plotted impedance as the test systems are kept balanced.*

- *As the method is being developed and tested it is sufficient to use a balanced system in order to keep the system simple. Later the method can be modified to also be able to represent unbalanced systems in order to be applied to real systems, which generally are unbalanced.*
- * *The power system is often highly asymmetrical and thus unbalanced. Using only positive sequence will neglect the unbalance of the power system and consequently also the couplings between the sequences. This neglection will cause resonances from the sequence couplings to not be observed, and the resonances might therefore occur at other frequencies, or not be seen, due to the unbalance between the lines.*

Chapter 4

Analysis of Resonance Points in Small System

In this chapter a small four busbar example system comprising a radial line and a ring circuit will be analysed in order to determine the origins of the resonance points in the system. Furthermore harmonic propagation in the system is investigated.

The objective of this chapter is to get a brief understanding of how a system is affected by analysing the frequency scan of the system, before and after system changes. First the length of the lines in a system is changed in order to see how each line length affect the frequency scan. Secondly it is investigated how filters and their different impedance profiles affect the frequency scan of a system.

The single line diagram of the system to be used is given in Figure 4.1 and will be referred to as the Small System. The system consist of four busbars, an ideal voltage source and four lines each of 25 km, for which parameters are given in Appendix B.

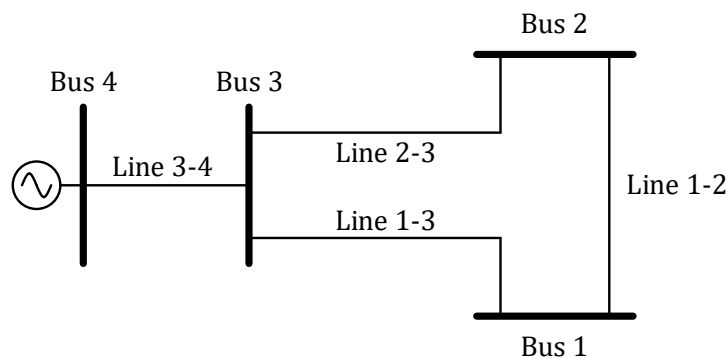


Figure 4.1: Single line diagram of the Small System.

In order to investigate the impact of the various changes the frequency scan before and after the changes is to be calculated. This is done using Equation 4.1, which was previously shown and explained in Section 2.4 before and after the system changes, in MATLAB.

$$\mathbf{V} = \mathbf{Y}^{-1}\mathbf{I} \quad (4.1)$$

The admittance matrix of the system is given in Equation 4.2 where Y_{ij} is the shunt admittance of the components between Bus i and Bus j . Z_{ij} is the series impedance of the components between Bus i and Bus j . Y_{shc} in Bus 4, position $[4,4]$ in the matrix, is

the short-circuit admittance of the voltage source which is assumed very large in order to represent an ideal voltage source. The admittances and impedances are calculated using distributed parameters and as such Y_{ij} and Z_{ij} are calculated by Equations 2.10 - 2.13.

$$\mathbf{Y} = \begin{bmatrix} Y_{12} + Y_{13} + \frac{1}{Z_{12}} + \frac{1}{Z_{13}} & -\frac{1}{Z_{12}} & -\frac{1}{Z_{13}} & 0 \\ -\frac{1}{Z_{12}} & Y_{12} + Y_{23} + \frac{1}{Z_{12}} + \frac{1}{Z_{23}} & -\frac{1}{Z_{23}} & 0 \\ -\frac{1}{Z_{13}} & -\frac{1}{Z_{23}} & Y_{23} + Y_{13} + Y_{34} + \frac{1}{Z_{23}} + \frac{1}{Z_{13}} + \frac{1}{Z_{34}} & -\frac{1}{Z_{34}} \\ 0 & 0 & -\frac{1}{Z_{34}} & Y_{34} + \frac{1}{Z_{34}} + Y_{shc} \end{bmatrix} \quad (4.2)$$

4.1 Impact of Different Line Lengths

In order to analyse the effect of changing the length of the lines in the Small System each line's length is changed individually. This is done by doubling their lengths and the frequency scan from each busbar is investigated to analyse the effect of different line lengths. Bus 4 will not be investigated as an ideal source is connected at that busbar and all the injected current will flow through the ideal voltage source, as it act like a short-circuit. From this five scenarios are set up where each scenario represent a doubling of the length of a line. The scenarios are given in Table 4.1 and shows which line is changed for each scenario. The symmetrical structure of the Small System makes the impedance scan observed from Bus 1 and Bus 2 equal therefore the impedance scan observed from Bus 2 will not be shown or commented on as it would be a repetition of the results from Bus 1.

	Scenario 1	Scenario 2	Scenario 3	Scenario 4	Scenario 5
Affected Line	None	Line 1-2	Line 2-3	Line 1-3	Line 3-4

Table 4.1: The five scenarios, where in each scenario a line length in the system is doubled, with Scenario 1 being the reference case, which is the system where all lines are 25 km.

Frequency Scan from Bus 1

First the frequency scan is calculated for each scenario by observing Bus 1 with a current injection in Bus 1, meaning $Z_{1,1}$, as shown in Figure 4.2, where the blue line is the reference case where no line length is changed.

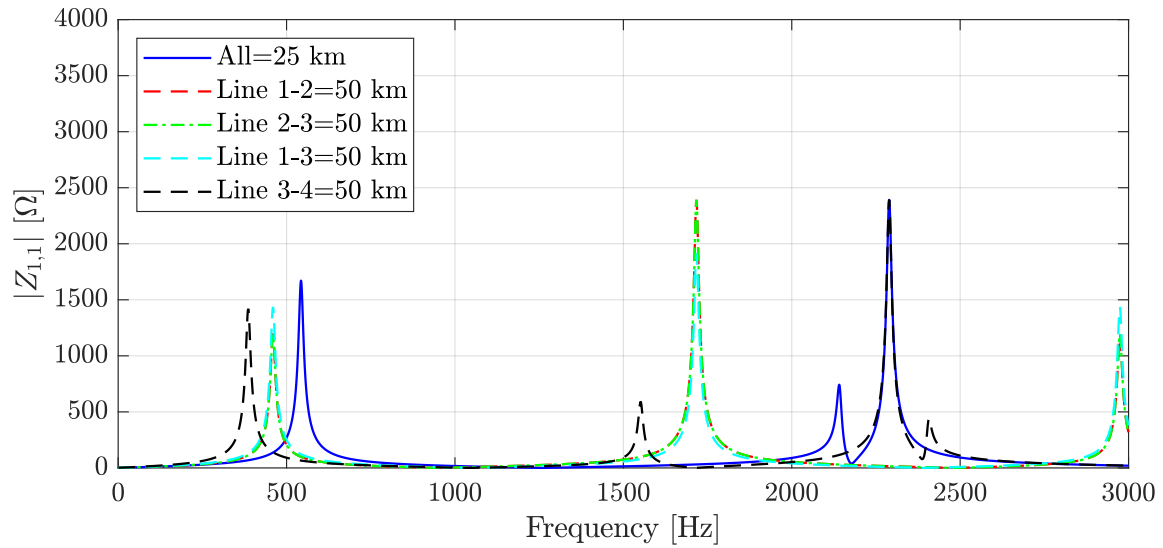


Figure 4.2: Frequency scan from the Small System, seen from Bus 1 with each of the five scenarios, with the length of each line being changed individually.

The results for the frequency scan, meaning the frequencies of the resonance peaks and their impedance values are given in Table 4.2, where the symbol (*) means that the resonance peak has the same resonance peak as another resonance peak, meaning that two resonance peaks joined together to become one. This is due to the structure of the system, where the doubling of length of specific lines causes two equally long parallel sections towards the measured busbar, which moves two resonance peaks together.

Frequency Scan observed from Bus 1

Resonance peak 1	Scenario 1	Scenario 2	Scenario 3	Scenario 4	Scenario 5
Frequency [Hz]	543	460	460	460	386
Impedance [Ω]	1671	1195	1195	1434	1420
Resonance peak 2	Scenario 1	Scenario 2	Scenario 3	Scenario 4	Scenario 5
Frequency [Hz]	2141	1717*	1717*	1717*	1551
Impedance [Ω]	742.7	2392*	2392*	1913*	591.2
Resonance peak 3	Scenario 1	Scenario 2	Scenario 3	Scenario 4	Scenario 5
Frequency [Hz]	2289	1717*	1717*	1717*	2289
Impedance [Ω]	2392	2392*	2392*	1913*	2392

Table 4.2: The frequency and impedance of each resonance peak from the frequency scan observed from Bus 1. The symbol (*) means that the given resonance peak is at the same frequency as a another resonance peak, meaning that two resonance peaks joined together to become one.

From Table 4.2 looking at Resonance peak 1 it is seen that for Scenario 2, 3 and 4 its frequency is lowered compared to Scenario 1, however Scenario 4 has a higher impedance. Scenario 5 has the lowest frequency with an impedance similar to Scenario 4, therefore Line 3-4 has the most impact on the frequency of the first resonance peak, but not as much on its impedance. Line 3-4 is the radial line in the system, connecting the ideal voltage source to the meshed part of the Small System, as seen in Figure 4.1 and it therefore makes sense to have a larger impact, than the other lines as they are in the meshed part of the system.

When looking at Resonance peak 2 in Table 4.2 similar results to what was observed for Resonance peak 1 is observed, in that Scenario 5 has the lowest frequency, and in this case also the lowest impedance. Scenario 2, 3 and 4 are a special case as the frequency and impedance for Resonance peak 2 and 3 are equal, as it was seen when the lengths of the lines were increased the two resonance peaks merged to become one resonance peak. The frequency and impedance for these scenarios share the same tendency as seen for Resonance peak 1, as their frequencies are equal, but with Scenario 4 having a lower impedance.

For Resonance peak 3 in Table 4.2 Scenario 2, 3 and 4 will not be explained as their results were explained for Resonance peak 2. However, an interesting result is observed as Scenario 1 and Scenario 5 have the same values for both frequency and impedance. The result then indicates that Resonance peak 3 is not affected by the radial line, Line 3-4, and a further investigation follows later.

Scan from Bus 3

The frequency scan seen from Bus 3, can be seen in Figure 4.3.

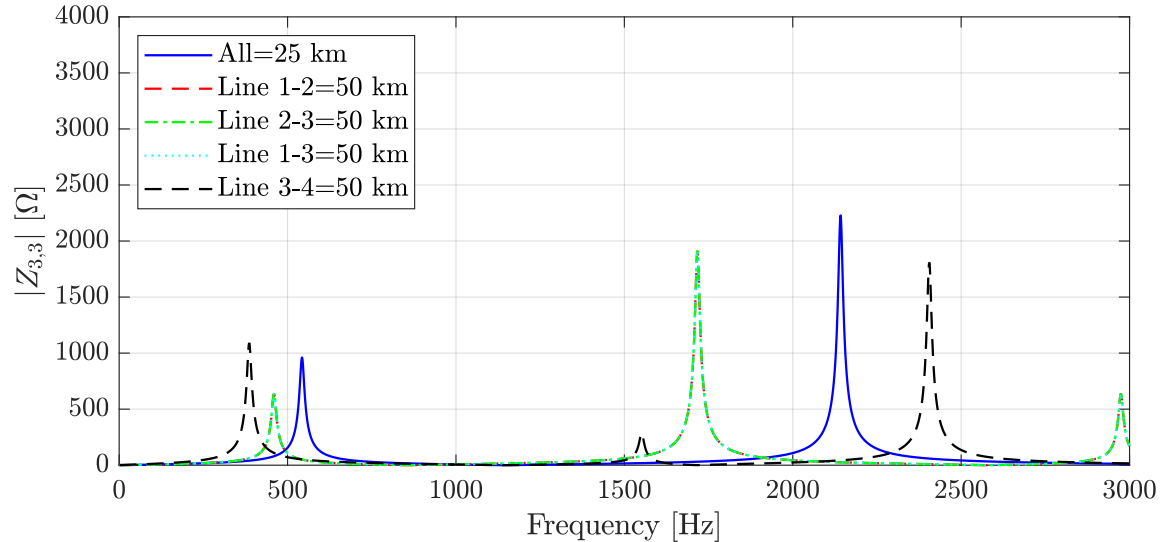


Figure 4.3: Frequency scan from the Small System with equivalent-PI, seen from Bus 3 with the length of the four lines being changed individually.

The frequency of the resonance peaks is the same as when seen from Bus 1, except the radial independent resonance peak, which is not present when seen from Bus 3. Therefore the line changes impact all the observed resonance peaks. It should be noticed that even though some of the resonance peaks are at the same frequencies, when observing from different busbars the magnitudes are not the same.

Radial Independent Resonance

In order to investigate the impact of the individual lines on the impedance, specifically the impact of Line 3-4 on the third resonance peak, the Jacobian of Equation 4.1 is investigated. By setting up Equation 4.1 for the Small System in MATLAB, with the lines implemented as equivalent-PI, the symbolic expression of the impedance, $Z_{i,j}$, is obtained. It should be noted that $Z_{i,j}$ is the same as $V_{i,j}$ in Equation 4.1 for the busbar where the current is being injected. By taking the partial differentials of $Z_{i,j}$ in respect to the individual lines a Jacobian matrix is obtained, as seen in Equation 4.3, where x is the variables which are to be investigated, in this case being the four line lengths.

$$\mathbf{J} = \left[\frac{\partial \mathbf{Z}}{\partial x_1} \cdots \frac{\partial \mathbf{Z}}{\partial x_n} \right] \quad (4.3)$$

When the symbolic partial derivatives have been obtained the symbolic variables are assigned values to get the raw sensitivities of the partial derivatives. This method is a local sensitivity method, which means that one value of $Z_{i,j}$ is being evaluated at a time, being the value of $Z_{i,j}$ at a specific frequency, as seen in Equation 4.4.

$$\mathbf{J}(Z_{i,j}) = \left. \frac{\partial Z_{i,j}}{\partial x_n} \right|_f \quad (4.4)$$

The raw sensitivities indicate how much a change in x_n , which is a specific line, causes a change in $Z_{i,j}$. A for-loop is used in MATLAB to make a frequency scan of the Jacobian and this way the raw sensitivities of $|Z_{1,1}|$ are obtained over the frequency scan for the individual lines, as seen in Figure 4.4.

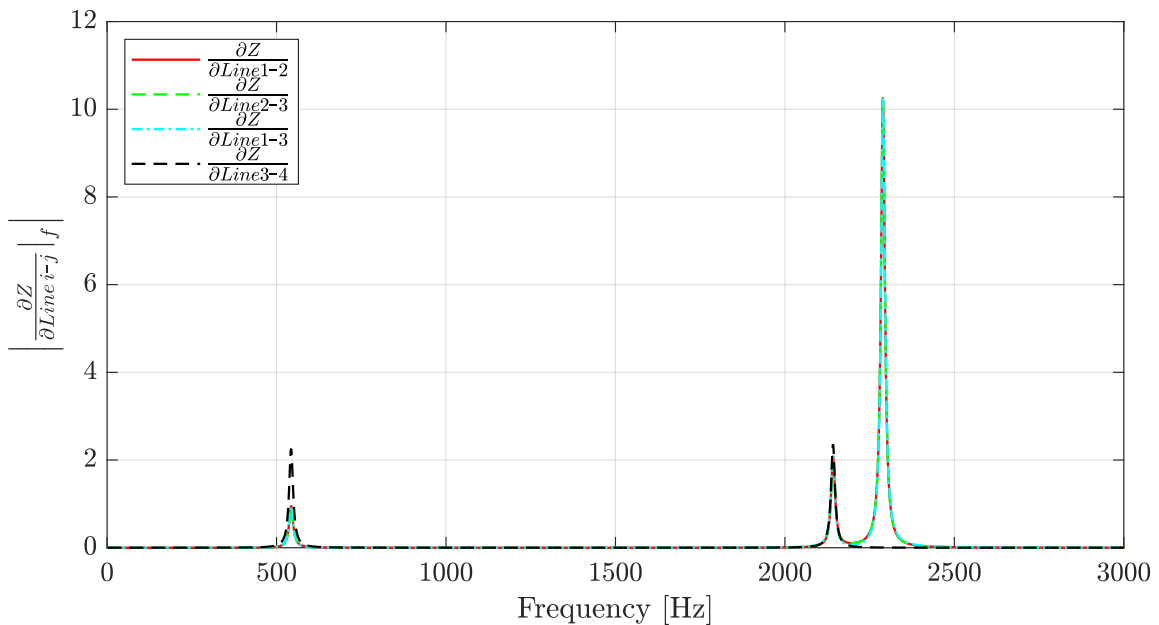


Figure 4.4: Raw sensitivity of partial derivatives of the line lengths.

From Figure 4.4 it is seen that the raw sensitivities are large at the frequencies of the resonance peaks. Noticeably Line 3-4 is seen to have zero impact at the third resonance peak, which confirms the results of Table 4.2. This means that the third resonance peak is created exclusive by interactions in the ring circuit. Appendix C gives a mathematical explanation on how to find the radial independent resonance point in the Small System with the lines modelled as nominal-PI, where the line parameters and lengths are the same for all four lines. In the appendix it is found that the resonance peak unaffected by the radial line, is located at a frequency which can be calculated through the ring circuit lines only. In addition an explanation is given for why the third resonance peak

is not seen, when Bus 3 is the observed and injected busbar. For more advanced systems these specific resonance points become harder to locate and the method of differentiating the impedance to see the impact of specific parameters becomes computationally heavier as more variables are introduced. Naturally if the frequency of the resonance peaks are known beforehand the tested frequencies can be greatly limited.

4.2 Impact of Different Filter Positions

In order to investigate the impact of implementing a filter in the Small System it is chosen to implement three flat admittance profiles, which can be identified in Table 4.3 where the fixed impedance values are shown. The flat admittance profile filter is defined as a filter which admittance is equal at all frequencies, and the filter is thus not frequency dependent. No actual filters will have this kind of profile, however this is done as a mathematical trick in order to have the same filter impact at all frequencies. By inserting flat admittance profiles the clear impact of a filter can be found across the frequency scan, without specifically tuning to a specific frequency. Later these results are compared to a C-type filter in order to see if the results fits the tendency found for the flat admittance profile filters. This section will comment on the results of implementing different types of filters but will not go into a depth on what mathematically causes the results as this is not manageable even for a simple system. The results are all observed from Bus 1, with injection at Bus 1, with the filters being implemented in Bus 1, 2 and 3 respectively. Due to the ideal voltage source essentially acting as a short-circuit no filter is placed in Bus 4, as it would not have an impact.

Filter name	Resistance [Ω]	Reactance [Ω]
Resistive	500	0
Inductive	0	500
Capacitive	0	-500

Table 4.3: Flat impedance profiles of filters.

Resistive Filter

The first filter which is implemented in the three busbars is a purely resistive filter with a flat admittance profile. Figure 4.5 shows $|Z_{1,1}|$ for the different filter positions. Noticeably a filter in Bus 3 has no effect on the third resonance peak. This result proposes that if a resonance peak is created by a certain section of the system the filter should be placed in that section, to achieve the best mitigation effect. In the frequency region between the second and third resonance peak a filter in either Bus 2 or Bus 3 is seen to amplify $Z_{1,1}$

and effectively remove the resonance valley. An interesting tendency which will become more apparent in the next figures is that the purely resistive filter not only dampens the resonance peaks but also leads to a small shift in the resonance frequencies.

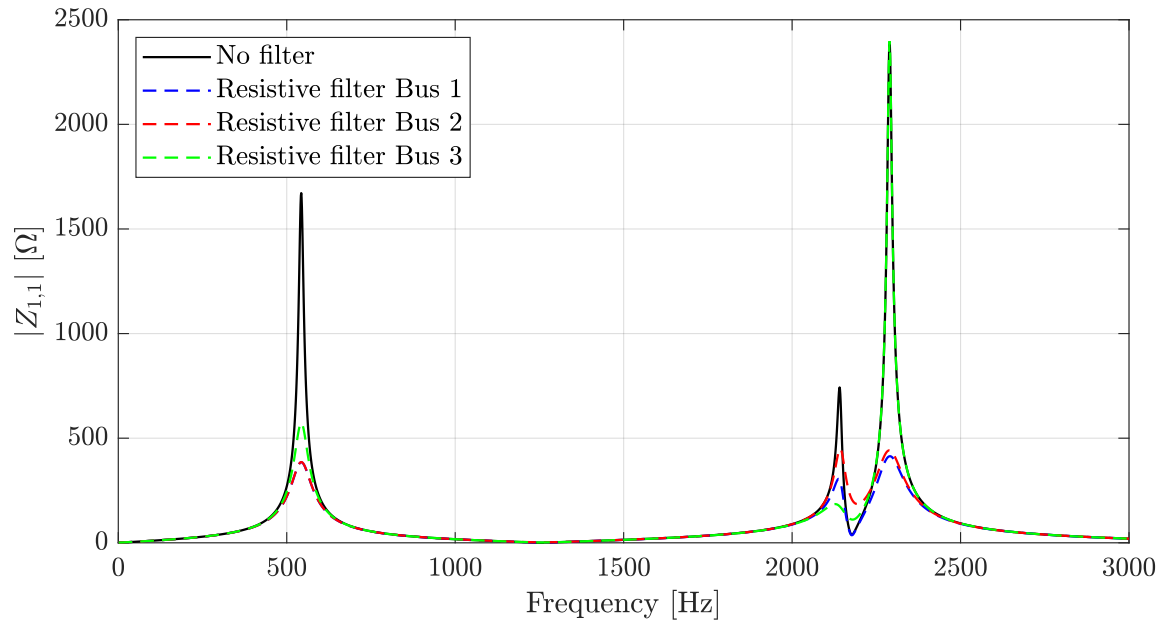


Figure 4.5: Absolute impedance scan of the Small System seen from Bus 1 before and after a purely resistive filter is connected in the different busbars.

Figure 4.6 shows the imaginary part $X_{1,1}$ for the different filter positions of the resistive filter. Noticeably it is seen that the magnitude of $X_{1,1}$ is affected by the resistive filter, thus there is a connection between the resistive parts of a filter and the imaginary value of the impedance after the filter is implemented. In the zoom in part of the figure it can be seen that the resistive filter causes the peaks to shift.

Figure 4.7 shows $R_{1,1}$ for the different filter positions of the resistive filter. The noticeable tendencies described before continues for $R_{1,1}$, while it should be noticed that the values around the resonance peaks are sharper for $R_{1,1}$ compared to $Z_{1,1}$.

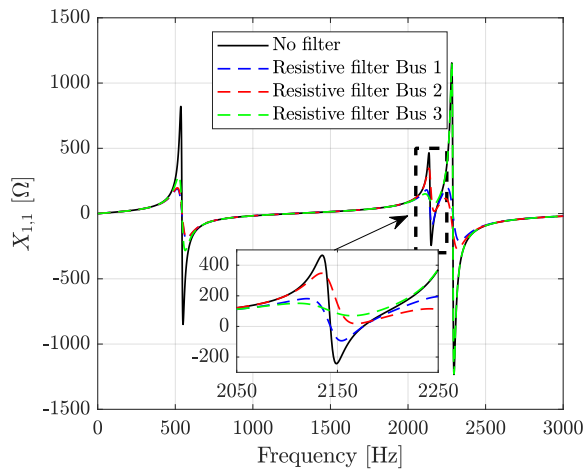


Figure 4.6: Reactance scan of the Small System seen from Bus 1 before and after a purely resistive filter is connected to Bus 1.

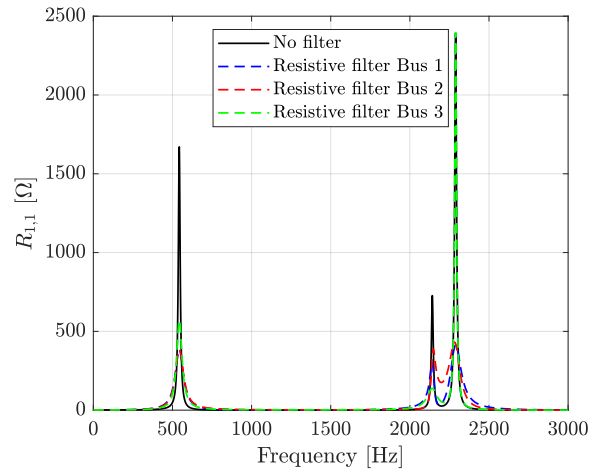


Figure 4.7: Resistance scan of the Small System seen from Bus 1 before and after a purely resistive filter is connected to Bus 1

Capacitive and Inductive Filter

Next a purely capacitive and a purely inductive filter are placed in Bus 1, 2 and 3 respectively, with one filter implemented each time. Figure 4.8 shows $Z_{1,1}$ for the different filter positions. It becomes apparent that filters with imaginary values shifts the resonance peaks. As seen in the zoom in of the figure capacitive filters lowers the resonance frequency while inductive filters increases the resonance frequency. At the first resonance peak there is a tendency in that the lower the resonance frequency is the lower is the magnitude of the resonance peak. The same tendency is not seen at the other resonance peaks, which indicates that because the resonance peaks are created by different parts of the system, no general rule can be set up for the magnitudes of the resonance peaks after a filter implementation. It should also be noticed that the filters with imaginary values does not provide significant damping of the resonance peaks as was seen for the resistive filter. No real filter has a flat admittance profile and therefore this result is not something that can be directly compared with the performance of an actual filter.

The filters with imaginary filter values does not impact the frequency region between the second and third resonance peaks the same way as the resistive filter, as it is seen that the resonance valley is mostly shifted for all the filter position cases and not significantly amplified.

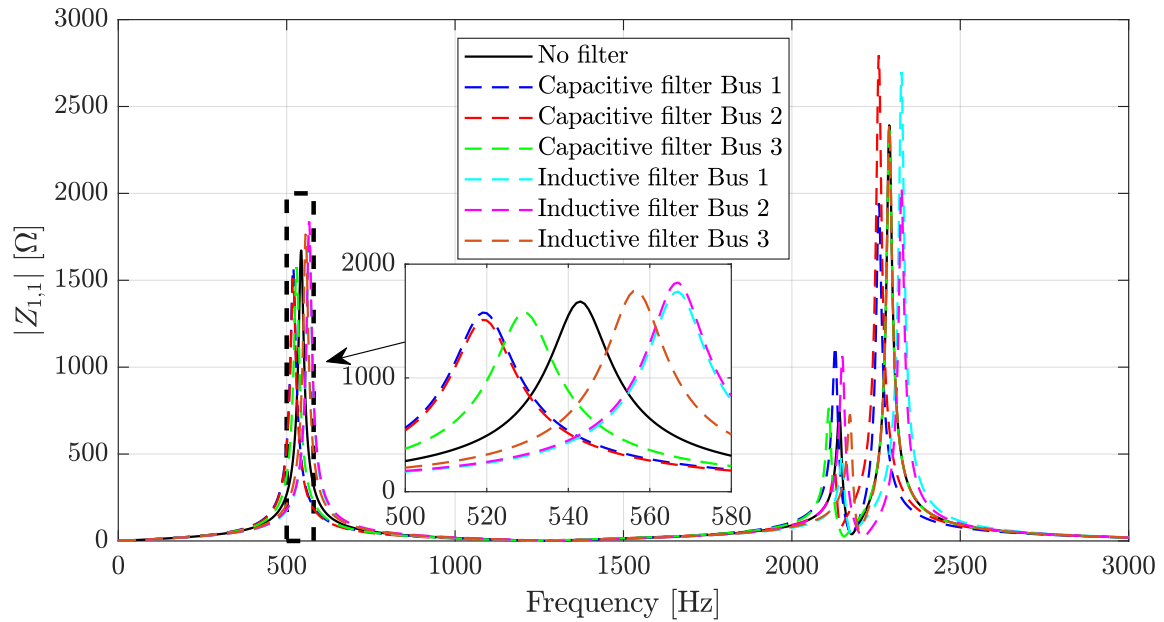


Figure 4.8: Absolute impedance scan of Small System, observed from Bus 1, before and after a purely capacitive and inductive filter are connected at different busbars.

Figure 4.9 and 4.10 show $X_{1,1}$ and $R_{1,1}$, for the different filter positions with the capacitive and inductive filters implemented, respectively. As expected the zero crossings of $X_{1,1}$ are shifted depending on the filter being capacitive or inductive. In general the resonance peaks of $R_{1,1}$ follow the zero crossings of $X_{1,1}$ as would be expected. This highlights that the system is purely resistive at the resonance peaks.

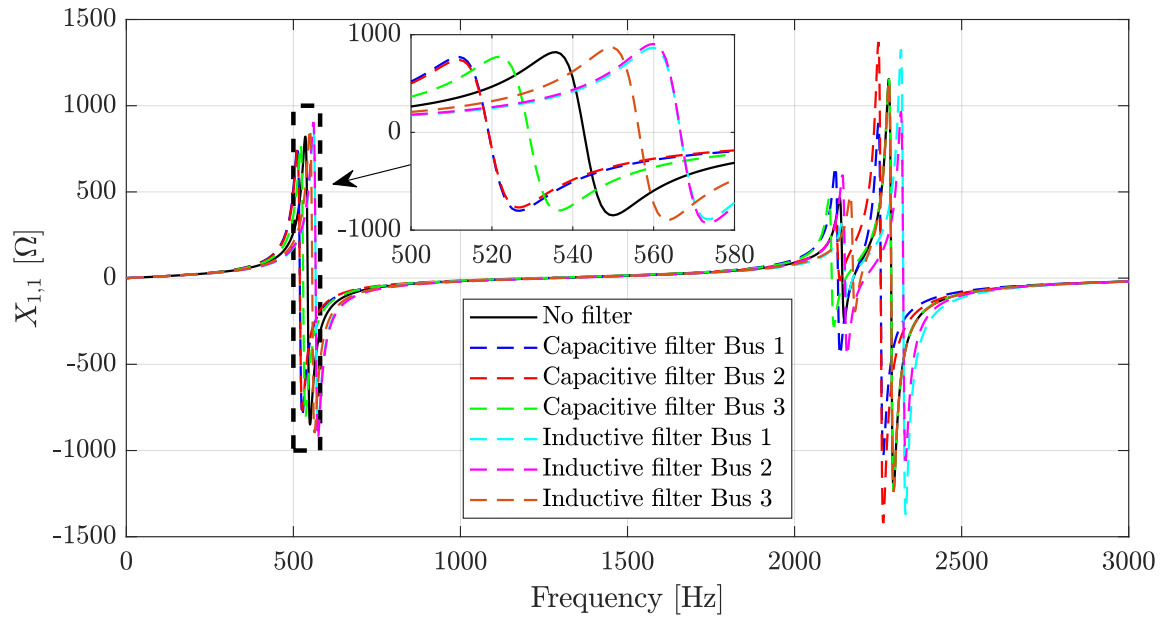


Figure 4.9: Reactance scan of the Small System seen from Bus 1 before and after a purely capacitive and inductive filter are connected at different busbars.

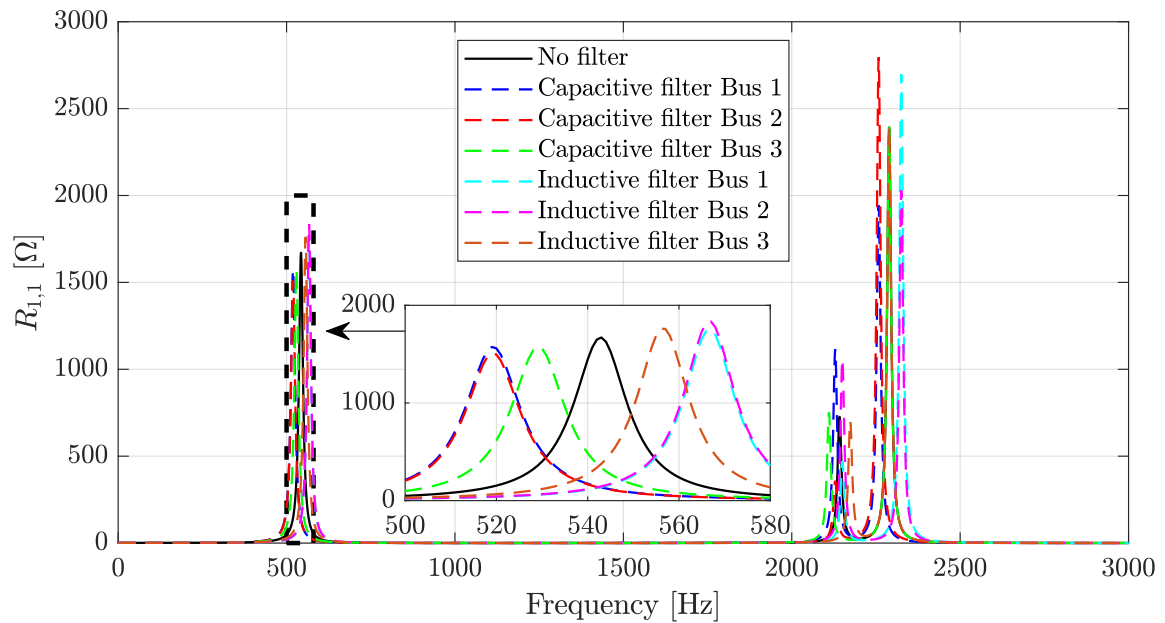


Figure 4.10: Resistance scan of the Small System seen from Bus 1 before and after a purely capacitive and inductive filter are connected at different busbars.

C-type Filter

Now that the flat admittance profile filters have been tested the results are compared with the implementation of a realistic filter. A C-type filter is chosen and implemented at the available busbars. The C-type filter is tuned to the 11th harmonic order, in order to dampen most at the first resonance peak, and is set to have $Q_1 = 100$ Mvar and $q = 2$, thus allowing for damping of the second and third resonance peak, due to the low quality factor of the filter. Figure 4.11 shows the impedance profile and the angle of the impedance of the C-type filter. In the first frequency region, before the tuning frequency, the C-type filter is predominantly capacitive, as can be seen by observing θ , which is the angle of the impedance. After the tuning frequency the filter is predominately resistive while still being slightly inductive.

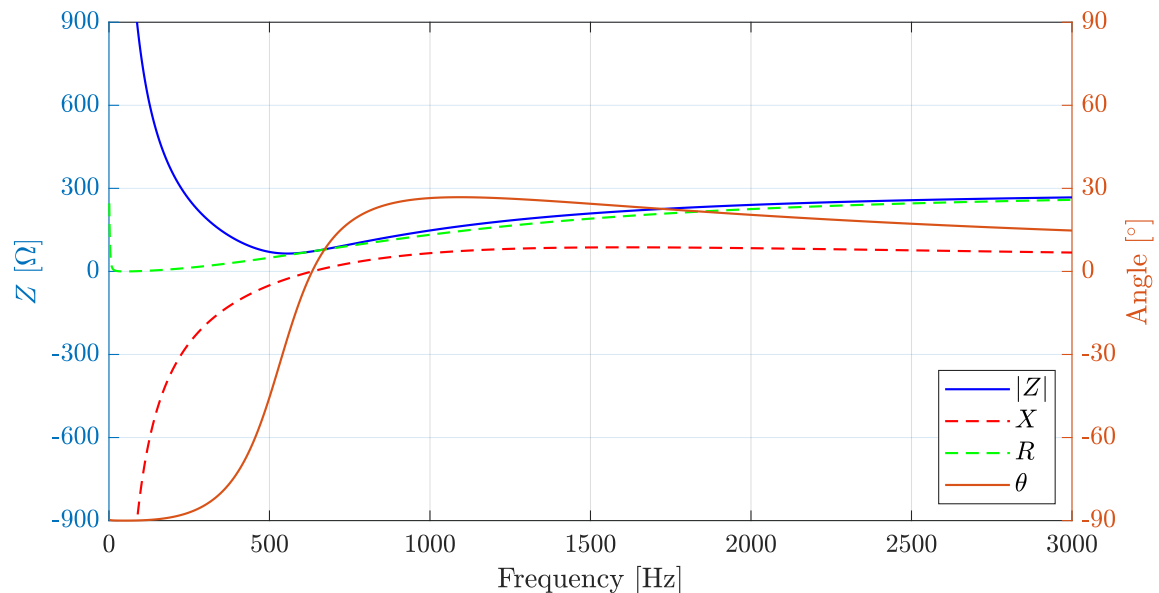


Figure 4.11: Absolute impedance, reactance and resistance scan of a C-type filter with the parameters: $h_0 = 11^{th}$, $Q_1 = 100$ & $q = 2$

Figure 4.12 shows $Z_{1,1}$ for the different filter positions. Due to the capacitive nature of the filter, before the tuning frequency, the first resonance peak has shifted to lower frequencies, although with significantly lower magnitude, which can mostly be attributed to the resistive damping of the filter. The movement of the resonance peaks can cause anti-resonances. The frequency of the second and third resonance peak is shifted slightly to a higher frequency due to the inductive nature of the filter after the tuning frequency, however not as significantly as the first resonance peak, due to the relatively low inductive nature at the second and third resonance peak compared to the capacitive nature at the

first resonance peak. The third resonance peak is still unaffected by a filter in Bus 3.

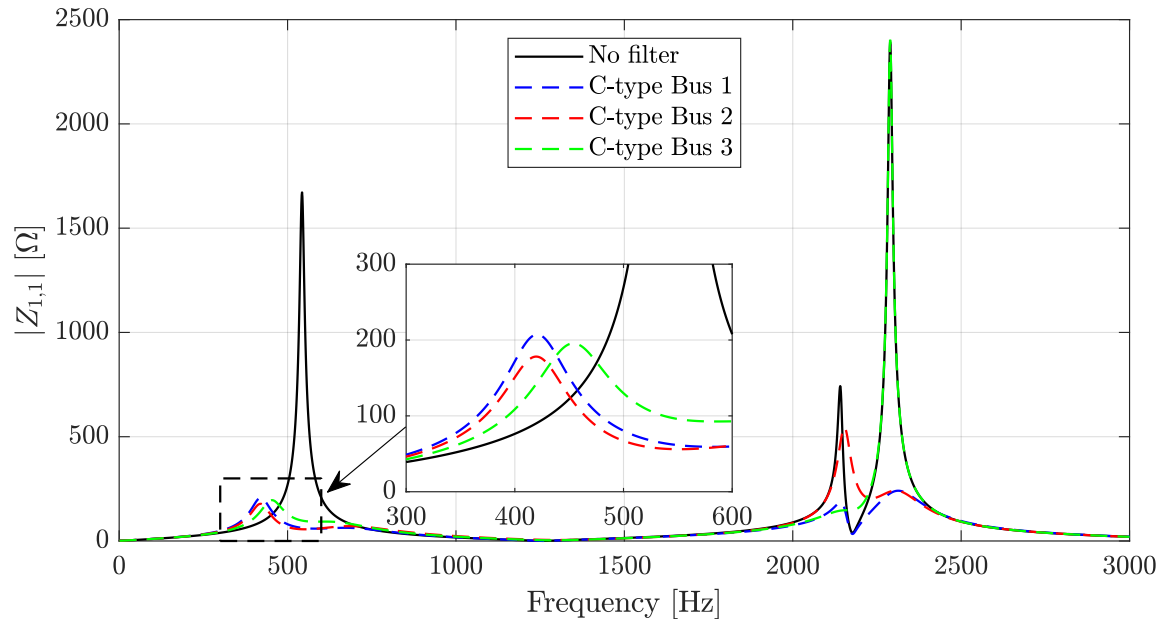


Figure 4.12: Absolute impedance scan of the Small System seen from Bus 1 before and after C-type filters are connected at different busbars.

In general it has been found that the C-type filter had the expected impact on the resonance frequencies, however it was also found that an intuitive understanding of how a certain filter in a specific filter position impacts the shift in frequency and magnitude of a resonance peaks is not readily obtained. For more complex systems this becomes increasingly difficult and the engineer has to conduct frequency scans to follow the movement of the resonance points or use other mathematical methods to find the optimum filter position and filter values.

4.3 Summary of Chapter

In this chapter a four busbar example system is presented, consisting of a radial line and a ring circuit, where the impact on resonance points, due to changes in the system, is investigated. First it was examined how changing each line length affected the resonance points. It was found that there exist a resonance peak which is independent of the radial line. This resonance condition is verified through examining the Jacobian matrix of the system.

It is also examined how different filters in different positions affect the impedance

envelope seen from a selected busbar. The following list describes the main observations:

- Generally the changing of line lengths affect both the magnitude and frequency of resonance points.
 - Specific sections of the system affects certain resonance points more than other sections.
- The resistive part of a filter mostly dampens the resonance peaks.
- The capacitive and inductive parts of a filter mostly causes shifts in the resonance peaks' frequency.
 - Resonance peaks with frequencies in the capacitive region of a filter shifts to lower frequencies.
 - Resonance peaks with frequencies in the inductive region of a filter shifts to higher frequencies.
- A C-type filter is capacitive in the frequency region before the tuned frequency. After the tuned frequency the C-type filter is inductive but starts to become more dominated by the resistive part of the filter as the frequency increases, especially if the C-type filter has a low quality factor.

Chapter 5

Methods for Assessing Optimum Filter Location

This chapter presents different methods for finding the points in a power system where the implementation of a filter will have the most effect in reducing harmonics. A brute force method is described but not investigated in depth. The new method which is presented is the First Order Coefficient Homotopy Method, which is developed and described in depth.

In harmonic propagation studies it is first identified if there is busbars, which have harmonic distortion that exceeds the limits set by the TSO. If these limits are exceeded a passive filter is typically implemented, which is tuned to the frequency which had harmonic distortion exceeding the limit. This is done on a case-by-case basis and as such problems in other busbars might occur, due to the filter changing the impedance envelopes of the system, and a second filter may have to be implemented to mitigate the problems caused by the first filter. This can also occur if a new OHL or cable is installed in the system such that the system impedance is changed. This procedure of potentially having to keep adding filters to the system, essentially moving the problem around the system without fixing it, is costly and should be avoided.

The goal of this chapter is to examine methods which can help identify the optimal locations of filters in the power system by giving indications of which resonances, seen from a given busbar, are most affected by each possible filter position. The methods presented will give indications on how a filter in each busbar affect the impedance scan for all the busbars in the system.

In order to assess the usefulness of the presented methods, the methods are assessed against three objectives as listed below.

1. Ability to identify which resonance peaks are affected by implementation of filters in different busbars.
2. Ability to identify which filter position in a system will have the most impact on resonance points, at a given busbar, in term of magnitude reduction.
3. Ability to identify which direction in terms of frequency each resonance point will move after the filter implementation.

The first objective assesses if the method is able to indicate whether resonance peaks are being affected by the implementation of a filter in the different busbars. As seen in

Chapter 4 there was a resonance peak which was unaffected by a specific filter position, and the minimum criterion is that the method should be able to indicate this. If a given resonance point is of concern the filter will have to be placed in a location which will impact the resonance point. Thus if the given method fulfils objective one it is possible to identify the filter positions in the system which impact a given resonance peak.

The second objective assesses the method's ability to give information on how much each resonance point is affected by different filter locations, and then the filter location which have the most impact can be chosen. A method for utilising this information is to put weight on specific frequency ranges, such as the characteristic 5th, 7th, 11th and 13th harmonic orders, which is where harmonic issues are more common compared to frequency ranges around the 8th to 10th harmonic orders. This way a filter location which has more impact on a characteristic harmonic is seen as more beneficial, than a filter with more impact on the 8th to 10th order harmonics.

The third objective will give information on how much each individual resonance point change in frequency and in which direction, as a resonance point close to a harmonic order which is common to have harmonic injections can go from being non-problematic to problematic, if it is moved closer to a characteristic harmonic order. If this objective is fulfilled it enables the ability to track anti-resonances.

Normally the method of implementing a passive filter in power systems have been to put in a passive filter at the specific location where there is a problem due to harmonics distortion. These methods will then show the impact of the filter in that busbar and surrounding busbars by that filter.

The following section describes a brute force method which have been identified as being able to fulfil some of the set up objectives, but is chosen to not be investigated further due to the described drawbacks.

5.1 Brute Force Method

The Brute Force Method is a method which calculates all possible solutions and assesses the solutions to a given criteria. In this filter optimisation case it would mean to set up the admittance matrix of the system and iteratively place filters in all the possible locations and through preset criteria find the optimal filter placement. However this method has significant drawbacks, the first one being the ever increasing scale and simulation time as the system size is increased and the problem with determining the filter values to be used beforehand, as otherwise the scale of the problem increases drastically. If the filter and filter values that are to be implemented are known, this method is more useful and could be used to check if the filter location suggested by another method is the optimal

solution. Another problem with this method, which is the main reason for it not being investigated further, is that it gives no inherent knowledge of why the found solution is the optimal solution, as the Brute Force Method only provides the best solution. This method does not need to take into account where the resonance peaks are before the filter is placed, as another method shown later have to, however this also means that the movement of resonance points are not tracked and as such no understanding of how the system was impacted is obtained. If a better understanding of the system's behaviour is wanted one would have to track back through all the possible solutions and manually access why one solution is better than the other.

5.2 Homotopy Method

The method which will be presented in depth is based on the homotopy analysis method, which is a semi-analytic method [23].

Following is a mathematical explanation behind the method, being applied to the frequency scan method, and demonstrated on the Small System from Chapter 4. The single line diagram of the Small System is shown in Figure 5.1.

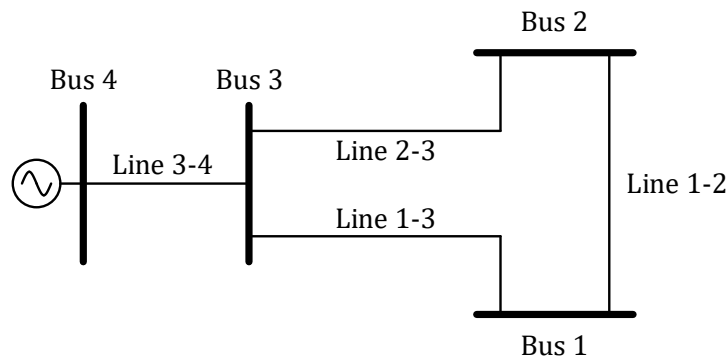


Figure 5.1: Single line diagram of the Small System.

The admittance matrix of the Small System which contains the self-admittances on the diagonal and mutual-admittances on the off-diagonal, of the system elements, is given in Equation 5.1. Y_{shc} in Bus 4, position [4,4] in the matrix, is the short-circuit admittance of

the generator which is assumed very large in order to represent an ideal voltage source.

$$\begin{bmatrix} Y_{12} + Y_{13} + \frac{1}{Z_{12}} + \frac{1}{Z_{13}} & -\frac{1}{Z_{12}} & -\frac{1}{Z_{13}} & 0 \\ -\frac{1}{Z_{12}} & Y_{12} + Y_{23} + \frac{1}{Z_{12}} + \frac{1}{Z_{23}} & -\frac{1}{Z_{23}} & 0 \\ -\frac{1}{Z_{13}} & -\frac{1}{Z_{23}} & Y_{23} + Y_{13} + Y_{34} + \frac{1}{Z_{23}} + \frac{1}{Z_{13}} + \frac{1}{Z_{34}} & -\frac{1}{Z_{34}} \\ 0 & 0 & -\frac{1}{Z_{34}} & Y_{34} + \frac{1}{Z_{34}} + Y_{shc} \end{bmatrix} \quad (5.1)$$

For visual purposes the admittances in Equation 5.1 are represented by Y , where Y_{ii} is the self-admittance and Y_{ij} is the mutual-admittance, for example $Y_{11} = Y_{12} + Y_{13} + \frac{1}{Z_{12}} + \frac{1}{Z_{13}}$. The admittance matrix depends on the frequency and it will therefore be calculated at each frequency step, where the steps depend on the resolution that is used for the frequency. The reduced matrix is denoted \mathbf{Y} and can be seen in Equation 5.2. It should be noted that a bold symbol represents a matrix.

$$\mathbf{Y} = \begin{bmatrix} Y_{11} & Y_{12} & Y_{13} & 0 \\ Y_{12} & Y_{22} & Y_{23} & 0 \\ Y_{13} & Y_{23} & Y_{33} & Y_{34} \\ 0 & 0 & Y_{34} & Y_{44} \end{bmatrix} \quad (5.2)$$

The admittance matrix \mathbf{Y} is now used in the equation for the frequency scan, which was shown in Equation 2.19 and given here again in Equation 5.3.

$$\mathbf{I} = \mathbf{YV} \quad (5.3)$$

Where \mathbf{I} is the current injection matrix given by Equation 5.4, where the entries on the diagonal represent current injections in each busbar, which means an entry of 1 in $[1, 1]$ corresponds to an injection of 1 A at Bus 1. \mathbf{V} is the harmonic voltage matrix given in Equation 5.5.

$$\mathbf{I} = \begin{bmatrix} 1 & 0 & 0 & 0 \\ 0 & 1 & 0 & 0 \\ 0 & 0 & 1 & 0 \\ 0 & 0 & 0 & 1 \end{bmatrix} \quad (5.4)$$

$$\mathbf{V} = \begin{bmatrix} V_{1,1} & V_{1,2} & V_{1,3} & V_{1,4} \\ V_{2,1} & V_{2,2} & V_{2,3} & V_{2,4} \\ V_{3,1} & V_{3,2} & V_{3,3} & V_{3,4} \\ V_{4,1} & V_{4,2} & V_{4,3} & V_{4,4} \end{bmatrix} \quad (5.5)$$

Inserting the matrices for \mathbf{I} , \mathbf{Y} and \mathbf{V} into Equation 5.3, Equation 5.6 is obtained.

$$\begin{bmatrix} Y_{11} & Y_{12} & Y_{13} & 0 \\ Y_{12} & Y_{22} & Y_{23} & 0 \\ Y_{13} & Y_{23} & Y_{33} & Y_{34} \\ 0 & 0 & Y_{34} & Y_{44} \end{bmatrix} \begin{bmatrix} V_{1,1} & V_{1,2} & V_{1,3} & V_{1,4} \\ V_{2,1} & V_{2,2} & V_{2,3} & V_{2,4} \\ V_{3,1} & V_{3,2} & V_{3,3} & V_{3,4} \\ V_{4,1} & V_{4,2} & V_{4,3} & V_{4,4} \end{bmatrix} = \begin{bmatrix} 1 & 0 & 0 & 0 \\ 0 & 1 & 0 & 0 \\ 0 & 0 & 1 & 0 \\ 0 & 0 & 0 & 1 \end{bmatrix} \quad (5.6)$$

A filter y_{fil} , represented by its admittance values, is implemented in Bus 2 by adding it to the admittance matrix, which makes the voltages depend on the filter, and thus the voltages can be defined as $V_{i,j}(y_{fil})$. The filter position in Bus 2 is one out of four possible filter position scenarios for the Small System, and is chosen for this example. A non-zero auxiliary parameter a , multiplied to the filter y_{fil} , is introduced as a convergence-control parameter, which was proposed in [23] as a simple way to adjust and control the convergence regions of the Homotopy Method. From the addition of the convergence-control parameter a and the filter y_{fil} Equation 5.7 is obtained. From Equation 5.7 it can be seen that when $a = 0$ the filter has no impact and refers back to Equation 5.6 and when $a = 1$ the filter is fully implemented in the Small System. The method of obtaining the value of a will be shown later in this section.

$$\begin{bmatrix} Y_{11} & Y_{12} & Y_{13} & 0 \\ Y_{12} & Y_{22} + a \cdot y_{fil} & Y_{23} & 0 \\ Y_{13} & Y_{23} & Y_{33} & Y_{34} \\ 0 & 0 & Y_{34} & Y_{44} \end{bmatrix} \begin{bmatrix} V_{1,1}(y_{fil}) & V_{1,2}(y_{fil}) & V_{1,3}(y_{fil}) & V_{1,4}(y_{fil}) \\ V_{2,1}(y_{fil}) & V_{2,2}(y_{fil}) & V_{2,3}(y_{fil}) & V_{2,4}(y_{fil}) \\ V_{3,1}(y_{fil}) & V_{3,2}(y_{fil}) & V_{3,3}(y_{fil}) & V_{3,4}(y_{fil}) \\ V_{4,1}(y_{fil}) & V_{4,2}(y_{fil}) & V_{4,3}(y_{fil}) & V_{4,4}(y_{fil}) \end{bmatrix} = \begin{bmatrix} 1 & 0 & 0 & 0 \\ 0 & 1 & 0 & 0 \\ 0 & 0 & 1 & 0 \\ 0 & 0 & 0 & 1 \end{bmatrix} \quad (5.7)$$

The homotopy analysis method is used to approximate series solutions to solve non-linear equations [23], and thus to get a series solution the voltages $V_{i,j}(y_{fil})$ are set as a power series, as seen in Equation 5.8. Semi-analytical methods such as the homotopy analysis method are based on finding the unknown coefficients in the power series from initial conditions [24].

$$V_{i,j}(y_{fil}) = V_{i,j}[0] + V_{i,j}[1]a \cdot y_{fil} + V_{i,j}[2](a \cdot y_{fil})^2 + \cdots + V_{i,j}[m](a \cdot y_{fil})^m \quad (5.8)$$

The power series in Equation 5.8 is now substituted into Equation 5.7, which results in Equation 5.9. For visual simplicity the equation is only shown with a current injection in Bus 1, which represents one current injection scenario. The other current injection scenarios should however still be specified when setting up the method.

$$\begin{bmatrix} Y_{11} & Y_{12} & Y_{13} & 0 \\ Y_{12} & Y_{22} + a \cdot y_{fil} & Y_{23} & 0 \\ Y_{13} & Y_{23} & Y_{33} & Y_{34} \\ 0 & 0 & Y_{34} & Y_{44} \end{bmatrix} \begin{bmatrix} V_{1,1}[0] + V_{1,1}[1]a \cdot y_{fil} + \cdots + V_{1,1}[m](a \cdot y_{fil})^m \\ V_{2,1}[0] + V_{2,1}[1]a \cdot y_{fil} + \cdots + V_{2,1}[m](a \cdot y_{fil})^m \\ V_{3,1}[0] + V_{3,1}[1]a \cdot y_{fil} + \cdots + V_{3,1}[m](a \cdot y_{fil})^m \\ V_{4,1}[0] + V_{4,1}[1]a \cdot y_{fil} + \cdots + V_{4,1}[m](a \cdot y_{fil})^m \end{bmatrix} = \begin{bmatrix} 1 \\ 0 \\ 0 \\ 0 \end{bmatrix} \quad (5.9)$$

5.2.1 Calculation of Power Series Coefficients

The next step in the method is to calculate the coefficients of the power series, which are given as $V_{i,j}[m]$ where m denotes the order. $V_{i,j}[0]$ is given by the admittance matrix without the filter component, and thus represents the voltage before the filter is implemented, while the rest of the orders of $V_{i,j}[m]$ in the power series are multiplied by the filter component and the convergence control parameter to the power of the order, being $(a \cdot y_{fil})^m$. Starting with the calculation of $V_{i,j}[1]$ a decision has to be made on how many orders of the power series is needed in order to calculate $V_{i,j}[1]$. This decision and subsequent example is only shown as a mathematical proof of the calculation of $V_{i,j}[1]$, as it will later be seen that the calculation of any $V_{i,j}[m]$ can be greatly simplified compared to the following example. As an example it is chosen to calculate $V_{i,j}[1]$ using the power series up to the 4th order. In this example the assumption is made that terms higher than the 4th order does not have an impact on the calculation of $V_{i,j}[1]$. The admittance matrix of Equation 5.9, which contains the original admittance matrix and the added filter, with the convergence parameter a , is split into two matrices. The first matrix is the original admittance matrix which is denoted \mathbf{Y} and shown in Equation 5.10. The second matrix is the filter position matrix which is denoted \mathbf{A} and shown in Equation 5.11.

$$\mathbf{Y} = \begin{bmatrix} Y_{11} & Y_{12} & Y_{13} & 0 \\ Y_{12} & Y_{22} & Y_{23} & 0 \\ Y_{13} & Y_{23} & Y_{33} & Y_{34} \\ 0 & 0 & Y_{34} & Y_{44} \end{bmatrix} \quad (5.10)$$

$$\mathbf{A} = \begin{bmatrix} 0 & 0 & 0 & 0 \\ 0 & a \cdot y_{fil} & 0 & 0 \\ 0 & 0 & 0 & 0 \\ 0 & 0 & 0 & 0 \end{bmatrix} \quad (5.11)$$

For the case shown the filter is placed in Bus 2. If the filter were to be placed in Bus 1 the term $a \cdot y_{fil}$ would be in position $\mathbf{A}_{1,1}$ instead of $\mathbf{A}_{2,2}$ in this case.

The extension of the admittance matrix forms Equation 5.12. The power series terms are denoted $\mathbf{V}'[m]$ as shown in Equation 5.13. The prime (') indicates that the value of $V_{i,j}[m]$ has been multiplied with the constant a^m such that $V'_{i,j}[m] = V_{i,j}[m] \cdot a^m$. It should be noticed that $\mathbf{V}[0]$ in Equation 5.12 is not scaled to a^m , due to it being the original voltages before the filter implementation, and $\mathbf{V}[0]$ is therefore written without the prime. Finally the current injection matrix can be denoted as \mathbf{I} , as seen in Equation

5.14.

$$\left[\mathbf{Y} + \mathbf{A} \right] \begin{bmatrix} V_{1,1}[0] + V_{1,1}[1]a \cdot y_{fil} + \dots + V_{1,1}[m](a \cdot y_{fil})^m \\ V_{2,1}[0] + V_{2,1}[1]a \cdot y_{fil} + \dots + V_{2,1}[m](a \cdot y_{fil})^m \\ V_{3,1}[0] + V_{3,1}[1]a \cdot y_{fil} + \dots + V_{3,1}[m](a \cdot y_{fil})^m \\ V_{4,1}[0] + V_{4,1}[1]a \cdot y_{fil} + \dots + V_{4,1}[m](a \cdot y_{fil})^m \end{bmatrix} = \begin{bmatrix} 1 \\ 0 \\ 0 \\ 0 \end{bmatrix} \quad (5.12)$$

$$\mathbf{V}'[m] = \begin{bmatrix} V'_{11}[m] \cdot y_{fil}^m & V'_{12}[m] \cdot y_{fil}^m & V'_{13}[m] \cdot y_{fil}^m & V'_{14}[m] \cdot y_{fil}^m \\ V'_{12}[m] \cdot y_{fil}^m & V'_{22}[m] \cdot y_{fil}^m & V'_{23}[m] \cdot y_{fil}^m & V'_{24}[m] \cdot y_{fil}^m \\ V'_{13}[m] \cdot y_{fil}^m & V'_{23}[m] \cdot y_{fil}^m & V'_{33}[m] \cdot y_{fil}^m & V'_{34}[m] \cdot y_{fil}^m \\ V'_{14}[m] \cdot y_{fil}^m & V'_{24}[m] \cdot y_{fil}^m & V'_{34}[m] \cdot y_{fil}^m & V'_{44}[m] \cdot y_{fil}^m \end{bmatrix} \quad (5.13)$$

$$\mathbf{I} = \begin{bmatrix} 1 & 0 & 0 & 0 \\ 0 & 1 & 0 & 0 \\ 0 & 0 & 1 & 0 \\ 0 & 0 & 0 & 1 \end{bmatrix} \quad (5.14)$$

Having denoted all the matrices Equation 5.15 can be formed, which shows all the parts up to the 4th order of the power series in a simplified matrix form.

$$\left[\mathbf{Y} + \mathbf{A} \right] \left[\mathbf{V}[0] + \mathbf{V}'[1] + \mathbf{V}'[2] + \mathbf{V}'[3] + \mathbf{V}'[4] \right] = \mathbf{I} \quad (5.15)$$

Multiplying the admittance parts, \mathbf{Y} and \mathbf{A} , together with the voltage parts forms Equation 5.16.

$$\begin{aligned} \mathbf{AV}[0] + \mathbf{YV}[0] + \mathbf{AV}'[1] + \mathbf{YV}'[1] + \mathbf{AV}'[2] + \mathbf{YV}'[2] \\ + \mathbf{AV}'[3] + \mathbf{YV}'[3] + \mathbf{AV}'[4] + \mathbf{YV}'[4] = \mathbf{I} \end{aligned} \quad (5.16)$$

The part containing $\mathbf{YV}[0]$ equals the identity matrix, as $\mathbf{V}[0] = \mathbf{Y}^{-1}$. In this case the identity matrix and the current injection matrix \mathbf{I} are the same. \mathbf{I} can therefore be subtracted from both sides of Equation 5.16 forming Equation 5.17. The zero matrix $\mathbf{0}$, which remains on the right side of the equal sign in the equation, is shown in Equation 5.18.

$$\mathbf{AV}[0] + \mathbf{AV}'[1] + \mathbf{YV}'[1] + \mathbf{AV}'[2] + \mathbf{YV}'[2] + \mathbf{AV}'[3] + \mathbf{YV}'[3] + \mathbf{AV}'[4] + \mathbf{YV}'[4] = \mathbf{0} \quad (5.17)$$

$$\mathbf{0} = \begin{bmatrix} 0 & 0 & 0 & 0 \\ 0 & 0 & 0 & 0 \\ 0 & 0 & 0 & 0 \\ 0 & 0 & 0 & 0 \end{bmatrix} \quad (5.18)$$

In order to start the isolation of $\mathbf{V}'[1]$ the part of Equation 5.17 containing $\mathbf{YV}'[1]$ is chosen to be kept on the left side of the equal sign, while everything else is subtracted from both sides, thus moving to the right side of the equal sign, which forms Equation 5.19.

$$\mathbf{YV}'[1] = -\mathbf{AV}[0] - \mathbf{AV}'[1] - \mathbf{AV}'[2] - \mathbf{YV}'[2] - \mathbf{AV}'[3] - \mathbf{YV}'[3] - \mathbf{AV}'[4] - \mathbf{YV}'[4] \quad (5.19)$$

In order to make the final isolation of $\mathbf{V}'[1]$ the inverse of \mathbf{Y} is multiplied on both sides of the equation, which forms Equation 5.20.

$$\mathbf{V}'[1] = -\mathbf{Y}^{-1}\mathbf{AV}[0] - \mathbf{Y}^{-1}\mathbf{AV}'[1] - \mathbf{Y}^{-1}\mathbf{AV}'[2] - \mathbf{Y}^{-1}\mathbf{YV}'[2] - \mathbf{Y}^{-1}\mathbf{AV}'[3] - \mathbf{Y}^{-1}\mathbf{YV}'[3] - \mathbf{Y}^{-1}\mathbf{AV}'[4] - \mathbf{Y}^{-1}\mathbf{YV}'[4] \quad (5.20)$$

Several parts of Equation 5.20 has $\mathbf{Y}^{-1}\mathbf{Y}$ which equals the identity matrix. Multiplying a matrix with the identity matrix recovers the original matrix as $-\mathbf{Y}^{-1}\mathbf{YV}'[m] = -\mathbf{V}'[m]$.

Using the property that $\mathbf{V}'[m] = -\mathbf{Y}^{-1}\mathbf{AV}'[m-1]$, Equation 5.20 can be simplified, as seen in Equation 5.21. At this point in the proof example the property is an educated guess, however later it is shown to be valid.

$$\mathbf{V}'[1] = \mathbf{V}'[1] + \mathbf{V}'[2] - \mathbf{V}'[2] + \mathbf{V}'[3] - \mathbf{V}'[3] + \mathbf{V}'[4] - \mathbf{V}'[4] + \mathbf{V}'[5] \quad (5.21)$$

Observing Equation 5.21 it can be seen that several parts cancel each other out, which leaves the remaining terms as seen in Equation 5.22, where $\mathbf{V}'[1]$ from the right side of the equal sign in Equation 5.21 is written out.

$$\mathbf{V}'[1] = -\mathbf{Y}^{-1}\mathbf{AV}[0] + \mathbf{V}'[5] \quad (5.22)$$

At the start of this example, which shows the isolation process of $\mathbf{V}'[1]$, up to the 4th order of the voltage power series was used. The result of Equation 5.22 shows that by using the property $\mathbf{V}'[m] = -\mathbf{Y}^{-1}\mathbf{AV}'[m-1]$ a 5th order remainder term is left, besides the expected 1st order term. However it can be generalised that if m terms of the power series is used to calculate $\mathbf{V}'[1]$ the last term will be of $(m+1)^{th}$ order. Under the condition $\mathbf{V}'[m] < \mathbf{V}'[m-1]$ the remainder term is small and as m goes towards infinity the remainder term goes towards zero and can thus be assumed neglectable. This condition is examined later. Any $\mathbf{V}'[m]$ can be calculated by Equation 5.23 and therefore the calculation of the voltage power series coefficients becomes a recursive process as each order of $\mathbf{V}'[m]$ is calculated using the previous order $\mathbf{V}'[m-1]$.

$$\mathbf{V}'[m] = -\mathbf{Y}^{-1}\mathbf{AV}'[m-1] \quad (5.23)$$

The extended version of Equation 5.23 for $\mathbf{V}'[1]$, with current injection in Bus 1, is shown in Equation 5.24.

$$\begin{bmatrix} V'_{1,1}[1] \cdot y_{fil} \\ V'_{2,1}[1] \cdot y_{fil} \\ V'_{3,1}[1] \cdot y_{fil} \\ V'_{4,1}[1] \cdot y_{fil} \end{bmatrix} = - \begin{bmatrix} Y_{11} & Y_{12} & Y_{13} & 0 \\ Y_{12} & Y_{22} & Y_{23} & 0 \\ Y_{13} & Y_{23} & Y_{33} & Y_{34} \\ 0 & 0 & Y_{34} & Y_{44} \end{bmatrix}^{-1} \begin{bmatrix} 0 & 0 & 0 & 0 \\ 0 & a \cdot y_{fil} & 0 & 0 \\ 0 & 0 & 0 & 0 \\ 0 & 0 & 0 & 0 \end{bmatrix} \begin{bmatrix} V_{1,1}[0] \\ V_{2,1}[0] \\ V_{3,1}[0] \\ V_{4,1}[0] \end{bmatrix} \quad (5.24)$$

The y_{fil} terms can be moved out of their respective matrices, as seen in Equation 5.25.

$$\begin{bmatrix} V'_{1,1}[1] \\ V'_{2,1}[1] \\ V'_{3,1}[1] \\ V'_{4,1}[1] \end{bmatrix} y_{fil} = - \begin{bmatrix} Y_{11} & Y_{12} & Y_{13} & 0 \\ Y_{12} & Y_{22} & Y_{23} & 0 \\ Y_{13} & Y_{23} & Y_{33} & Y_{34} \\ 0 & 0 & Y_{34} & Y_{44} \end{bmatrix}^{-1} \begin{bmatrix} 0 & 0 & 0 & 0 \\ 0 & a & 0 & 0 \\ 0 & 0 & 0 & 0 \\ 0 & 0 & 0 & 0 \end{bmatrix} y_{fil} \begin{bmatrix} V_{1,1}[0] \\ V_{2,1}[0] \\ V_{3,1}[0] \\ V_{4,1}[0] \end{bmatrix} \quad (5.25)$$

Dividing with y_{fil} on both sides of Equation 5.25 removes y_{fil} , which leaves the final equation for $V_{i,1}[1]$, as seen in Equation 5.26.

$$\begin{bmatrix} V'_{1,1}[1] \\ V'_{2,1}[1] \\ V'_{3,1}[1] \\ V'_{4,1}[1] \end{bmatrix} = - \begin{bmatrix} Y_{11} & Y_{12} & Y_{13} & 0 \\ Y_{12} & Y_{22} & Y_{23} & 0 \\ Y_{13} & Y_{23} & Y_{33} & Y_{34} \\ 0 & 0 & Y_{34} & Y_{44} \end{bmatrix}^{-1} \begin{bmatrix} 0 & 0 & 0 & 0 \\ 0 & a & 0 & 0 \\ 0 & 0 & 0 & 0 \\ 0 & 0 & 0 & 0 \end{bmatrix} \begin{bmatrix} V_{1,1}[0] \\ V_{2,1}[0] \\ V_{3,1}[0] \\ V_{4,1}[0] \end{bmatrix} \quad (5.26)$$

This result means that any $\mathbf{V}'[m]$ can be calculated without y_{fil} through Equation 5.27, where \mathbf{A}^* and $\mathbf{V}^*[m]$ do not have y_{fil} multiplied, as seen in Equation 5.28 and Equation 5.29 respectively.

$$\mathbf{V}^*[m] = -\mathbf{Y}^{-1} \mathbf{A}^* \mathbf{V}^*[m-1] \quad (5.27)$$

$$\mathbf{A}^* = \begin{bmatrix} 0 & 0 & 0 & 0 \\ 0 & a & 0 & 0 \\ 0 & 0 & 0 & 0 \\ 0 & 0 & 0 & 0 \end{bmatrix} \quad (5.28)$$

$$\mathbf{V}^*[m] = \begin{bmatrix} V'_{11}[m] & V'_{12}[m] & V'_{13}[m] & V'_{14}[m] \\ V'_{12}[m] & V'_{22}[m] & V'_{23}[m] & V'_{24}[m] \\ V'_{13}[m] & V'_{23}[m] & V'_{33}[m] & V'_{34}[m] \\ V'_{14}[m] & V'_{24}[m] & V'_{34}[m] & V'_{44}[m] \end{bmatrix} \quad (5.29)$$

Calculation of a Constant

From Equation 5.27 the part containing $-\mathbf{Y}^{-1}\mathbf{A}^*$ is the same for the calculation of all orders of the power series coefficients. This is where the convergence control parameter a is used. To ensure convergence the magnitude of the largest eigenvalue of Equation 5.30 has to be less than 1 [25]. A starting value of a is chosen first, and next a loop is run in MATLAB which checks if the eigenvalues of \mathbf{T} is less than 1 for a given y_{fil} . If the absolute eigenvalues are not less than 1 a is multiplied by a constant b , which is chosen to be $0 < b < 1$, thus reducing a until the eigenvalues of \mathbf{T} are less than 1. This loop is run before the power series coefficients $\mathbf{V}'[m]$ are calculated in order to determine the value of a .

$$\mathbf{T} = \mathbf{Y}^{-1}\mathbf{A}^* = - \begin{bmatrix} Y_{11} & Y_{12} & Y_{13} & 0 \\ Y_{12} & Y_{22} & Y_{23} & 0 \\ Y_{13} & Y_{23} & Y_{33} & Y_{34} \\ 0 & 0 & Y_{34} & Y_{44} \end{bmatrix}^{-1} \begin{bmatrix} 0 & 0 & 0 & 0 \\ 0 & a \cdot y_{fil} & 0 & 0 \\ 0 & 0 & 0 & 0 \\ 0 & 0 & 0 & 0 \end{bmatrix} \quad (5.30)$$

It is also found that in order for the condition $\mathbf{V}'[m] < \mathbf{V}'[m-1]$ to be true the absolute values of \mathbf{T} should be less than 1. This condition is important for Equation 5.22 where the higher order term is removed due to being of insignificant size.

Generally if a larger value of y_{fil} is chosen at the start of the process a will become smaller in order to keep the absolute value of the eigenvalues of \mathbf{T} below 1. Therefore can any starting value of y_{fil} in theory be used as a will be scaled accordingly, however it is found that if the starting value of y_{fil} is too low the absolute values of \mathbf{T} will be larger than 1, thus not fulfilling the condition of $\mathbf{V}'[m] < \mathbf{V}'[m-1]$. A starting value of $y_{fil} = 1$ has been found to be a good option.

5.2.2 Power Series Convergence

After all the coefficients are calculated they can be summed up in the power series and the voltage at the different busbars, with the filter implemented, can be calculated by Equation 5.31. A filter that is different from the starting filter y_{fil} can be used next, which is denoted $y_{fil-new}$. In principle any $y_{fil-new}$ can be implemented in the equation, but the convergence radius of the power series is defined by the original filter y_{fil} that was used in the start of the process as y_{fil} determines the value of a . It is found that for convergence to occur $a \cdot y_{fil} > y_{fil-new}$. This makes sense as a is used to scale y_{fil} in order to get the absolute values of the eigenvalues of \mathbf{T} below 1 and therefore if $a \cdot y_{fil} < y_{fil-new}$ convergence is not achieved. If a large filter is to be implemented the method should be run a number of times with small increments of the final filter, in order to assure

convergence at each small step, until the total filter has been implemented.

$$V_{i,j}(y_{fil-new}) = V_{i,j}[0] + \left(\frac{V'_{i,j}[1]}{a}\right)y_{fil-new} + \dots + \left(\frac{V'_{i,j}[m]}{a^m}\right)y_{fil-new}^m \quad (5.31)$$

In order to limit the number of terms used from the power series $V_{i,j}(y_{fil-new})$ is inserted into Equation 5.32, which is the frequency scan equation with the new filter $y_{fil-new}$ inserted. Equation 5.32 consists of a new admittance matrix and a new voltage matrix. The new admittance matrix has $y_{fil-new}$ added at the chosen busbar, as seen in Equation 5.33. The new voltage matrix which is shown in Equation 5.34, consists of entries calculated from Equation 5.31.

$$\mathbf{Y}_{fil-new} \mathbf{V}_{fil-new} = \begin{bmatrix} 1 & 0 & 0 & 0 \\ 0 & 1 & 0 & 0 \\ 0 & 0 & 1 & 0 \\ 0 & 0 & 0 & 1 \end{bmatrix} \quad (5.32)$$

$$\mathbf{Y}_{fil-new} = \begin{bmatrix} Y_{11} & Y_{12} & Y_{13} & 0 \\ Y_{12} & Y_{22} + y_{fil-new} & Y_{23} & 0 \\ Y_{13} & Y_{23} & Y_{33} & Y_{34} \\ 0 & 0 & Y_{34} & Y_{44} \end{bmatrix} \quad (5.33)$$

$$\mathbf{V}_{fil-new} = \begin{bmatrix} V_{1,1}(y_{fil-new}) & V_{1,2}(y_{fil-new}) & V_{1,3}(y_{fil-new}) & V_{1,4}(y_{fil-new}) \\ V_{2,1}(y_{fil-new}) & V_{2,2}(y_{fil-new}) & V_{2,3}(y_{fil-new}) & V_{2,4}(y_{fil-new}) \\ V_{3,1}(y_{fil-new}) & V_{3,2}(y_{fil-new}) & V_{3,3}(y_{fil-new}) & V_{3,4}(y_{fil-new}) \\ V_{4,1}(y_{fil-new}) & V_{4,2}(y_{fil-new}) & V_{4,3}(y_{fil-new}) & V_{4,4}(y_{fil-new}) \end{bmatrix} \quad (5.34)$$

A loop is run which calculates one $V_{i,j}[m]$ term for each iteration and inserts the calculated term into Equation 5.31, thus expanding the power series one term for each iteration. If the voltage power series converges, the result of Equation 5.32 approximates the current injection matrix. Therefore Equation 5.35 is set up which subtracts the current injection matrix from Equation 5.32, thus as more terms are added to the power series the result approximates a zero matrix. The loop stops adding terms to the power series when the largest entry of the resulting matrix from Equation 5.35 is below a pre-specified value ϵ .

$$\mathbf{Y}_{fil-new} \mathbf{V}_{fil-new} - \begin{bmatrix} 1 & 0 & 0 & 0 \\ 0 & 1 & 0 & 0 \\ 0 & 0 & 1 & 0 \\ 0 & 0 & 0 & 1 \end{bmatrix} \approx \begin{bmatrix} 0 & 0 & 0 & 0 \\ 0 & 0 & 0 & 0 \\ 0 & 0 & 0 & 0 \\ 0 & 0 & 0 & 0 \end{bmatrix} \quad (5.35)$$

Figure 5.2 shows the power series convergence of $V_{1,1}(y_{fil-new})$ for a specific frequency, being the frequency at the first resonance peak from the Small System. The filter that is added is a purely resistive filter with a value of $1 \cdot 10^{-4}$ Siemens. The value of the filter is chosen in order to be below a , which for the specific frequency is $a = 1.5474 \cdot 10^{-4}$. It should be noted that there does not exist a purely resistive filter, however the filter is chosen to show the mathematical principle of the power series convergence. The power series converges within a tolerance of $\epsilon = 1 \cdot 10^{-4}$ after the 5th order term is added to the power series and the final result is identified in the figure with the horizontal black dashed line. The value of ϵ is in this case chosen as an academic value. As can be seen on the figure each term added slightly overshoots the final value and thus for each term that is added the direction changes.

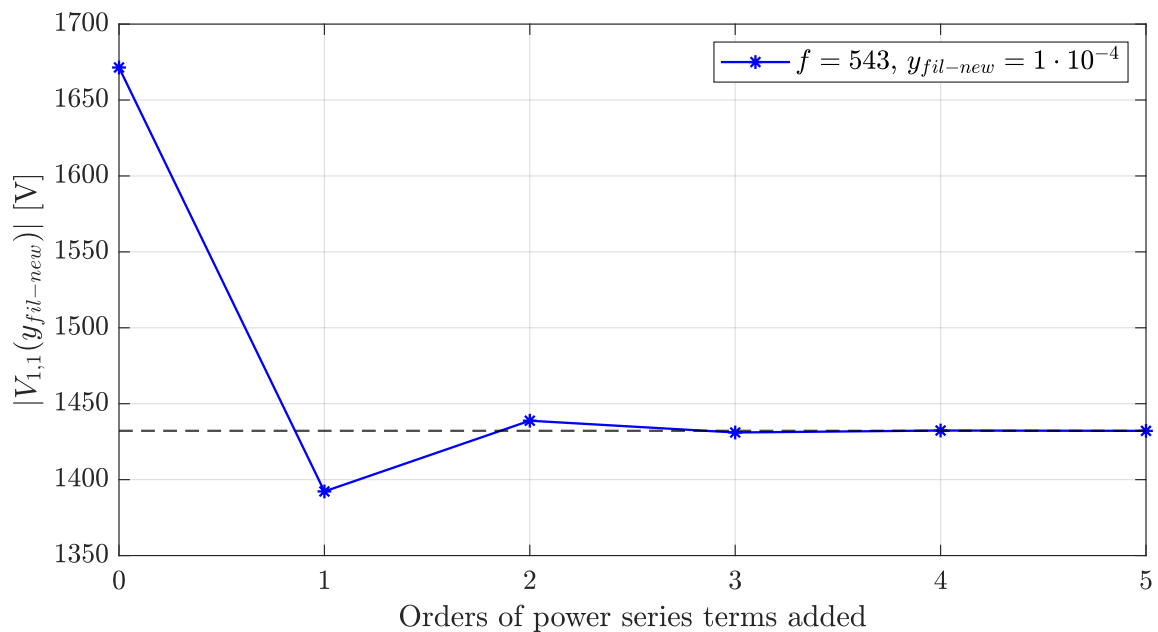


Figure 5.2: Power series convergence of $V_{1,1}(y_{fil-new})$ for a specific frequency and filter implementation.

Table 5.1 shows the values of the power series for the specific frequency and filter shown in Figure 5.2. The final column shows the percentage error between the power series and $|V_{1,1}(y_{fil-new})|$, which is the absolute value when the filter is implemented. $V_{1,1}[0]$ is the voltage before the filter is implemented. It should be noticed that $V'_{1,1}[1]$ is the largest of the terms which is added and thus has the largest impact. The sign of the $V'_{1,1}[m]$ terms change at each step of m , which was also visible in Figure 5.2.

Terms	$V'_{1,1}[m]$		$\frac{V'_{1,1}[m]}{a} \cdot y_{fil-new}^m$		Error [%]
0	1670.5	- 54.977i*	-	-	16.71
1	-431.36	+ 28.42i	-278.75	+ 18.368i	2.794
2	111.26	- 11.02i	46.466	- 4.6009i	0.467
3	-28.668	+ 3.7945i	-7.7370	+ 1.0240i	0.078
4	7.3784	- 1.2248i	1.2868	- 0.2136i	0.013
5	-1.8969	+ 0.3794i	-0.2138	+ 0.0428i	0.002

Table 5.1: Example of power series convergence for the same frequency and filter as presented in Figure 5.2.

* $V_{1,1}[0]$ is not scaled to a . The constant $a = 0.00015474$.

5.2.3 Usability of the Homotopy Method

If convergence is achieved, Equation 5.31 can give the voltage profile after the filter is implemented. This is however the same result as would be achieved if the filter was inserted directly into the admittance matrix and solved using the classical frequency scan equation $\mathbf{Y}^{-1}\mathbf{I} = \mathbf{V}$, which would be a faster approach to calculate the result after the specific filter is implemented. However, the usefulness of the Homotopy Method is that by calculating the voltage coefficient terms for the power series it is possible to get a general indication of how the resonance peaks are affected by different filter positions without having specified the filter. This is done by observing $V'_{i,j}[1]$, which as shown in Equation 5.27, can be calculated using only the filter position and not the specific filter values. It is important to scale back $V'_{i,j}[1]$, as seen in Equation 5.36, and obtain $V_{i,j}[1]$ before comparing different frequencies, as different frequencies might have different values of a .

$$V_{i,j}[1] = \frac{V'_{i,j}[1]}{a} \quad (5.36)$$

If only a specific frequency is to be examined $V'_{i,j}[1]$ can be used, as the relative impacts of the filter positions are still the same as $V_{i,j}[1]$, since a is only a scale.

5.2.4 First Order Coefficient Homotopy Method

$V_{i,j}[1]$ is the first order coefficient of the power series and can be viewed as the first order linear rate of change at the specific frequency at bus i, j . As $V_{i,j}[1]$ is larger than all the other higher order terms it has the most impact and thus gives the best indication of how the resonances are affected. The largest values of $V_{i,j}[1]$ are seen at the frequencies of the resonance peaks, as this is where a potential filter will have the largest impact.

What makes the use of $V_{i,j}[1]$ from the Homotopy Method very valuable is that it is not needed to set up all the calculations shown in Section 5.2.1 as only $V_{i,j}[1]$ for the different

frequencies and filter locations, is needed. This means that whether the power series converges or not does not matter as $V_{i,j}[1]$ is used before the new filter is implemented. As can be seen in Equation 5.37, which is a reprint of Equation 5.26, the calculation of $V'_{i,j}[1]$ contains a , which is dependent of the starting filter y_{fil} as seen in Section 5.2.1.

$$\begin{bmatrix} V'_{1,1}[1] \\ V'_{2,1}[1] \\ V'_{3,1}[1] \\ V'_{4,1}[1] \end{bmatrix} = - \begin{bmatrix} Y_{11} & Y_{12} & Y_{13} & 0 \\ Y_{12} & Y_{22} & Y_{23} & 0 \\ Y_{13} & Y_{23} & Y_{33} & Y_{34} \\ 0 & 0 & Y_{34} & Y_{44} \end{bmatrix}^{-1} \begin{bmatrix} 0 & 0 & 0 & 0 \\ 0 & a & 0 & 0 \\ 0 & 0 & 0 & 0 \\ 0 & 0 & 0 & 0 \end{bmatrix} \begin{bmatrix} V_{1,1}[0] \\ V_{2,1}[0] \\ V_{3,1}[0] \\ V_{4,1}[0] \end{bmatrix} \quad (5.37)$$

Multiplying a out its matrix forms Equation 5.38, which leaves 1 at the chosen filter position in the filter position matrix.

$$\begin{bmatrix} V^*_{1,1}[1]a \\ V^*_{2,1}[1]a \\ V^*_{3,1}[1]a \\ V^*_{4,1}[1]a \end{bmatrix} = - \begin{bmatrix} Y_{11} & Y_{12} & Y_{13} & 0 \\ Y_{12} & Y_{22} & Y_{23} & 0 \\ Y_{13} & Y_{23} & Y_{33} & Y_{34} \\ 0 & 0 & Y_{34} & Y_{44} \end{bmatrix}^{-1} \begin{bmatrix} 0 & 0 & 0 & 0 \\ 0 & 1 & 0 & 0 \\ 0 & 0 & 0 & 0 \\ 0 & 0 & 0 & 0 \end{bmatrix} \cdot a \cdot \begin{bmatrix} V_{1,1}[0] \\ V_{2,1}[0] \\ V_{3,1}[0] \\ V_{4,1}[0] \end{bmatrix} \quad (5.38)$$

Dividing both sides of the equal sign of Equation 5.38 with a forms Equation 5.39, where a is removed.

$$\begin{bmatrix} V_{1,1}[1] \\ V_{2,1}[1] \\ V_{3,1}[1] \\ V_{4,1}[1] \end{bmatrix} = - \begin{bmatrix} Y_{11} & Y_{12} & Y_{13} & 0 \\ Y_{12} & Y_{22} & Y_{23} & 0 \\ Y_{13} & Y_{23} & Y_{33} & Y_{34} \\ 0 & 0 & Y_{34} & Y_{44} \end{bmatrix}^{-1} \begin{bmatrix} 0 & 0 & 0 & 0 \\ 0 & 1 & 0 & 0 \\ 0 & 0 & 0 & 0 \\ 0 & 0 & 0 & 0 \end{bmatrix} \begin{bmatrix} V_{1,1}[0] \\ V_{2,1}[0] \\ V_{3,1}[0] \\ V_{4,1}[0] \end{bmatrix} \quad (5.39)$$

There is no impact from the starting filter y_{fil} left on Equation 5.39, and only the admittance of the system and the chosen filter position have an impact. In fact the First Order Coefficient Homotopy Method can be rewritten as Equation 5.40, due to $\mathbf{Y}^{-1} = \mathbf{V}[0]$. The filter position matrix contains the chosen filter position which impact, at the given frequency, is to be investigated. By setting a loop which moves the value 1 along the diagonal of the filter position matrix one step per iteration, the impact of each filter position at the given frequency can be obtained.

$$\mathbf{V}[1] = -\mathbf{Y}^{-1} \begin{bmatrix} 0 & 0 & 0 & 0 \\ 0 & 1 & 0 & 0 \\ 0 & 0 & 0 & 0 \\ 0 & 0 & 0 & 0 \end{bmatrix} \mathbf{Y}^{-1} \quad (5.40)$$

The method is then able to identify the resonance peaks which will be affected by different filter positions without specifying the filter beforehand. This way it also provides an intuitive feeling of the system's harmonic behaviour. The method will not be able to

give a quantitative output, but will give a relative output between the different filter positions, meaning that if one filter position's value is higher than another filter position's value the first filter will have a larger effect. It is important to notice that the value of $V_{i,j}[1]$ can not be correlated to a final impedance value, at the given frequency, after a filter with specific values is implemented, as $V_{i,j}[1]$ itself is not based on filter values. As will be shown later there are naturally some drawbacks to only using $V[1]$, in terms of not being able to accurately predict the frequencies where the resonance peaks end up after the actual filter is inserted.

Implementation with PowerFactory

The method can be applied to a pre-designed power system in PowerFactory by using the frequency sweep function to extract $V_{i,j}[0]$. Given that for the frequency scan method $\mathbf{Y}^{-1} = \mathbf{Z} = \mathbf{V}[0]$ the impedance matrix \mathbf{Z} can be used in order to set up Equation 5.40. In order to acquire the off-diagonal values of the system impedance matrix the mutual impedance between two busbars has to be defined. An example of this could be the mutual impedance between Bus 1 and Bus 2, which would be denoted $Z_{1,2}$. This is done through defining "ElmMut" elements in PowerFactory, thus enabling the possibility to obtain what PowerFactory calls coupling impedances between two busbars which are the off-diagonal values of the system impedance matrix.

5.2.5 Test of First Order Coefficient Homotopy Method on Small System

The following section shows a test with the First Order Coefficient Homotopy Method being applied on the Small System, which single line diagram is shown in Figure 5.1. This is done through examining $|V_{1,1}[1]|$ at the resonance peaks for different filter positions and comparing the output of the method to a frequency scan of the system, showing $|Z_{1,1}|$, when an actual filter is implemented in the different busbars. In order to distinguish between the results of the First Order Coefficient Homotopy Method and the results of the frequency scan, with actual filters implemented, it is chosen to keep the output of the First Order Coefficient Homotopy Method as $V_{i,j}[1]$ due to it being obtained from the voltage power series, and represent the frequency scan results as $|Z_{i,j}|$ instead of $|V_{i,j}|$, due to $|Z_{i,j}| = |V_{i,j}|$ in the frequency scan method, where $|V_{i,j}|$ is the new voltage at the given busbar after the actual filter is implemented.

In Figure 5.3 the absolute value of $V_{1,1}[1]$, meaning $|V_{1,1}[1]|$, which is the value of $V[1]$ from the Homotopy Method seen from Bus 1 with current injection in Bus 1, is plotted over frequency with the filter position in either Bus 1, Bus 2 or Bus 3, to give an indication of which filter position have the most impact on each resonance peak. A higher value of $|V_{i,j}[1]|$ at a specific frequency means a filter in that position will have a larger impact at

that frequency. This is only to be seen as a relative analysis between the filter positions as the values of $|V_{i,j}[1]|$ for different filter positions depend on the value of the impedance of the system at the specific frequency.

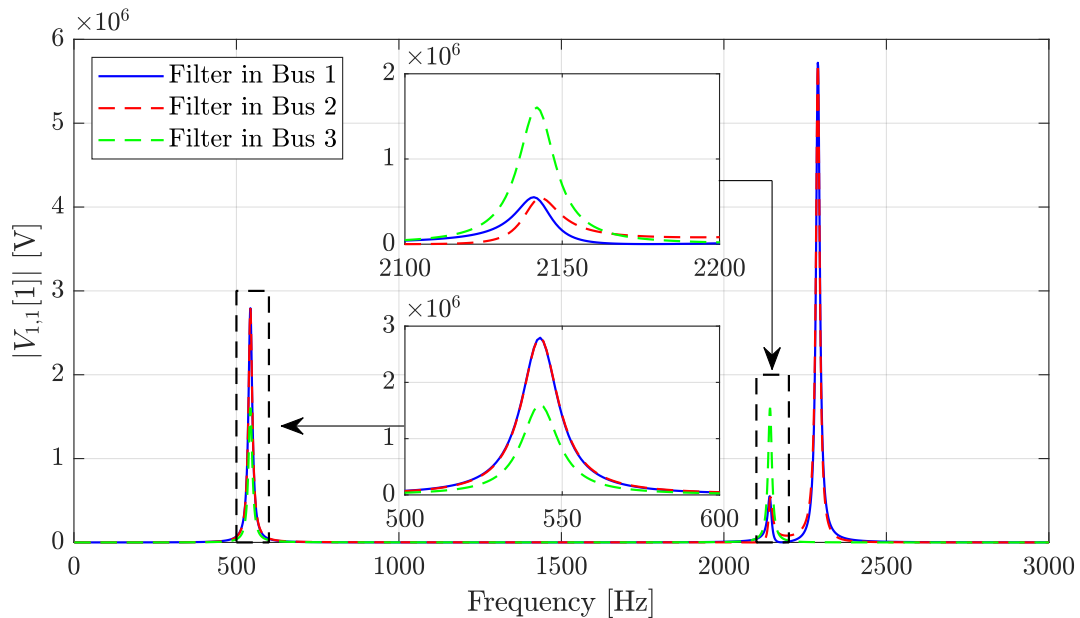


Figure 5.3: $|V_{1,1}[1]|$ from the Homotopy Method, for different filter locations, with observation and injection at Bus 1.

Figure 5.3 shows $|V_{1,1}[1]|$, which indicates that for the first resonance peak a filter in Bus 1 or Bus 2 will have equal, but more impact than a filter in Bus 3. For the second resonance peak, a filter in Bus 3 have the most impact, while a filter in Bus 1 or 2 have almost the same magnitude, but at different frequencies, which will be commented upon later. The results of the second resonance peak are also noteworthy, due to the best filter position not being in the busbar with the injection, which indicates that a filter in Bus 3 does more to dampen the resonance peak, than the other filter positions. At the third resonance peak the method indicates that only a filter in Bus 1 or Bus 2 will affect the system, when observed from Bus 1 and a filter in Bus 3, will thus not have an impact at this resonance.

Figure 5.4 shows $|Z_{1,1}|$ with no filter and with C-type filters located in the different busbars, with the C-type filter tuned to the 11th harmonic order, $Q_1 = 100$ Mvar and $q = 2$.

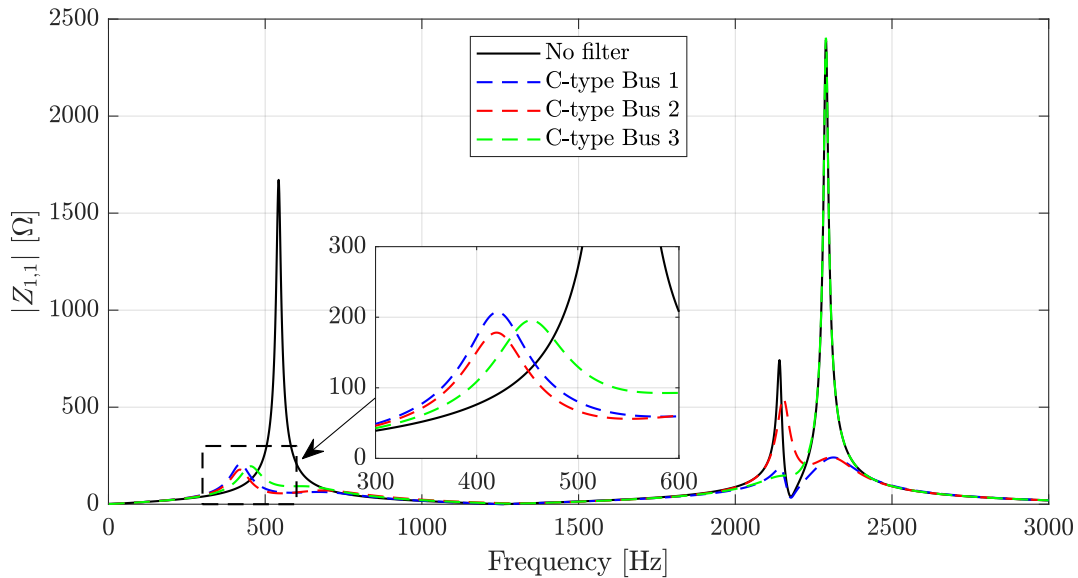


Figure 5.4: Absolute impedance seen from Bus 1, when C-type filter is implemented in different positions.

In Figure 5.4 the First Order Coefficient Homotopy Method is seen to indicate correctly the effect of implementing a filter. A fast way to compare results of $|V_{1,1}[1]|$ and $|Z_{1,1}|$ is to set up rankings for the different filter positions in terms of both $|V_{1,1}[1]|$ and $|Z_{1,1}|$ and see if they correlate as this would indicate that the method is predicting correctly. The filter position with the largest value of $|V_{1,1}[1]|$, at the resonance peak, gets a ranking of 1, as this indicates that the filter position will have the largest impact at the given resonance peak. For $|Z_{1,1}|$ the ranking of 1 is given to the filter position, with the actual C-type filter implemented, which has the lowest value of $|Z_{1,1}|$ at the frequency of the original resonance peak.

It was found that all the rankings of $|V_{1,1}[1]|$ and $|Z_{1,1}|$ matched thus indicating that the method predicted correct at the three resonance peaks. In order to further examine the results a grading is added to each filter position, as even though the method predicted the right ranking there is differences in how well the results can be used. Table 5.2 shows the grades and gives an explanation of what the grading entails.

Grade	Explanation of grade
Perfect	<ul style="list-style-type: none"> • Method perfectly indicates the impact at resonance peak, when an actual filter is implemented. • Can give clear indications of the final impedance value after an actual filter is implemented.
Good	<ul style="list-style-type: none"> • Method indicates correctly the filter position's ranking in terms of most impactful filter positions. • Can give some indication of the final impedance value, after an actual filter is implemented, in terms of the expected difference in the final impedance between two actual filter positions.
Lacking	<ul style="list-style-type: none"> • Method indicates correctly the filter position's ranking in terms of most impactful filter positions. • The method does not provide a clear distinction between damping and amplification of given resonance point after implementation of an actual filter. • Typically seen for resonance peak followed immediately by resonance valley.
Bad	<ul style="list-style-type: none"> • Method wrongly indicates the filter position's ranking in terms of most impactful filter positions.
-	<ul style="list-style-type: none"> • Resonance peak is not present from observed busbar.

Table 5.2: Description of grades to determine First Order Coefficient Homotopy Method's usefulness.

Table 5.3 shows the grade of the different filter positions for the different peaks and also show the results for when Bus 2 and Bus 3 are the observed and injected busbars. It is seen that the grade Bad is not used due the rankings of $|V_{1,1}[1]|$ and $|Z_{1,1}|$ matching for the tested cases. The plots for $|V_{2,2}[1]|$, $|Z_{2,2}|$, $|V_{3,3}[1]|$ and $|Z_{3,3}|$ are shown in Appendix D where a brief description of the results is given.

From the results here and in Appendix D it is seen that for this system the best filter position is not always the location with the harmonic emission, depending on which resonance point is of interest. The best filter position is the location which have most effect on the resonance point. Therefore there is an indication that the best possible filter position, for a specific resonance point, is at the busbars which created the resonance or has the largest effect on the resonance point.

Observation and injection at Bus 1								
Filter at Bus 1			Filter at Bus 2			Filter at Bus 3		
Res. 1	Res. 2	Res. 3	Res. 1	Res. 2	Res. 3	Res. 1	Res. 2	Res. 3
Good	Good	Good	Good	Lacking	Good	Good	Lacking	Perfect

Observation and injection at Bus 2								
Filter at Bus 1			Filter at Bus 2			Filter at Bus 3		
Res. 1	Res. 2	Res. 3	Res. 1	Res. 2	Res. 3	Res. 1	Res. 2	Res. 3
Good	Lacking	Good	Good	Good	Good	Good	Lacking	Perfect

Observation and injection at Bus 3								
Filter at Bus 1			Filter at Bus 2			Filter at Bus 3		
Res. 1	Res. 2	Res. 3	Res. 1	Res. 2	Res. 3	Res. 1	Res. 2	Res. 3
Good	Good	-	Good	Good	-	Good	Good	-

Table 5.3: The performance of the First Order Coefficient Homotopy Method seen from Bus 1, Bus 2 and Bus 3 respectively with filter position in Bus 1, Bus 2 and Bus 3 respectively.

It is found that if a resonance peak is immediately followed by a resonance valley, $|V_{1,1}[1]|$ of a filter position can be affected, if the filter position has an impact on both the resonance peak and the resonance valley. For the given case there was 36 Hz between the frequency of the resonance peak and the frequency of the lowest magnitude of the resonance valley. Due to $|V_{1,1}[1]|$ being the absolute value it is not able to indicate whether the impact of the filter position is damping or amplification. This was seen when observing $|V_{1,1}[1]|$ for the second resonance peak in the case of a filter position in Bus 2 or Bus 3. In Figure 5.4 it is seen that a filter in Bus 2 or Bus 3 gives an amplification at the resonance valley, which immediately follows the second resonance peak. $|V_{1,1}[1]|$ is thus affected, as it seem to indicate a larger impact at the resonance peak, for a filter in Bus 2 or Bus 3, than what is observed in Figure 5.4 after the actual filter is implemented. As noted earlier the rankings of $|V_{1,1}[1]|$ and $|Z_{1,1}|$ still matched, so the method predicted correctly, however if only the rankings are used and the final $|Z_{1,1}|$ after implementation of the actual filter is not observed, information is lost.

As is seen the method can correctly predict the rankings of $|V_{1,1}[1]|$ and $|Z_{1,1}|$, but not give a final value of the impedance, and therefore the method should be limited to an early screening of the power system for finding potential filter position candidates.

The value of $V_{i,j}[1]$ that has been used is the absolute value, so to examine if there is more information to be gained from the method by observing the real and imaginary part of $V_{i,j}[1]$ an analysis is done in Appendix E. The analysis indicated that even though the observation of the real and imaginary values independently could provide some more

information, especially the real values, the information is not reliable for all frequencies, as the method is still only relying on the filter-less first order coefficient. Using the real values enables the ability see whether the indication is an increase or a decrease in the impedance magnitude, which is very useful in the case of resonance peaks being followed by resonance valleys. Given the fact that the use of $V_{i,j}[1]$ should be limited to an early screening of which filter positions have the largest impact, it is sufficient to use the absolute value of $V_{i,j}[1]$. Potentially a case could be made for using the real values to indicate whether the impedance is increasing or decreasing, however the actual filter values will still determine the final impedance value, and as such $V_{i,j}[1]$ can not predict the final impedance value alone.

As seen in Chapter 4 different filter positions of the same filter causes different shifts in the resonance peak frequency. Investigating the imaginary values of $V_{i,j}[1]$ it would be possible to get an indication of how an actual filter, in different filter positions, will shift the resonance peak relative to each other, however it will never be possible to obtain the final frequency of the resonance peak before an actual filter is implemented.

The main findings of this section describing the Homotopy Method and its application to the Small System are given here in bullet points:

- Through the use of the Homotopy Method a voltage power series can be obtained which, if it converges, can give the new voltages in the system after implementation of an actual filter.
 - The Homotopy Method provides a semi-analytical solution to the implementation of a filter, however a direct usage of the frequency scan method, with the filter implemented, provides a faster and easier solution if only the final value of the voltages is needed.
- Using the first order coefficient of the power series it is possible to get indications of different filter positions' impact on resonance peaks without specifying an actual filter.
 - The noticeable advantage of the method is that it is independent of an actual filter, and can therefore be used early in the process of selecting filter position candidates in a given system.
 - Applying the first order coefficient method to the Small System showed that the method correctly indicated the most impactful filter position for all the resonance points tested for, when compared to the implementation of a C-type filter.
- More understanding of the potential filter impact can be gained by observing the

real and imaginary values of the first order coefficient, however the absolute value is found to be sufficient for most cases.

- The real part of the first order coefficient can indicate whether a given filter position causes a damping or amplification at the given frequency.
- The imaginary part of the first order coefficient can indicate the relative movement of resonance peaks in terms of frequency between different filter positions.
- A major drawback of the First Order Coefficient Homotopy Method is that it can only give indications of the final voltages in the system after the implementation of an actual filter, as the values of the actual filter will determine the final voltages.
 - The First Order Coefficient Homotopy Method can not give final values for resonance shifts and potential anti-resonances.
- For a global filter placement study the method's usefulness is in the early stages in order to select a number of candidates for the best filter positions before an actual filter is designed and implemented in the models.

A general discussion of the results and the usefulness of the First Order Coefficient Homotopy Method is reserved to Chapter 7, where the results from this section will be compared to the results from Chapter 6 which shows the First Order Coefficient Homotopy Method being applied to a larger system.

Chapter 6

First Order Coefficient Homotopy Method Applied to Large System

This chapter examines the use of the First Order Coefficient Homotopy Method, when the method is applied to a large system, and how well the method works when a change occur in the system, such as implementation of a new line.

6.1 Description of Large System

The system that is used in this chapter is based on the 400 kV skeleton of the western Danish transmission system known as the DK1 grid, as seen in Figure 6.1 and will be referred to as the Large System. The lines are modelled as equivalent-PI with the line data being fundamental frequency values from [26], which is load flow data from the Danish TSO. In order to keep the system relatively simple for implementation in MATLAB only the 400 kV substations and lines are modelled, and thus the 150 kV transmission level is not modelled nor aggregated. Four ideal voltage sources are implemented, of which three are placed at 400 kV busbars which does not have a transformer to the 150 kV level of the grid in the real system, being FVO, MKS and SVS. In the real system these busbars are used as connections for large generators through EHV-MV transformers. This is in no way an accurate representation of the generators and the EHV-MV transformers in terms of an accurate harmonic study, but it is decided to use the ideal voltage sources in order to keep the system simple, so that it easily can be implemented in MATLAB. The final busbar which is chosen to have an ideal source connected is the UCTE busbar which represents the German border. As the data from [26] does not give any indications of the structure of the grid on the German side of the border all the lines going to Germany is connected at the UCTE busbar. The goal of this oversimplified representation of the DK1 grid is thus not to try to represent the Danish grid accurately, as this is out of the scope of the project, but instead test the method on a known grid structure, with real line data. This also means that the results presented later should not be taken as accurate for the real system, but rather as a means to show how the method works on a larger system.

As stated earlier one of the objectives is to compare how the results of the First Order Coefficient Homotopy Method are affected when a change to the system is implemented. The chosen change will be an implementation of a line between the EDR and IDU busbars, thus resembling a change in the system that will occur in reality [3].

The busbar that is chosen as the focus busbar is the TJE busbar as this is a fairly central busbar in the system, which also have an HVDC-LCC connected making the busbar a source of harmonic emission. In principle any busbar could be chosen for this analysis, however as only one will be shown, TJE is chosen as it is relatively close to the busbars where the new EDR-IDU line is to be implemented.

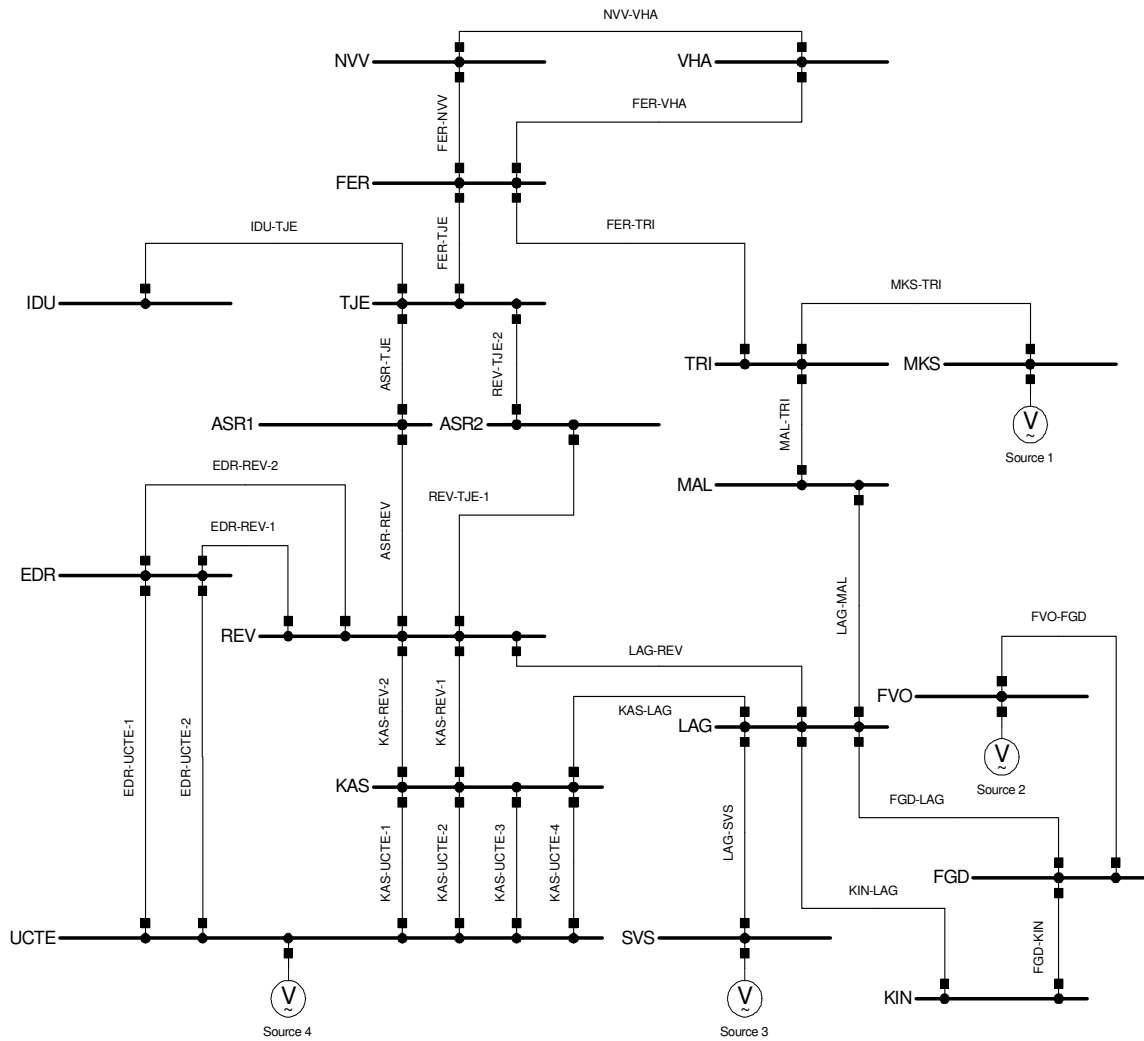


Figure 6.1: Single-line diagram of the Large System, with ideal voltage sources at pre-specified busbars.

6.2 Movement of Resonance Peaks during EDR-IDU Line Implementation

A new line in a system will most likely have an impact on the resonance points of the system, therefore when comparing the impact of filters using the First Order Coefficient Homotopy Method, before and after a new line is implemented in the Large System, the same resonance peaks should be compared. It will therefore be necessary to track the movement of the resonance peaks as the system is changed. This is done by scaling the impedance and admittance of the EDR-IDU line by the scaling factor k , as seen in Equation 6.1 and 6.2 respectively, and observing the impedance plot graphically.

$$Z'_{EDR-IDU} = \frac{Z_{EDR-IDU}}{k} \quad (6.1)$$

When $k = 0 \iff Z'_{EDR-IDU} = \infty$ and thus have no impact on the system.

$$Y'_{EDR-IDU} = Y_{EDR-IDU} \cdot k \quad (6.2)$$

When $k = 0 \iff Y'_{EDR-IDU} = 0$ and thus have no impact on the system. $Z'_{EDR-IDU}$ and $Y'_{EDR-IDU}$ are implemented in the system admittance matrix. By running a loop which gradually increases k from 0 to 1 the line is gradually implemented in the system and the movement of the resonance peaks can be tracked. Figure 6.2 shows the impedance scan observed from TJE with current injection in TJE, for the scaled implementation of the EDR-IDU line. The three zooms are of the first three resonance peaks which are investigated later.

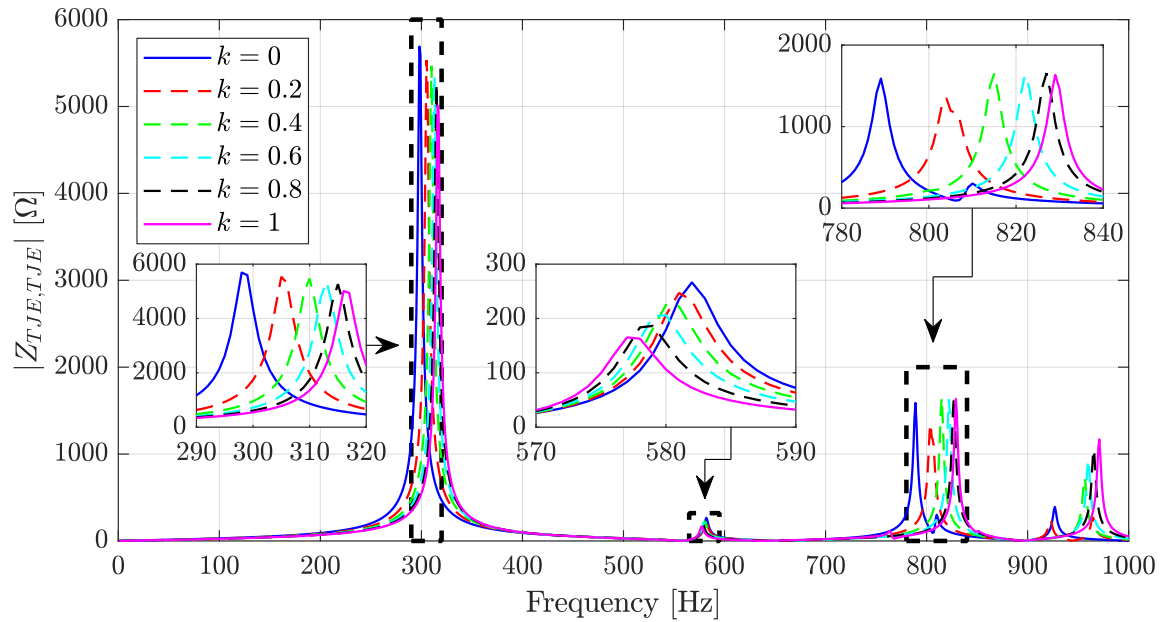


Figure 6.2: Movement of resonance peaks observed from TJE, with injection in TJE, for the scaled implementation of EDR-IDU line.

Table 6.1 shows the frequency of the three resonance peaks of interest. When $k = 0$ the implemented line has no impact and when $k = 1$ the line is fully implemented.

Resonance peak #	$k = 0$	$k = 1$
1	298 Hz	316 Hz
2	582 Hz	577 Hz
3	789 Hz	829 Hz

Table 6.1: Frequency of resonance peaks before and after implementation of the EDR-IDU line.

6.3 Results of First Order Coefficient Homotopy Method

Results of Peak 1

Figure 6.3 shows the absolute value of $V_{TJE,TJE}[1]$, as calculated by the use of the First Order Coefficient Homotopy Method, before the EDR-IDU line is implemented. Again it should be noticed that a large value of $|V_{TJE,TJE}[1]|$ indicates that a potential filter will have a large impact on the impedance at the specific frequency. The results from the busbars with ideal voltage sources are not shown as these busbars act as ideal short-circuits meaning a filter will have no effect by being implemented there. The results will

be summarised and discussed later.

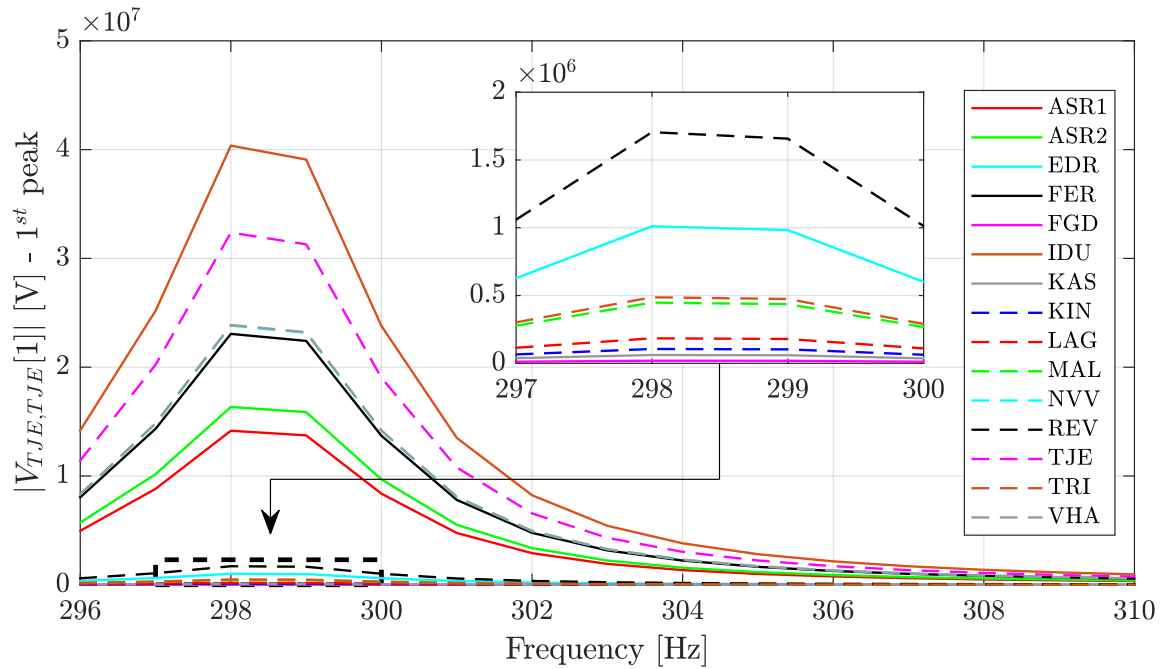


Figure 6.3: $|V_{TJE,TJE}[1]|$ for the first resonance peak, before the EDR-IDU line is implemented.

In order to compare the results of Figure 6.3 to a situation where an actual filter is implemented in the system a pre-specified filter is implemented at each available busbar to see if the filters have the predicted impact of the First Order Coefficient Homotopy Method. The chosen filter is a C-type filter tuned to the 5th harmonic order, with $Q_1 = 100$ Mvar and $q = 2$. The values for Q_1 and q are standard values, while the tuned frequency is chosen as the 5th harmonic order because of the 5th harmonic order being a characteristic frequency, and thus it is more likely to have harmonics injections at this frequency, compared to the 6th harmonic order. If the filter was tuned to the 6th harmonic order there would be a large risk of creating a resonance peak at the 5th harmonic order. The impedance profile of the C-type filter should be able to give mitigation at all three resonance peaks of interest.

Figure 6.4 shows the absolute impedance, $|Z_{TJE,TJE}[1]|$, of the first resonance peak when the filter is implemented at the different busbars, before the EDR-IDU line is implemented.

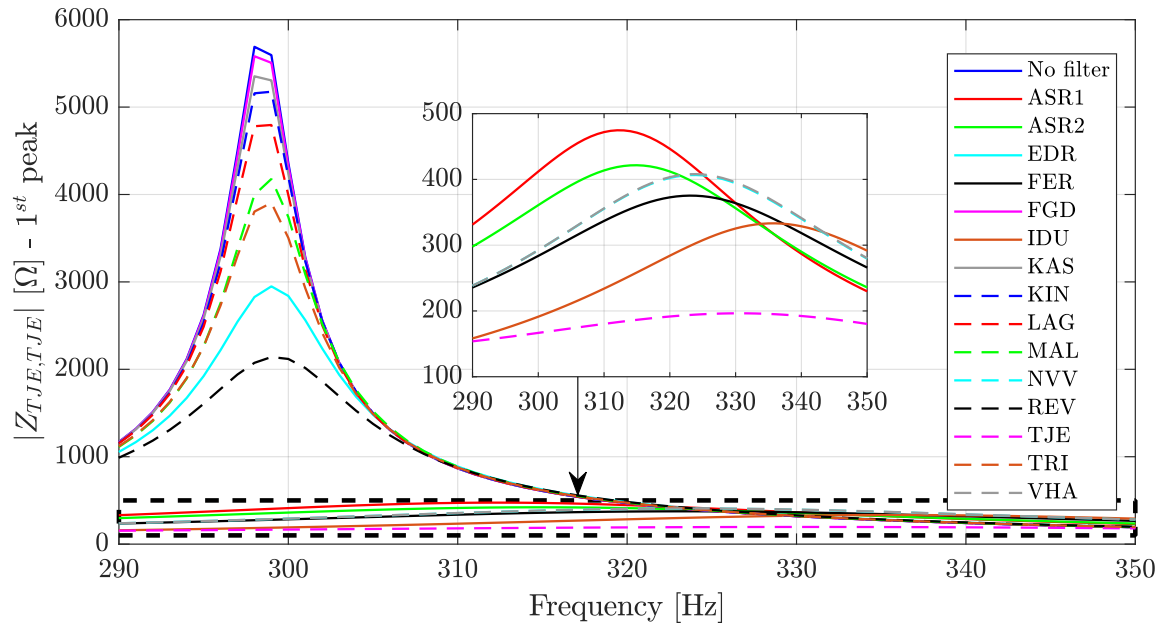


Figure 6.4: $|Z_{TJE,TJE}[1]|$ at the first resonance peak after implementation of a C-type filter tuned to the 5th harmonic order, before the EDR-IDU line is implemented.

Figure 6.5 shows the absolute value of $V_{TJE,TJE}[1]$, as calculated by the use of the First Order Coefficient Homotopy Method, after the EDR-IDU line is implemented.

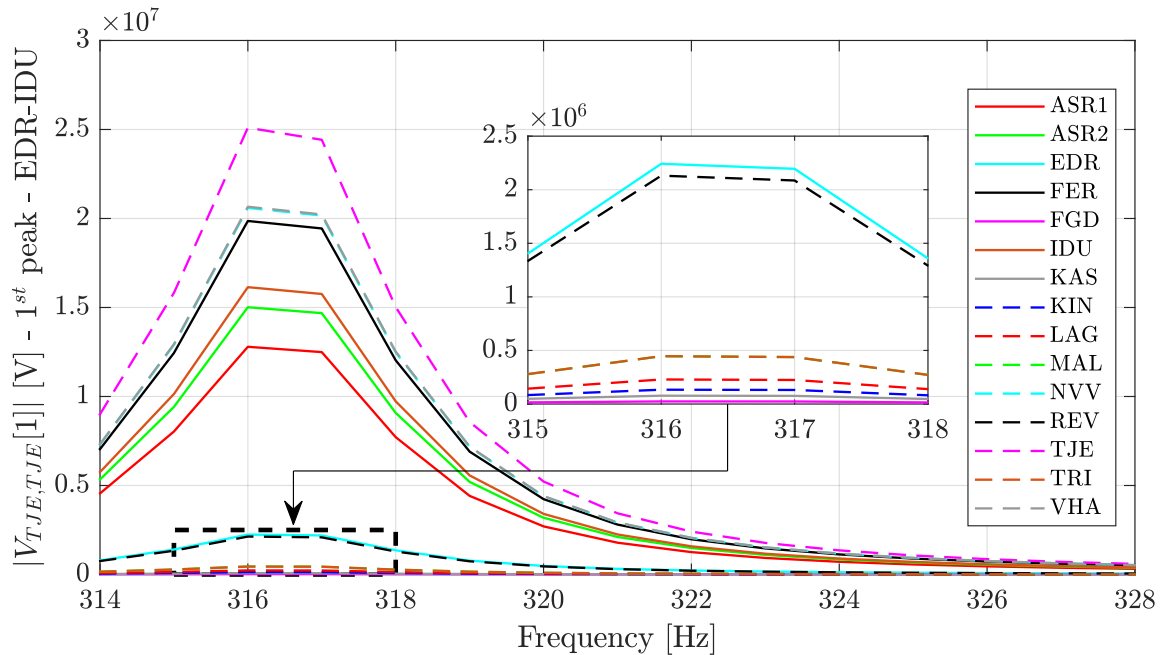


Figure 6.5: $|V_{TJE,TJE}[1]|$ for the first resonance peak, after the EDR-IDU line is implemented.

Figure 6.6 shows $|Z_{TJE,TJE}|$ of the first resonance peak when the filter is implemented at different busbars, after the EDR-IDU line is implemented.

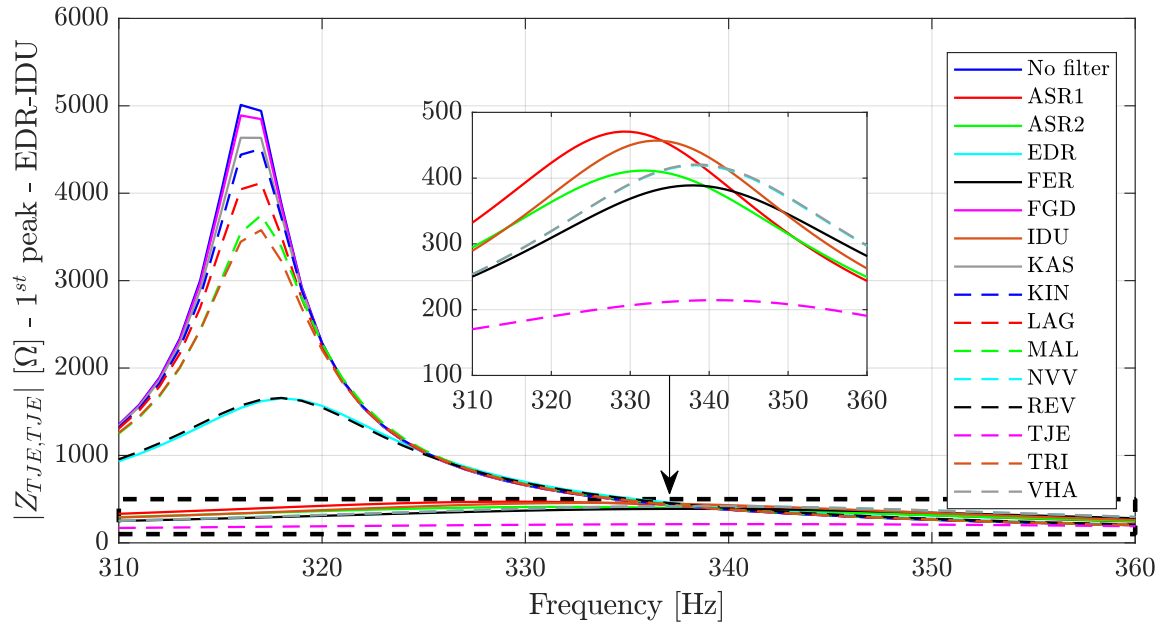


Figure 6.6: $|Z_{TJE,TJE}[1]|$ at the first resonance peak after implementation of a C-type filter tuned to the 5th harmonic order, after the EDR-IDU line is implemented.

In order to compare the results of the First Order Coefficient Homotopy Method to the implementation of a filter with actual values, both before and after the implementation of the EDR-IDU line, Table 6.2 is set up.

The table shows $|V_{TJE,TJE}[1]|$ and $|Z_{TJE,TJE}|$ before and after the implementation of the EDR-IDU line. It should be noticed that comparing values of $|V_{TJE,TJE}[1]|$ and $|Z_{TJE,TJE}|$ for the same filter position before and after the implementation of the EDR-IDU line is not conclusive as the shift of the resonance peaks also caused a change in the absolute impedance before the actual filter is implemented. The table also ranks $|V_{TJE,TJE}[1]|$ and $|Z_{TJE,TJE}|$ so that it can be compared whether the filter position which indicated the largest impact, also is the position that have the largest impact when an actual filter is implemented. For $V_{TJE,TJE}[1]$ a rank of 1 indicates that the filter position have the largest impact, meaning the largest value of $|V_{TJE,TJE}[1]|$. For $|Z_{TJE,TJE}|$ a rank of 1 indicates that the filter position has the lowest value of $|Z_{TJE,TJE}|$ at the specific frequency where the resonance peak was before the filter was implemented.

The rank indicates nothing about potential anti-resonances as this is not part of the focus when using this method, as anti-resonances will be dependent on the actual filter values. The meaning behind displaying the ranking is twofold. First it is to see if the rank be-

tween $|V_{TJE,TJE}[1]|$ and $|Z_{TJE,TJE}|$ is the same, or close to the same, as this indicates that the method accurately predicts which filter position has the most affect at the specific resonance frequency. Secondly, it is to compare the ranks before and after the implementation of the EDR-IDU line to see how the change in the system affects which filter position is most impactful.

Peak 1	Before EDR-IDU				After EDR-IDU			
	$ V[1] $	Rank	$ Z $	Rank	$ V[1] $	Rank	$ Z $	Rank
No Filter	-	-	5690	16	-	-	5010	16
ASR1	$1.416 \cdot 10^7$	7	395.4	7	$1.279 \cdot 10^7$	7	386.7	7
ASR2	$1.634 \cdot 10^7$	6	347.9	6	$1.501 \cdot 10^7$	6	335.8	5
EDR	$1.011 \cdot 10^6$	9	2827	9	$2.242 \cdot 10^6$	8	1544	8
FER	$2.306 \cdot 10^7$	5	273.4	3	$1.986 \cdot 10^7$	4	284.4	2
FGD	$1.900 \cdot 10^4$	15	5582	15	$2.423 \cdot 10^4$	15	4890	15
IDU	$4.037 \cdot 10^7$	1	184.0	2	$1.614 \cdot 10^7$	5	338.4	6
KAS	$6.108 \cdot 10^4$	14	5352	14	$7.762 \cdot 10^4$	14	4635	14
KIN	$1.057 \cdot 10^5$	13	5158	13	$1.337 \cdot 10^5$	13	4440	13
LAG	$1.844 \cdot 10^5$	12	4781	12	$2.292 \cdot 10^5$	12	4045	12
MAL	$4.478 \cdot 10^5$	11	3997	11	$4.462 \cdot 10^5$	11	3547	11
NVV	$2.382 \cdot 10^7$	4	280.5	4	$2.059 \cdot 10^7$	3	291.2	3
REV	$1.705 \cdot 10^6$	8	2074	8	$2.131 \cdot 10^6$	9	1571	9
TJE	$3.237 \cdot 10^7$	2	163.9	1	$2.510 \cdot 10^7$	1	181.9	1
TRI	$4.870 \cdot 10^5$	10	3805	10	$4.467 \cdot 10^5$	10	3445	10
VHA	$2.389 \cdot 10^7$	3	280.6	5	$2.066 \cdot 10^7$	2	291.3	4

Table 6.2: Comparison of $|V_{TJE,TJE}[1]|$ and $|Z_{TJE,TJE}|$ before and after implementation of the EDR-IDU line, for the first resonance peak.

Before Implementation of the EDR-IDU Line

Comparing the filter position ranks of $|V_{TJE,TJE}[1]|$ and $|Z_{TJE,TJE}|$ in Table 6.2, before the implementation of the EDR-IDU line, there is a maximum difference of two rankings for the same filter position. This indicates that the use of $V_{TJE,TJE}[1]$ predicts quite well how much an actual filter impacts at the resonance frequency. The filter positions with the most deviating ranks are FER and VHA, however the values of $|V_{TJE,TJE}[1]|$ is close between the two positions and their values of $|Z_{TJE,TJE}|$ are also very close, with NVV having values of $|V_{TJE,TJE}[1]|$ and $|Z_{TJE,TJE}|$ between FER and VHA. The grading system used in Chapter 5 would assign the grade Bad for these filter positions, however as the three busbars are having values very close to each other, the ranks of these busbars can almost be seen as being equal. The difference in ranks for the two filter positions FER and

VHA is not because of the method having a large uncertainty, but because of the close values between the busbars, thus a small error gave the difference in ranks. Therefore the rank system is also not the most precise indicator of how impactful a filter position is, as a single difference in rank can mean a very small or very large difference in the final value of $|Z_{TJE,TJE}|$. The lowest value of $|Z_{TJE,TJE}|$ is achieved by the filter in TJE, which is also ranked second in terms of $|V_{TJE,TJE}[1]|$. This would be somewhat expected as it makes sense that the filter in the busbar being observed will have a large impact on the impedance envelopes, however as will be seen for the other resonance peaks this is not always the case.

Finally it can be seen that there are some geographical tendencies in the results. The three busbars FER, NVV and VHA have close to the same results and if Figure 6.1 is observed the three busbars are also all located in the same area, relatively to TJE. The results for NVV and VHA are almost equal, most notably in terms of $|Z_{TJE,TJE}|$. This suggest a similar tendency as was seen in the Small System, where Bus 1 and Bus 2 shared similar results when observing from Bus 3. The structure of the FER, NVV and VHA ring share similarities with the Bus 1, Bus 2 and Bus 3 ring from the Small System, where Bus 3 has the same role as FER. The lengths from FER towards NVV and VHA are 20.4 km and 24.5 km respectively, and even though the lines do not share the same electrical parameters, one could make the approximation that they are seen as being equal from TJE, which would then give the same results when seen from TJE, independent of which busbar the filter was placed in. This result was also seen when observing from Bus 3 in the Small System and having the filter in either Bus 1 or Bus 2, due to the line lengths to the two busbars being equal. The least impactful filter positions are the group of FGD, KAS, KIN and LAG, which are all located relatively far away from TJE in the same direction. Some of this can be explained by the interaction with the ideal voltage sources located in the vicinity of these four busbars. The ideal voltage sources essentially acts as perfect filters and thus the impact of placing a filter with actual values in the busbar next to the busbar, with an assumed perfect filter, could be expected to be low. However as will be seen later this is not always the case and the structure of the system will also be seen to have an impact.

After Implementation of the EDR-IDU Line

Comparing the filter position ranks of $|V_{TJE,TJE}[1]|$ and $|Z_{TJE,TJE}|$, after the implementation of the EDR-IDU line, for the first resonance peak, there is again a maximum difference of two rankings for the same filter position. Again the filter positions with the largest ranking deviations are due to the same three filter positions, being NVV, FER and VHA, as before the implementation of the line, as their results are very close to each other.

Comparing the rankings before and after the implementation of the EDR-IDU line the only major change is the ranking of IDU which goes from being ranked 1st and 2nd in terms of $|V_{TJE,TJE}[1]|$ and $|Z_{TJE,TJE}|$ respectively, to being ranked 5th and 6th respectively. It makes sense that the filter position in IDU would be impacted as the major change in the system occurs at that busbar. Even though EDR, which is the other busbar being directly impacted by the change in the system, only gains one ranking better in terms of $|V_{TJE,TJE}[1]|$ and $|Z_{TJE,TJE}|$, EDR's impact also changes significantly. Even though the values of $|V_{TJE,TJE}[1]|$ and $|Z_{TJE,TJE}|$ can not be directly compared before and after the implementation of the EDR-IDU line, EDR sees a doubling in terms of $|V_{TJE,TJE}[1]|$, which can not alone be explained by the change in the absolute impedance of the resonance peak before and after the change in the system. The reason EDR did not gain more ranks is due to the results of other busbars being far away from the results of EDR. These two results from IDU and EDR highlights that for this resonance peak changing the system had a significant impact on the filter effectiveness at the busbars being directly impacted by the change in the system.

The results and plots for the second and third resonance peak can be found in Appendix F. The main findings from examining the results for the second resonance peak are:

- A filter in VHA, NVV and FER have the largest values of $|V_{TJE,TJE}[1]|$ and lowest values of $|Z_{TJE,TJE}|$, meaning the method accurately indicates the filter position with the largest impact.
- A filter in TJE is ranked 10 in terms of $|V_{TJE,TJE}[1]|$ and ranked 9 in terms of $|Z_{TJE,TJE}|$ and is therefore not a good filter position to reduce the second resonance peak.
- The FER, VHA and NVV ring circuit was the reason for the second resonance peak, as a filter in the ring circuit removed the resonance peak. A disconnection of these lines also resulted in the resonance peak disappearing.
- The implementation of the EDR-IDU line had no significant effect on the values of $|V_{TJE,TJE}[1]|$ and $|Z_{TJE,TJE}|$, which indicates that the resonance peak is not influenced by the changed part of the system.

The main findings from examining the results for the third resonance peak are:

- A filter in IDU had the largest value of $|V_{TJE,TJE}[1]|$ and lowest value of $|Z_{TJE,TJE}|$, before the implementation of the line and thus TJE was not the best filter position to reduce the third resonance peak.

- A filter in ASR1 had a rank difference of three between $|V_{TJE,TJE}[1]|$ and $|Z_{TJE,TJE}|$, which was not because other filter positions had close values of $|V_{TJE,TJE}[1]|$ and $|Z_{TJE,TJE}|$ to those of ASR1, which shows that there are inaccuracies in the method. The reason could however be explained by using the real and imaginary values instead of absolute values, as for ASR1 the frequencies right after the resonance peak were seen to be amplified.
- The implementation of the EDR-IDU line had a large impact on the values of $|V_{TJE,TJE}[1]|$ and $|Z_{TJE,TJE}|$ for the different filter locations as one of the most impactful locations before the implementation of the line, being IDU, is one of the worst after the implementation, and ASR1 which had a low impact before the implementation is one of the most impactful after the implementation.
- The busbars close to the ideal voltage sources were seen to not be the least impactful filter positions, thus indicating that the structure of the system has a large impact at the different resonance peaks.

Conclusion

The main findings of the result of using the First Order Coefficient Homotopy Method on the Large System are given here in bullet points:

- The method is able to give valuable indication of which resonances, seen from a specific busbar and specific current injection, are affected by different filter locations.
- The method is able to give relative information of which filter position has the most effect on each resonance peak.
- The method indicates that a filter position in the busbar which created a resonance point is sometimes more effective, than a filter position in the busbar where the injection is.
- The filter position in the busbar where the injection is, has a tendency to perform better when the actual filter is implemented than what the method indicates.
- The method is not able to give precise indications of the final impedance value after an actual filter is implemented, due to the lack of actual filter values in the method. This means the indications of the method are not completely precise, but still indicated satisfactorily the most impactful filter positions.
- After implementation of a new line in the system between EDR and IDU it was seen to change the system impedance and also the values of the First Order Coefficient

Homotopy Method, thus the method would be needed to be used after each change in the system. Generally the filter positions which are in busbars directly impacted by the change in the system see the largest change in their impact.

Chapter 7

Discussion

This chapter presents a discussion of the First Order Coefficient Homotopy Method in terms of the results from earlier chapters and the method's usefulness. Included is also a more general discussion on why, for practical reasons, the method have some drawbacks.

7.1 Results from Chapter 5 and 6

The results of the First Order Coefficient Homotopy Method from the Small System and the Large System show that the First Order Coefficient Homotopy Method is able to give valuable indication of which resonances, seen from a specific busbar and with current injection in a specific busbars, are affected by different filter locations, and give relative information of which filter position has the most effect on each resonance peak. The major advantage of the method is that it does not utilise filter values, and only needs the filter position. The method was seen to not be able to give precise indications of the final impedance value, after an actual filter is implemented, due to the lack of actual filter values. In Chapter 6 a ranking system was used to rank the filter positions in terms of the magnitude of $|V_{i,j}[1]|$, and rank the filter positions in terms of the $|Z_{i,j}|$ in a system where a filter with pre-specified values was inserted at the filter positions. Comparing the two rankings they were mostly seen to correlate with each other, however a few instances there was a difference between the rankings. These differences were generally either of 1 or 2 ranks, with one instance being a ranking difference of 3. Therefore the First Order Coefficient Homotopy Method is not able to accurately predict which filter position will results in the most damping at the specific resonance frequency, when an actual filter is implemented. However as the maximum ranking difference seen was 3 out of a possible 15, the method never predicted that a filter position would be among the best where the final damping turned out to be among the worst. When there was a difference in ranks, the absolute impedance between the ranks were often very close, an example being a difference of 11.4 % between TJE and IDU with a rank difference of one and 2.56 % between VHA and FER which had a rank difference of two, both for the first resonance. Therefore the method can be used to give the three to five best filter positions and further analysis could be conducted on those positions to get the best filter position by implementing actual filter values.

Due to the resonance peaks being in focus in the example systems the absolute value of $V_{i,j}[1]$ has been sufficient, as it would be difficult to imagine a scenario where the implementation of a filter resulted in an amplification at the specific frequency where

the resonance peak was. For the special case where a resonance peak is followed very closely by a resonance valley the absolute value of $V_{i,j}[1]$ is seen to cause inaccuracies. The method predicts a damping at the resonance peak and an amplification at the resonance valley, which is difficult to distinguish when observing the absolute value. Using the real part of $V_{i,j}[1]$, it can be observed which frequencies are expected to have a damping and which are expected to have an amplification. This is helped by the resonance peaks and valleys being purely resistive. Therefore it can be assumed that observing the sign of the real part of $V_{i,j}[1]$ it is possible to accurately indicate whether the impact of a filter is damping or amplification at the specific resonance point.

The accuracy of the First Order Coefficient Homotopy Method depends on how well the power system is modelled, as a more detailed modelled power system will give a more precise admittance matrix, which the method is based on. It is not clear at this point how much the results are being impacted by not modelling the lower voltage transmission levels and the distribution grid.

Several of the results of the First Order Coefficient Homotopy Method, shown for the Large System, indicated that the busbar with the injection would not be the best busbar to place a filter in. Two things are typically needed to create harmonic voltage distortion somewhere in the system, one being a harmonic current injection and second a resonance condition. If a filter is placed at the busbar with the harmonic injection and the filter does not affect the resonance condition the harmonic distortion is likely to remain high. If a filter is placed in a busbar which removes or severely dampens the resonance condition the harmonic voltage distortion will be significantly reduced.

Actual Filter Importance

After the First Order Coefficient Homotopy Method has identified a number of potential filter position candidates an actual filter has to be implemented, so the final system voltages after filter implementation can be obtained. If the method showed that several resonance peaks at different frequencies could be mitigated with a specific filter position, the filter still needs to be designed to be able to mitigate at the given frequencies. If a ST filter is tuned to the first resonance peak, and implemented at the found filter location, it is possible that the mitigation will not be seen at a resonance peak at a higher frequency, as the ST filter will have a small impact at the higher frequency, due to its impedance profile. So even though the First Order Coefficient Homotopy Method identifies a potentially good filter location for a resonance peak, the final mitigation will depend on if the actual filter is designed to mitigate at the specific frequency of the resonance points. Due to the C-type filter's damped characteristics the results from Chapter 6 showed that even though the specific filter tested for was tuned to be most effectful close to the first resonance peak, the other two resonance peaks also saw significant mitigation, due to the

C-type filters impedance profile. A C-type filter with a low quality factor is therefore a very good filter candidate to be used for the purpose of global filter placement as it able to mitigate at several frequencies in the network.

The First Order Coefficient Homotopy Method gives relative differences between the impact of filters positions for specific frequencies when observing from a busbar. If a specific resonance peak is to be mitigated the values of $|V_{i,j}[1]|$ for the different filter positions will also indicate how large a filter that is needed to mitigate the specific resonance peak. A filter position with a large value of $|V_{i,j}[1]|$ will need a smaller filter in order to achieve the same level of mitigation as a filter position with a small value of $|V_{i,j}[1]|$. A smaller filter will mean less investment costs, therefore the incentive should be to select the most impactful filter position before starting on the filter design, as it is possible that a smaller filter will be sufficient.

7.2 Usability in Connection to Optimisation Methods

The First Order Coefficient Homotopy Method is in its current stage not to be used as a final optimisation method, as it will only give indications and not a final value of the impedance after implementation of a filter. What it can be used for is a screening of an established system, and thus the possible filter locations can be limited to those locations which are indicated to have the largest effect on resonance peaks of interest. What makes the First Order Coefficient Homotopy Method good as an early screening is that it does not require any filter parameters in order to give results about which resonances are being affected the most in each filter location.

After the screening has been done using the First Order Coefficient Homotopy Method, a brute force method can be used on the filter locations, which the method showed to have the most effect on the resonances of interest. How the brute force method is done depends on what type of filter is wanted and how many resonances the filter should attempt to dampen. The results shown in Chapter 6 is only showing results for one busbar with one injection, however the objective of a global filter placement would be to be able to attenuate several resonances, in a number of busbars throughout the system. It was found when examining different busbars in the Large System that in general the resonance peaks for the different busbars were at the same frequencies but with different magnitudes. If this keeps being the tendency for a more accurately modelled system it should be easier to use the method to indicate a global filter placement which is effective at several busbars.

It was also seen that a resonance peak could effectively be removed by placing a filter in one of the busbars in a ring circuit, if the ring circuit was the reason the resonance

peak was created. This was seen for the second resonance peak highlighted in Appendix F. The validity of this result depends on how much the detailed modelling of the system, including the 150 kV level, changes the impact of the ring circuit.

If the most dominant emission sources are known, an example being HVDC-LCC connections emitting characteristic harmonics, the amount of data that has to be checked can be limited to the system's busbars, with injection from the specific busbars where the harmonic sources are located. Traditionally filters have been placed at the sources of the harmonic emission in an attempt to prevent the spread of harmonic issues, a well known case being the filtering at HVDC-LCC connections. If the number of emission sources increases, an example being increased harmonic emission from lower voltage levels, it could become too excessive to place filters at all potential emission sources. It also becomes difficult to locate the emission sources and the angles of the emission. This is where the use of a global filter strategy could have its purpose, as less filters would be able to cover several busbars, by removing certain resonance conditions from the system. However if the 400 kV level continues to be dominated by the emission from HVDC-LCCs it would make more sense to investigate whether the filtering that is already in place at the HVDC-LCC locations is effective enough.

7.3 Effect of a Continues Changing Power System

The usefulness of the First Order Coefficient Homotopy Method can be limited by the uncertainties with a large and ever changing power system. A large power system results in lots of resonances which may overlap. The method will give indications for the resonances overlapping as a single resonance, therefore it will not be able to distinguish between these resonances. For that case the method will still indicate which filter position dampens the resonance frequency the most, but it can not be used to gain a clear understanding of what parts of the system impacts the seen resonances. Another problem with the Homotopy Method, and other harmonic studies in general, is that the impedance envelopes of the system changes, due to changes in the power system. The extent of the change depends on each individual power system as a more meshed system and strong system will likely be less impacted by the implementation of a component, like a new line in the system, compared to a less meshed system. There is an increase in the number of radial lines in the power system due to the continued establishment of offshore WPPs, which are being connected further away from shore, thus increasing the length of the radial lines.

An example of a large change in a power system is the grid strengthening of the southwest part of DK1 done by the Danish TSO Energinet. The grid strengthening is required in order to be able to handle the increased power flow from the upcoming

HVDC connections in that area, mainly due to the establishment of the Viking Link HVDC connection [3]. Not only is additional lines being installed resulting in a more meshed system, some existing OHLs are replaced by UGCs, which is seen to have a large impact on the system impedances, due to the larger capacitance and lower series impedance of UGCs compared to OHLs. The expansion of the power system is however mostly predictable as it is planned ahead of time and reports on the development of the power system are conducted, with Energinet having the RUS report [4], which predicts the future projects in the transmission system. However this starts to become difficult to manage when political decisions can change the planned grid changes, especially in terms of the ratio of OHLs to UGCs in the new projects. This was highlighted in Chapter 1 where it was described that by law the Danish TSO can be demanded to compensate for the establishment of new 400 kV OHLs by converting existing OHLs to UGCs on the lower voltage levels. This makes it extremely difficult to plan ahead in terms of filter positions. If it was completely fixed how the next 30 years of grid changes is going to be, it would be easy to select a number of filter positions, which would continuously give a good performance even as the grid changes. However as it was seen in Chapter 6 a major grid change, such as the implementation of a line can significantly affect a filter position's effectiveness, especially at the busbars which are directly affected by the grid change.

A change in the system impedance, such as when a line or power system component is implemented, also occurs when a line or power system component is disconnected from the grid. Therefore when a contingency occurs in the power system the impedance of the system can be affected. The system impedance thus changes depending on the operating condition of the system, which also includes the loading of the system, and can affect the effectiveness of the filters already implemented in the system. An example of this could be if the newly implemented EDR-IDU line had a fault and the line was disconnected from the rest of the system. In that case the filter positions' effectiveness would revert back to what was seen before the implementation of the line, which would again change the effectiveness of several filter positions.

The change of system impedance can affect already implemented filters, as the resonances might change enough that a filter which previously damped a resonance peak, has no effect on that resonance peak, as it will be at a lower or higher frequency. It will be even worse if the new frequency of the resonance peak is at a point with no damping from other filters and at a frequency which has seen to have harmonic emission. The use of C-type filters can to some degree alleviate the problem with the resonances moving away from the tuned frequency, due to their low quality factor.

A very advantages usage of the First Order Coefficient Homotopy Method is that if a certain part of the power system is the reason a specific resonance is created the method will illustrate this, as seen for the second resonance peak of the Large System

in Appendix F. If a change in the system is implemented far away from the part, which created the given resonance point, it can be expected that the resonance point will be mostly affected by the part of the system which created it, which was also seen to be the case for the second resonance peak in the Large System. If the resonance peak is created by a part of the system which is subject to a major change it clearly makes sense that the method's results, before the change in the system, will not necessarily be applicable after the change, and the method has to be run again for the new system configuration. It can thus in principle be mapped out, by using the method, which parts of the system affects specific resonance points. Having this knowledge it becomes easier to predict if a filter might become redundant after a specific change in the power system.

7.4 Data Management of Results

A problem with the Homotopy Method and other methods of its likeliness, especially for a large system, becomes the increasing amount of data the engineer has to handle. If only one busbar with one injection is being observed it is manageable, however the idea behind the global filter positioning is to mitigate at several busbars from one filter position. Therefore it may be too cumbersome to view the results graphically as was shown in Chapter 6 and a ranking system has to be implemented as was also shown in Chapter 6. If a filter position ranking is in top 5, for the resonance peaks, in all observed busbars with injections from other busbars, the method has indicated that the filter position would be a good candidate for a global filter solution. In order to use this type of ranking the frequency of the resonance peaks has to be known before the ranking can be applied to the specific resonance frequencies. Once a number of filter positions has been chosen a brute force method could be used with actual filter values to find the best filter position.

7.5 Implementation with PowerFactory

By extracting the system impedance matrix in PowerFactory through the frequency sweep function, the First Order Coefficient Homotopy Method can be implemented on large pre-built systems. This is a big advantage due to the difficulty of implementing lines modelled from geometrical input parameters in MATLAB. This is much easier in PowerFactory as the software has been designed specifically with the purpose of enabling the lines to be relatively easily modelled from geometrical input parameters. An example system was made in PowerFactory, which is not shown in the report, which included geometrically modelled UGCs, transformers and shunt reactors. By extracting the impedance matrix of the example system the First Order Coefficient Homotopy Method was applied.

It was found that the method predicted the most impactful filter locations correctly in the more detailed system, which would be expected as the method is based on the impedance matrix. TSOs and other operators most likely have a model of the system, and some even a planning model for the future. Therefore it would simply be a matter of pressing a button, if a script was prepared to extract the impedance matrix, to get the data required for the method and do the calculations.

7.6 Unbalanced Power System

The results of the First Order Coefficient Homotopy Method, shown in this report, have only been conducted using the positive sequence. The method should also be applicable on the negative and zero sequence. There can also be couplings between the three sequence components as the power system is often highly asymmetrical, with the coupling between the positive and negative sequence having the largest impact [11]. As long as the admittance matrix is detailed with significant accuracy, including inter-sequence couplings, the method should be able to indicate the correct filter position impacts for an asymmetrical system.

7.7 Summary of Discussion

As described in this chapter there is a number of advantages and disadvantages related to the First Order Coefficient Homotopy Method. The following lists are therefore created to provide an overview of the advantages and disadvantages of the method.

Advantages

- The method predicts with good accuracy the most impactful filter positions for an observed busbar, with injection at a chosen busbar.
 - The method only needs the admittance matrix of the system, however due to some commercial software not being able to extract the admittance matrix, the impedance matrix can also be used as it is the inverse of the admittance matrix.
- The method can predict the most impactful filter positions without the utilisation of a pre-designed filter.
 - If the most impactful filter locations were to be found by a pre-designed filter, a complicated process of choosing which type of filter to use, have to be conducted. Afterwards the pre-designed filter would most likely need to be

adjusted again after the most impactful filter position has been found. The First Order Coefficient Homotopy Method is therefore a faster method in obtaining the most impactful filter positions.

- Analysing the results of the method a better understanding of the harmonic behaviour of the system can be obtained.
 - The method can give an understanding of which sections of the system affects specific resonances. This is especially useful as changes to the system is implemented, so that it can be predicted if filters already installed become redundant.
 - Through the use of the imaginary values of the filter position results, an understanding of the relative shift in resonance frequencies between filter positions can be obtained and identify potential anti-resonances. Larger imaginary values around the resonance peak, for a specific filter position, indicate that the frequency shift for the resonance peak will be larger, compared to a filter position with lower imaginary values.
- The method can easily be combined with power system software like PowerFactory and alike, in order to apply the method on large and highly detailed power systems.

The work done in this report is only an initial introduction and exploratory work of the First Order Coefficient Homotopy Method, and therefore additional advantages might exist, with some potential advantages discussed in Chapter 9.

Disadvantages

- As the method does not utilise a pre-designed filter a final result for the harmonic distortion can not be obtained directly from the method.
- The method can not alone be used in a final optimisation method.
 - At some point after the most impactful filter positions have been obtained, an actual filter has to be designed and implemented in the system model in order to obtain the final results.
 - The final value of anti-resonances and shifts in frequency of resonance points can first be accessed after implementation of the designed filter.
- Using the absolute values of the results from the method is not accurate in the case of a resonance peak followed immediately by a resonance valley. In a case this was seen to be an issue when the frequency difference between the resonance peak and valley was 36 Hz.

- Using the real values of the method's results fixes this problem as the predicted damping and amplification can be separated.
- As for all methods of this kind data management can become an issue, especially for large systems.
 - Utilising a simple ranking system is a way to alleviate this issue, however the ranking solution has the problem of inaccuracy in that the same ranking will be given to a given filter position, whether the results of the filter position are close or far away from the results of other filter positions.

Chapter 8

Conclusion

The goal of this report is to investigate semi-analytical methods, which can be utilised to examine the impact of filter implementation in the power system, in order to further the idea of global filter placement. The method developed in this project is a homotopy analysis method, based on the frequency scan method typically used for harmonic studies. Setting the voltage as a power series, the voltages in the system can be obtained after a filter is implemented. It is found that examining the first order coefficient of the power series it is possible to get indications of the most impactful filter locations in the system, without specifying an actual filter. The first order coefficient can not give the final voltages in the system, after a filter implementation, as this will be determined by the actual filter. The first order coefficient can therefore not be used as a final optimisation method, as it gives a relative difference in impact of the filter positions and not a quantifiable value. The first order coefficient should therefore be used as an early screening of a system to identify a number of filter positions with large impacts, such that these filter positions can be further investigated with actual filters. The clear advantage of using the first order coefficient is therefore that the most impactful filter locations can be identified, without specifying an actual filter. In the Further Work chapter additional possible uses for the Homotopy Method is discussed, including; Optimisation method application, further development for better tracking of anti-resonances and application for other passive power system components.

The First Order Coefficient Homotopy Method was tested on a four busbar example system. The results showed that the method is capable of giving indications of the different filter positions' impact on resonance points, without implementing an actual filter. The method correctly indicated the most impactful filter positions for all the resonance peaks, in the frequencies of interest, when compared to the implementation of a C-type filter in the system. The First Order Coefficient Homotopy Method was also applied on a larger example system, with the structure and line data of the 400 kV Danish DK1 system. The method again proved to be able to predict the most impactful filter positions seen from a specific busbar in the system. By ranking the most impactful filter positions given by the First Order Coefficient Homotopy Method for specific resonances and comparing with a ranking of the most impactful filter positions when a C-type filter was implemented, it was found that the maximum ranking difference was 3 in a system of 15 possible filter locations. The ranking differences can be explained by the results of several filter positions being very close, or in the case of the largest ranking difference when a resonance peak is immediately followed by a resonance valley, which is a special case

where the use of the absolute values of the First Order Coefficient Homotopy Method leads to slightly inaccurate results.

An important finding by the use of the First Order Coefficient Homotopy Method was that for some resonance peaks the filter position in the busbar where the harmonic emission is located, will not always be the most impactful filter position. When a resonance peak, seen from a busbar with a harmonic injection at the same busbar, is created by an interaction with a specific part of the system the best filter placement is in some cases found to be in the specific part of the system, which has created the resonance and not in the observed busbar with the harmonic injection.

Implementing a change in the large example system, in this case a new line, changes the impact of the filter positions. Generally busbars directly impacted by the connection of the new line have the largest changes in the effectiveness of their filter positions, but the system change also affect the effectiveness of other filter positions in the system. As the power system continues to change filters may become redundant and unless the changes to the system can be known years beforehand it becomes problematic to select a global filter position, which can mitigate harmonic distortion in several parts of the system. However if the major changes to the grid can be predicted, it will be possible to compare the results for different grid scenarios, and select a number of filter positions which will continue being impactful as the system continues to change.

The absolute value of the first order coefficient can be used to indicate the most impactful filter positions for most cases. Using the real and imaginary parts of the first order coefficient will give a more detailed indication. The real part can indicate if the implementation of a filter will give damping or amplification, at the specific frequency, given by a negative or positive value respectively. The imaginary part will give indications of how much the resonance peak will shift in frequency. A filter position with a large imaginary value of the first order coefficient around the resonance point will move a given resonance peak more than a filter position with a lower imaginary part, if the same filter is implemented in one of the filter positions. This can help in understanding where anti-resonances will appear. The direction of the shift in frequency depends on the filter impedance profile at the frequencies at and around the given resonance peak. If the impedance profile at the resonance peak is inductive it has a tendency to shift to a higher frequency, while a capacitive impedance characteristic has a tendency to shift the resonance peak to a lower frequency. In order to get the final values for the resonance peak shift an actual filter has to be designed and implemented in the system.

As the first order coefficient method is based on the frequency scan of the system the detail of the admittance matrix will determine the accuracy of the results. Using PowerFactory and the frequency sweep function it is possible to implement the method to pre-designed systems, which makes it easy to construct an accurate admittance matrix.

Chapter 9

Further Work

This chapter present topics in the report that could be further investigated. The topics mentioned are additions to the methods presented earlier in the report or areas of the report which can be further explored.

Multiple Injections

In the report the First Order Coefficient Homotopy Method was used showing singular entries in the $\mathbf{V}[1]$ matrix. This means that the impact of different filter positions was tested on an observed busbar, with a single current injection. It would be beneficial if the method could be applied to a single busbar, with several injections at once, thus reducing the calculations needed to be made. If it is known that there are a number of large emission sources in the system it would be possible to set up a current injection matrix containing the known large emission sources.

Optimisation Method

In harmonic studies resonance points are of most interest if they are at or near characteristic harmonics, as these are the harmonics with the highest emission. A frequency scan can be used to locate resonance peaks which should be mitigated in order to reduce the harmonic distortion below the limits. Thus the objective is to minimise the maximum points in a frequency scan, and the optimisation algorithm type called minimax algorithms should fit to this objective [27]. The minimax algorithms will find the highest points, meaning the resonance peaks and minimise them. The objective function can be represented by $f(x, w)$ where the solution is to find a variable x that minimises the maximum of $f(x, w)$ as a function of w . The minimax problem pertaining to objective function $f(x, w)$ can be stated as in Equation 9.1 [27].

$$\text{minimise } \max f(x, w) \tag{9.1}$$

Various constraints can then be set up for the filters including filter type, filter parameters and number of filters. Other constrains would include the maximum allowed harmonic limit for each harmonic order.

Applying an optimisation method to the First Order Coefficient Homotopy Method would require a different type of optimisation method. The First Order Coefficient Homotopy Method is not accurate at determining the final impedance value and it will

therefore be difficult to implement as a final optimisation method. Instead the optimisation method should be set up to locate the most important resonance points in the system in need of mitigation. Applying the method for all the busbars in the system, the filter positions affecting the chosen resonance points the most can be found. In the end a select few filter positions, which shows good performance overall in the system can be chosen, and actual filters can be designed and implemented from that point on.

Homotopy Method Applied to Other Power System Elements

The First Order Coefficient Homotopy Method was able to give indications of how much each filter location would affect the resonance points in the system seen from a specific busbar. The method did not make use of the parameters of a filter. In theory other passive shunt elements components than a filter, should be able to be used. The value of $|V_{i,j}[1]|$ should be the same independent on the type of shunt element to be investigated. The effect of the shunt element on the impedance in the system will still depend on its impedance profile. An example could be the implementation of a shunt reactor, which will shift the resonance points slightly due to its inductive behaviour.

What would be interesting to investigate is if the First Order Coefficient Homotopy Method can be modified to be applicable on other passive power system components than shunt elements. This could be the addition of transmission lines or transformers in the system where the method would indicate how a new transmission line or transformer affects the different resonance peaks in the system. The filter position matrix **A** would have to include not only the shunt admittance on the diagonal, but also the series impedance on the off-diagonal and the method will then depend on two parameters, compared to a single parameter with a filter. It should be examined if the values of the line on the diagonal, is enough to get the correct indications. This could however lead to large errors as OHLs and transformers have larger values of series impedance than shunt admittance, the error might be smaller with a cable due to its higher shunt admittance. This is however all speculations as it is unclear how the method should be applied when there is several entries in the **A** matrix.

Homotopy Method for Tracking Resonance Shifts

An idea for a method based on extended use of the Homotopy Method is presented here briefly, with focus on its concepts. The method will be referred to as Small-signal Method as it is based on small-signal analysis, which is used to approximate non-linear equations with linear equations. This is done by assuming the non-linear equations are linear at the point of interest. The small-signal means its a small value, in this case the implementation

of a filter, compared to the rest of the system, in this case the system impedance, as the system impedance will act like a large-signal. The method should be able to satisfy the three objectives in Chapter 5 which were:

1. Ability to identify which resonance peaks are affected by implementation of filters in different busbars.
2. Ability to identify which filter position in a system will have the most impact on resonance points, at a given busbar, in term of magnitude reduction.
3. Ability to identify which direction in terms of frequency each resonance point will move after the filter implementation.

The Small-signal Method will depend on two variables, with the first being ω and the second being c . The first variable ω is naturally introduced as the method takes base in the frequency scan method, which uses the admittance matrix that depends on ω . The second variable c is introduced in the frequency scan method, by implementing a filter, with pre-specified parameters, and the variable c will work as an active scale from 0-1 multiplied with the filter to gradually shift the parameters of the filter. The goal of the method is to calculate the linearised change of the voltage, calculated by the frequency scan method, with respect to the active scale c at the resonance peaks when ω is changed. The directional derivatives are then used in which a graphical representation of this is to first find the change in voltage given as a direction (z) when c is changed, which will give one direction (x) and when ω is changed, which will give another direction (y). The two directions are then combined to form the directional derivatives.

To solve non-linear equations series solutions are often used, however since the method depends on two variables ω and c , the tensor multiplication is used as given in Equation 9.2, where the term $[1,0]$ means the term $V_{i,j}(\omega, c)$ only depends on the scale c , as ω is kept constant, and for $[0,1]$ the term $V_{i,j}(\omega, c)$ only depends on the angular velocity ω , as c is kept constant.

$$V_{i,j}(\omega, c) = V_{i,j}[0] + V_{i,j}[1,0]\Delta c + V_{i,j}[0,1]\Delta\omega + \dots \quad (9.2)$$

The term $V_{i,j}[0]$ is found from the frequency scan method with no filter implemented. The term $V_{i,j}[1,0]\Delta c$ is found using a similar method to the Homotopy Method and the term $V_{i,j}[0,1]\Delta\omega$ is found using partial derivatives.

After the terms $V_{i,j}[0]$, $V_{i,j}[1,0]\Delta c$ and $V_{i,j}[0,1]\Delta\omega$ have been calculated, the absolute value of the partial derivatives of $V_{i,j}(\omega, c)$ with respect to the angular velocity ω at the resonance peaks are to be calculated. The goal is to find a relation between Δc and $\Delta\omega$ at each resonance peak, such that the direction of the resonance peaks can be found, by seeing how much $\Delta\omega$ changes when Δc changes by one unit, which are the directional derivatives.

Bibliography

- [1] WG-C4/B4.38. *Network Modelling for Harmonic Studies*. CIGRE, 2018.
- [2] Filipe Faria da Silva and Claus Leth Bak. *Electromagnetic Transients in Power Cables*. Handbook ISBN:978-1-4471-5235-4. Springer, 2013.
- [3] Energinet. *Technical Issues Related to New Transmission Lines in Denmark - West Coast Line from German border to Endrup and Endrup-Idomlund*. Tech. rep. Energinet, 2018.
- [4] Energinet. *Reinvesterings-, Udbygnings- og Saneringsplan 2017 (RUS17)*. Tech. rep. Energinet, 2017.
- [5] Energinet.dk. *Kabelhandlingsplan*. Tech. rep. Energinet.dk, 2009.
- [6] Regeringen Lars Løkke Rasmussen III. *Energiaftale*. Tech. rep. Regeringen, 2018.
- [7] Energistyrelsen. *Offshore Wind Power in Denmark*. : 27-02-2018. <https://ens.dk/ansvarsomraader/vindenergi/eksisterende-havvindmoelleparker-og-aktuelle-projekter>, 2013.
- [8] C. F. Jensen, Ł. H. Kocewiak, and Z. Emin. *Amplification of harmonic background distortion in wind power plants with long high voltage connections*. Tech. rep. Cigre, 2017.
- [9] C. F. Jensen. *Harmonic background amplification in long asymmetrical highvoltage cable systems*. Tech. rep. Electric Power Systems Research, 2018.
- [10] Forsynings- og Klimaministeriet Energi-. *Markant færre master og luftledninger i Syd- og Vestjylland*. : 18-02-2019. <https://efkm.dk/aktuelt/nyheder/2018/dec/markant-faerre-master-og-luftledninger-i-syd-og-vestjylland/>, 2018.
- [11] Chris Skovgaard Hansen and Kristian Didriksen Lund. *Harmonic Modelling & Analysis of a Cable Based Transmission System*. Tech. rep. Aalborg University, 2016.
- [12] R. C. Dugan et al. *Electrical Power Systems Quality*. ISBN:0-07-138622-X. Tata McGraw-Hill, 2003.
- [13] J. C. Das. *Power System Harmonics and Passive Filter Design*. ISBN:978-1-118-86162-2. Wiley, 2015.
- [14] J. Arrillaga and N.R. Watson. *Power System Harmonics*. ISBN:978-0-470-85129-6. Wiley, 2004.
- [15] IEC. *Electromagnertic compatibility (EMC) - Part 3-6*. Tech. rep. IEC, 2008.
- [16] Ewald. F. Fuchs and Mohammad A. S. Masoum. *Power Quality in Power Systems and Electrical Machines*. ISBN:978-0-12-369536-9. Elsevier, 2008.
- [17] WG-14.30. *Guide to the specification and design evaluation of AC filters for HVDC systems*. Tech. rep. Cigre, 1999.

- [18] Yao Xiao, Jie Zhao, and Shijie Mao. *Theory for the Design of C-type filter*. Tech. rep. IEEE, 2004.
- [19] Wojciech Tomasz Wiechowski. *Harmonics in transmission power systems*. Tech. rep. Aalborg Universitet, 2006.
- [20] F. Faria da Silva. *Analysis and simulation of electromagnetic transients in HVAC cable transmission grids*. Tech. rep. AAU and Energinet, 2011.
- [21] F. Faria da Silva, C.L. Bak, and P.B. Holst. *Study of Harmonics in Cable-based Transmission Networks*. Tech. rep. CIGRE, 2012.
- [22] A. Medina et al. *Harmonic Analysis in Frequency and Time Domain*. Tech. rep. IEEE, 2013.
- [23] Shijun Liao. *Beyond Perturbation: Introduction to the Homotopy Analysis Method*. ISBN:9781584884071. Chapman and Hall/CRC, 2003.
- [24] Yavuz Ugurlu, Dogan Kaya, and Ibrahim E. Inan. *Comparison of three semi-analytical methods for solving (1 + 1)-dimensional dispersive long wave equations*. Tech. rep. Elsevier, 2010.
- [25] James V. Lambers and Amber C. Summer. *Explorations in numerical Analysis*. Handbook ISBN:978-9813209961. World Scientific, 2015.
- [26] Energinet. *Transmission System Data*. : 24-04-2019. <https://en.energinet.dk/Electricity/Energy-data/System-data>, 2017.
- [27] Andreas Antoniou and Wu Sheng Lu. *Practical Optimization*. Handbook ISBN:978-0-387-71106-5. Springer, 2007.
- [28] Shady H. E. Abdel Aleem and Ahmed F. Zobaa. *Optimal C-type filter for harmonics mitigation and resonance damping in industrial distribution systems*. Tech. rep. Springer, 2016.
- [29] Energinet. *Ancillary Services to be Delivered in Denmark. Tender Conditions*. Tech. rep. Energinet, 2017.
- [30] Oscar Lennerhag. *Power System Model for Resonance Studies*. Tech. rep. Independent Insulation Group, 2018.
- [31] ABB. *XLPE Land Cable Systems - User's Guide*. Tech. rep. ABB, 2012.

Appendix A

Sensitivity Analysis of C-type Filter Parameters

This appendix conducts a sensitivity analysis on the parameters of the C-type filter in order to see what parameters affect the filtering performance and the fundamental frequency losses. Figure A.1 shows impedance characteristics of C-type filters, modelled in PowerFactory, with different Q_1 and q values, but same tuned frequency and nominal voltage. For the three tested filters with a $Q_1 = 100$ it can be seen that the impedance characteristics are similar from the fundamental frequency up towards the 2nd harmonic order, due to the filters having the same Q_1 .

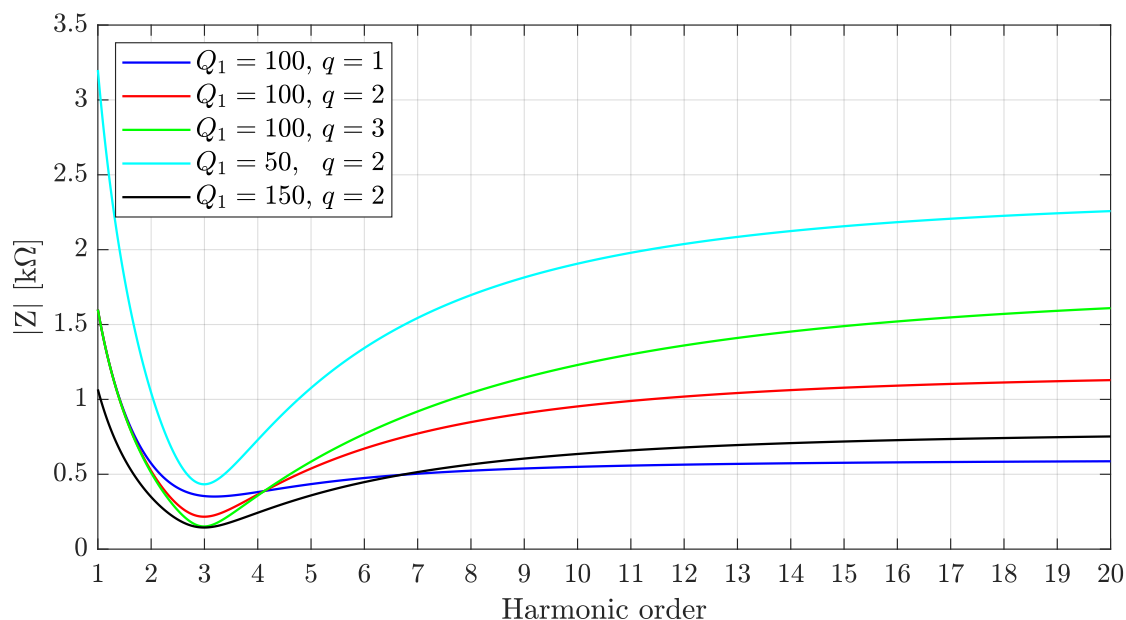


Figure A.1: C-type filter tuned to the 3rd harmonic order with different Q_1 and q values.

For the same filters it is also seen that the smaller the quality factor is, the flatter is the impedance characteristic, at and after the tuned frequency. A higher quality factor will thus give better attenuation at the tuned frequency, but will not mitigate the harmonics above the tuned frequency as effectively. From observing the three filters with the same q , but different Q_1 , it can be seen that a higher Q_1 will give better attenuation of all the harmonics shown within the spectrum. This also highlights that in theory a C-type filter can have as good attenuation at the tuned frequency as a ST filter, however a large Q_1 is

required, which can be expensive and cause problems related to the large flow of reactive power at fundamental frequency, which potentially has to be compensated with shunt reactors.

Losses at Fundamental Frequency

The power losses of the filter at fundamental frequency is a very important parameter as higher losses lead to higher operating costs. The C-type filter is specifically designed to have low losses at fundamental frequency by having C and L , in Figure A.2, resonate at the fundamental frequency, thus bypassing R . Under the conditions that the C and L branch is perfectly tuned to the fundamental frequency, there being no frequency deviation from the fundamental frequency and losses in the capacitors and inductor are neglected, the filter would have no losses at the fundamental frequency [28]. This is however all assumptions which by varying degrees are not true in a real system. Due to component manufacturing tolerances the C and L branch might not be perfectly tuned to the fundamental and furthermore the frequency of the power system is allowed to vary within ± 200 mHz of the fundamental before frequency regulation reserves are activated [29]. As neither capacitors or inductors are ideal components in reality resistive losses will occur. The following part will investigate the power losses at fundamental frequency when the winding resistance in the inductor R_L is taken into consideration. In Figure A.2 the schematic of a C-type filter is shown, with the dashed box indicating the inductor parameters.

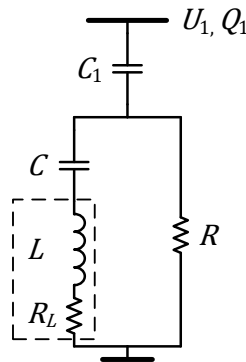


Figure A.2: C-type filter diagram, with winding resistance of inductor R_L .

It is assumed that the C and L branch is tuned perfectly to the fundamental frequency and that dielectric losses in the capacitor can be neglected. The resistance of the inductor R_L is determined by the quality factor of the inductor, q_L , which is calculated as seen in Equation A.1. It should be noted that the way the quality factor is calculated for the inductor itself is the inverse of the way the quality factor is calculated for the C-type filter

itself, which was shown in Equation 2.9. This is due to R and L being in parallel while R_L and L are in series.

$$q_L = \frac{2\pi fL}{R_L} \iff R_L = \frac{2\pi fL}{q_L} \quad (\text{A.1})$$

As the C and L branch acts as a short-circuit at the fundamental frequency the parallel branches only include resistances and Equation A.2 can be used to obtain the total resistance R_T .

$$R_T = \frac{R \cdot R_L}{R + R_L} \quad (\text{A.2})$$

Next the current through the filter, I_{filt} , has to be calculated, as seen in Equation A.3, where V_{filt} is the line-to-line voltage at the filter position. In the equation V_{filt} is converted to line-to-ground as the filter is a shunt element.

$$I_{filt} = \frac{V_{filt}}{Z \cdot \sqrt{3}} \quad (\text{A.3})$$

The earlier calculation for the impedance of the filter, seen in Equation A.4, can be updated to include R_L , as seen in Equation A.5. The difference in the impedance is not significant at the fundamental frequency, due to the impedance of C_1 being far larger than R_L at the fundamental frequency, as otherwise the losses in R_L would be unacceptable.

$$Z(\omega) = \left(\frac{1}{R} + \frac{1}{j\omega L - j(\omega C)^{-1}} \right)^{-1} + \frac{1}{j\omega C_1} \quad (\text{A.4})$$

$$Z(\omega) = \left(\frac{1}{R} + \frac{1}{R_L + j\omega L - j(\omega C)^{-1}} \right)^{-1} + \frac{1}{j\omega C_1} \quad (\text{A.5})$$

The power loss at fundamental frequency can then be calculated from Equation A.6. The multiplication by 3 is due to the power losses being for a three-phase filter.

$$P_{loss} = 3 \cdot I^2 \cdot R_T \quad (\text{A.6})$$

By using the symbolic toolbox in MATLAB a symbolic equation can be set up, as seen in Equation A.7, so that the different variables' impact on the fundamental frequency power loss can be examined.

$$P_{loss} = \left| \frac{Q_1 \cdot V_{filt}^2 \cdot \omega_F^2 \cdot \omega_0 \cdot q \cdot (\omega_0^2 - \omega_F^2) \cdot (\omega_F + \omega_0 \cdot q \cdot q_L)}{U_1^2 \cdot (\omega_F^2 \cdot \omega_0 \cdot q + \omega_0 \cdot j - \omega_0^3 \cdot q \cdot q_L \cdot j - \omega_0^2 \cdot \omega_F \cdot j + \omega_F^2 \cdot \omega_0 \cdot q \cdot q_L \cdot j)^2} \right| \quad (\text{A.7})$$

As ω_F is fixed at $2\pi 50$ it is not a variable and h_0 , being the harmonic order the filter is tuned to, can be used to simplify the equation further, as seen in Equation A.8. The results of the equation matches with PowerFactory when calculating the resistive losses of the filter during a fundamental frequency load flow.

$$P_{loss} = \left| \frac{Q_1 \cdot V_{filt}^2 \cdot h_0 \cdot q \cdot (q \cdot q_L \cdot h_0 + 1) \cdot (h_0^2 - 1)}{U_1^2 \cdot (h_0 \cdot q - h_0^2 \cdot j - h_0^3 \cdot q \cdot q_L \cdot j + h_0 \cdot q \cdot q_L \cdot j + j)^2} \right| \quad (\text{A.8})$$

The equation now has six variables which dependent on the filter design and operating conditions can change. Looking at the equation it becomes evident that if the voltage over the filter, V_{filt} , matches the nominal voltage of the filter, U_1 , the terms cancel each other out. This means that the losses of the filter at fundamental frequency does not depend on the voltage, if V_{filt} and U_1 are equal at the given operating conditions. If there is a difference between V_{filt} and U_1 it can be seen that there is a quadratic relationship between the voltage difference and the power loss, due to both V_{filt} and U_1 being squared in the equation. Another observation from Equation A.8 is that there is a linear relationship between Q_1 and the power loss at fundamental frequency. This means that if Q_1 is doubled then the power losses at fundamental frequency are also doubled.

In order to investigate the remaining variables each variable are investigated graphically, while the other variables are fixed. Unless otherwise noted on the following figures Table A.1 shows the fixed values for the variables. q_L remains a variable in all the figures and does therefore not appear in the table.

Variable	Value
Q_1 [Mvar]	100
q [-]	2
U_1 [kV]	400
V_{filt} [kV]	400
h_0 [-]	3

Table A.1: Fixed values for the variables in the equation for the resistive losses at the fundamental frequency.

Figure A.3 shows the fundamental frequency resistive losses in terms of the tuned harmonic order, h_0 , for different values for the quality factor of the inductor, q_L . It should be noted that the y-axis of the figure is set to a logarithmic scale. From the figure it is clear that the closer h_0 is to 1 the larger the resistive losses becomes. It can also be observed that a lower q_L results in larger losses, which would be expected as a lower q_L results in a larger resistance. The reason for the large reduction in the resistive losses as the tuning order gets larger can be found by examining how the inductor value is chosen, from Equation A.9. Due to the h_0 part being in the denominator and being squared the

calculated inductance value, when changing h_0 , will follow a similar tendency to the resistive losses shown in Figure A.3. This means that at a low h_0 the inductance value will be larger, and if the q_L is kept constant R_L will become larger, which results in larger fundamental frequency resistive losses.

$$L = \frac{U_1^2}{(h_0^2 - 1)\omega_F Q_1} \quad (\text{A.9})$$

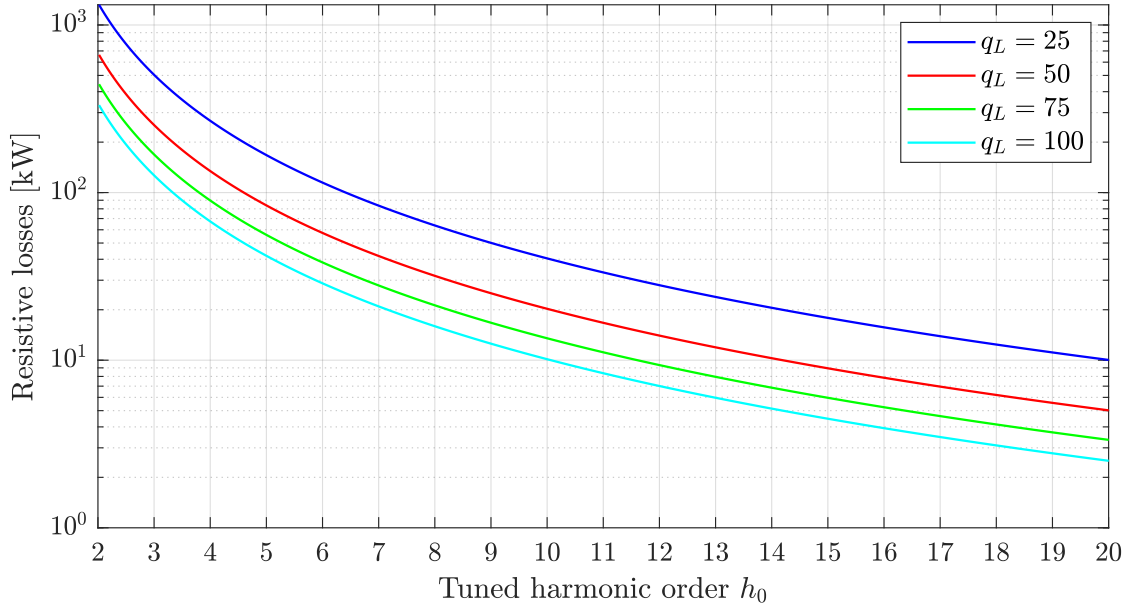


Figure A.3: Fundamental frequency resistive losses of the C-type filter in terms of the tuned harmonic order and the quality factor of the inductor. Y-axis is set as logarithmic scale.

Figure A.4 shows the fundamental frequency resistive losses in terms of the quality factor of the filter, q . It can be seen that if q is very low there is less losses, however within the region of existing filters in the literature [18], which is $q = 1 - 2.3$, the difference is very small, especially as q_L becomes larger. This relationship can be explained by examining Equation A.1, A.2 and A.10, where if q is the only variable, only R is impacted in the product over sum equation for the total resistance. As q is increased the value of R is increased linearly and when R increases its impact on the total resistance R_T decreases, which results in a increase in R_T , as R_T approximates R_L . This can also explain why the shapes of the relationships between the resistive losses and q is slightly different for different values of q_L , as can be seen in the region from $q = 0.1 - 1$ in Figure A.4. When q_L is decreased R_L becomes larger, which brings it closer to the value of R which normally is significantly larger than the value of R_L . For low values of q and q_L the values of the two parallel resistances R and R_L starts to go towards each other which causes relatively lower

losses compared to if q is increased. It should however still be noted, as seen in Figure A.4, that the value of q_L has far more importance for the amount of losses compared to the impact of q .

$$q = \frac{R}{\omega_0 L} \iff R = q \cdot \omega_0 L \quad (\text{A.10})$$

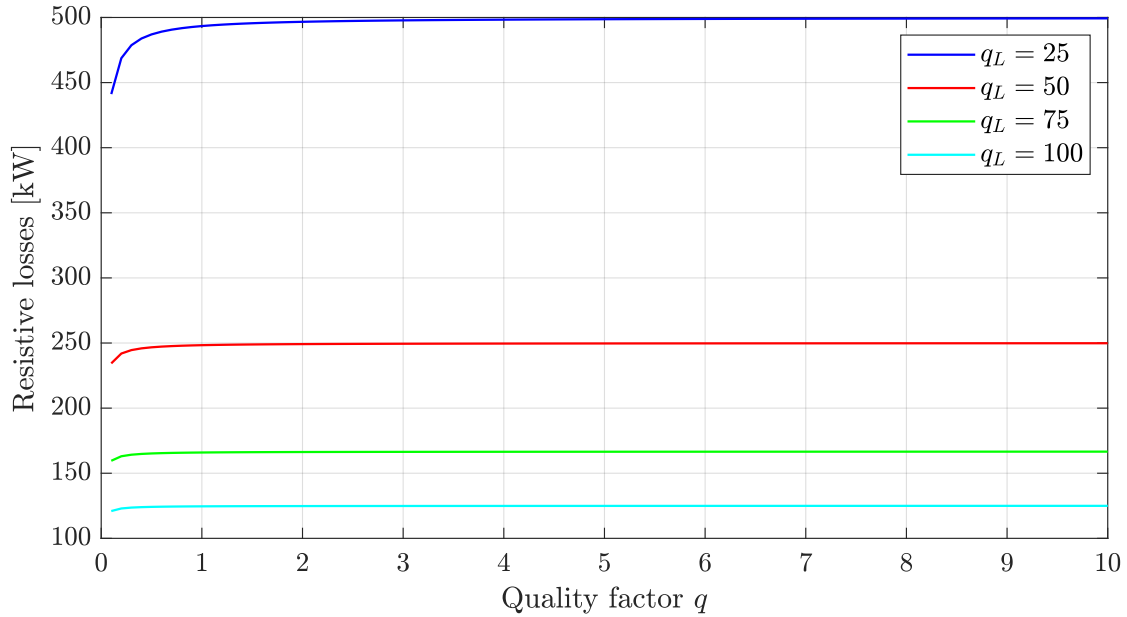


Figure A.4: Fundamental frequency resistive losses of the C-type filter in terms of the quality factor of the filter q and the quality factor of the inductor q_L .

Figure A.5 shows the relationship between the fundamental frequency resistive losses and the quality factor of the inductor, q_L , for a case where all the other variables are assigned values according to Table A.1. It is obvious that a lower q_L leads to larger losses as R_L increases. Again the shape of the relationship, seen in Figure A.5, is primarily determined by Equation A.2, being the product over sum calculation for the parallel resistances.

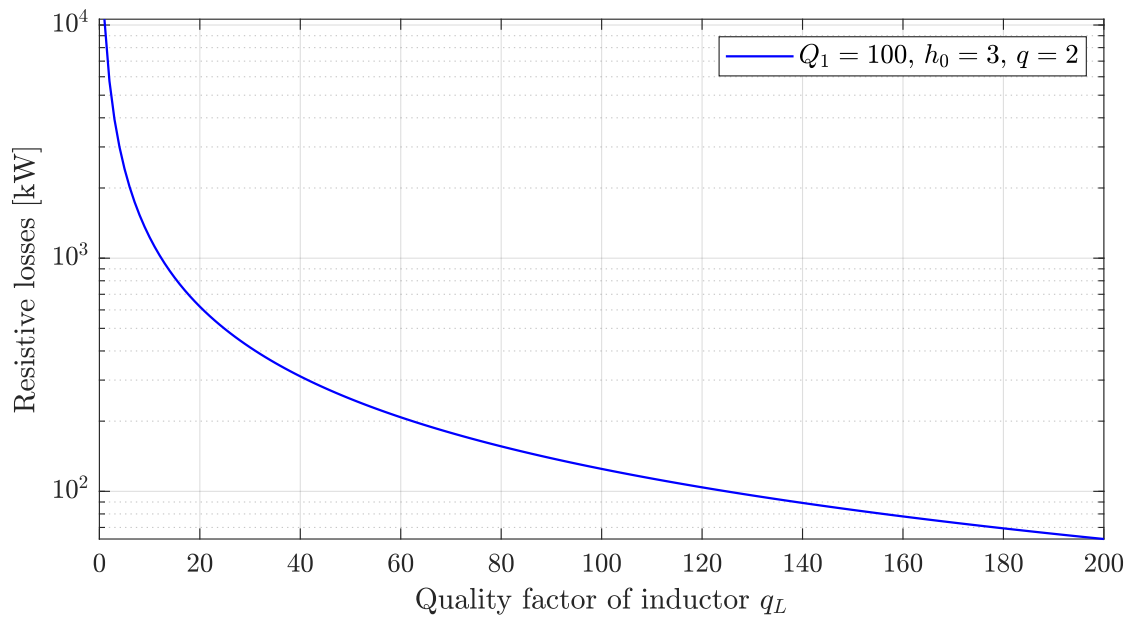


Figure A.5: Fundamental frequency resistive losses of the C-type filter in terms of the quality factor of the inductor q_L . Y-axis is set as logarithmic scale.

Fixing the variables means that special fixed cases are made which only shows the development of the resistive losses for the cases with the specific fixed values. Thus it is theoretically possible that the observed tendencies would change if other fixed values were used for the variables. However as indicated by the above figures there is no sign that radically different tendencies will appear if other fixed values are chosen for the variables.

Discussion of Sensitivity of Filter Values

When the C-type filter parameters have to be chosen a number of considerations have to be made, some of which are listed below.

- Fundamental frequency resistive losses.
- Harmonic mitigation performance.
- Reactive power injection at fundamental frequency.

The three main variables for designing the filter are Q_1 , q and h_0 . As shown above q_L can also be considered a variable, however in contrast to the other variables, which are varied to achieve a specific filter performance, q_L mainly affects the amount of resistive losses at the fundamental frequency.

The value of Q_1 not only determines the injection of reactive power at the fundamental frequency, but also significantly impacts the mitigation performance and the resistive losses at the fundamental frequency. As seen earlier the resistive losses increases linearly with the increase in Q_1 . It was also shown earlier in Figure A.1 that a larger Q_1 increases the harmonic attenuation, thus giving a better harmonic mitigation performance.

The choice of q carries a far larger importance in terms of the mitigation performance, compared to the limiting of the fundamental frequency resistive losses. In terms of harmonic mitigation q determines the value of R , which determines how sharp the attenuation is at the tuned frequency and how much attenuation there is at harmonic orders above the tuned frequency. As shown earlier the impact of q on the resistive losses at fundamental frequency is insignificant within the normal range of q , except if q_L is small, which is commented upon next.

q_L is the most important parameter to consider in terms of losses as it only has a significant affect on the amount of resistive losses. It should be noted that if q_L becomes very small it would in theory affect the impedance profile but for the values tested for above the difference is not significant. It could be expected that there will be larger investment costs for an inductor with a higher q_L . However if the TSO, as an example, has a cost estimate of 300 Danish kroner per megawatt-hour lost as resistive losses, and comparing with Figure A.5, it quickly becomes profitable to initially invest in an inductor with a high q_L .

In terms of harmonic mitigation performance h_0 is a very important parameter as it determines where the largest harmonic damping is located. One could argue that in order to achieve damping of as many harmonic orders as possible h_0 should be small, examples being 3rd or 5th. However as seen in Figure A.3 a lower h_0 leads to larger fundamental frequency resistive losses.

Table A.2 sums up the discussion made above for the different variables and their effect on the three major considerations discussed.

Variable	Fundamental losses	Mitigation	Mvar injection
Q_1	Important	Important	Very important
h_0	Important	Important	Not important
q	Less important	Important	Not important
q_L	Very important	Less important	Not important

Table A.2: Importance of variables on considerations for filter performance.

Another consideration, which lies under the harmonic mitigation performance, is how the choice of the filter parameters affects the system resonances, as anti-resonances can

become a problem. As mentioned in Chapter 1 Energinet's simulations has indicated that the use of C-type filters can lead to anti-resonances in other parts of the system, as the resonances across the system are affected by the installation of the C-type filter.

The third consideration, about the reactive power injection at fundamental frequency, is a bi-product from the original usage of the C-type filter, as the first usage of the C-type filter was for HVDC-LCC projects [13]. As HVDC-LCCs absorb reactive power in order to transfer active power, the use of C-type filters aided in delivering the reactive power needed, thus limiting the amount of shunt capacitors or synchronous condenser capacity needed. Thus essentially two problems were addressed with one solution, being mitigation of the harmonic distortion from the HVDC-LCC and supplying of the reactive power for the HVDC-LCC. In the Danish case the reactive power injection at the fundamental frequency has become a disadvantage if the filter is not used in connection to a HVDC-LCC project. This is because of the large share of UGCs in the Danish system, which already generate reactive power that has to be compensated by shunt reactors. If the C-type filter is to be connected in a busbar where there is not a HVDC-LCC connected, reactive power compensation is needed in order to not inject reactive power into the system. This reactive power compensation will typically be made by shunt reactors, thus leading to extra costs in the investment, when a C-type filter is found to be the solution for a harmonic issue in the system.

Currently there are six substations in Denmark which have HVDC-LCCs connected [26]. It is very preferable to have the reactive power generation located at the busbar where the HVDC-LCC is connected, as otherwise the transfer of reactive power in the system will lead to resistive losses and reduce the capacity of the active power transfer in the lines. Thus in general it can be predicted that if the C-type filter is installed in other substations than those with HVDC-LCCs connected, reactive power compensation by shunt reactors can be needed in order to limit the reactive power injection into the system.

Appendix B

Cable Data used in the Small System

In Table B.1 the data used for the 400 kV cable in the Small System is given. Furthermore the positive sequence power frequency parameters obtained in PowerFactory are also shown. The data for the cable comes from [30], which is an example grid suitable for investigation of the spread of harmonics, where lines are based on what is typical in the existing power system. The cable was originally a 400 kV sea cable but is adjusted to have land cable like parameters, by changing the relative permittivity of the oversheath, so that the permittivity matched an UGC variant also found in [30]. The reason for using the sea cable parameters was due to the UGC in [30] having a conductor cross-section of 2500 mm², which is the largest cross-section seen in [31], which gives tables for standard values of XLPE cables, and it was chosen to use a cable with smaller conductor cross-section to be in the middle of the range found in [31].

Parameter	Value
Cross-section of conductor [mm ²]	1200
Core diameter [mm]	46
Semiconductive layer thickness [mm]	1.5
Insulation thickness [mm]	27
Semiconductive layer thickness [mm]	1.5
Screen thickness [mm]	3.7
Oversheath thickness [mm]	4.0
DC-resistance of conductor at 20°C [Ω /km]	0.0151
DC-resistance of screen at 20°C [Ω /km]	0.1680
Relative permittivity of insulation [-]	2.5
Relative permittivity of oversheath [-]	2.4
Positive Sequence Power Frequency Parameters	Value
Resistance [Ω /km]	$3.236 \cdot 10^{-2}$
Inductance [H/km]	$3.623 \cdot 10^{-4}$
Capacitance [F/km]	$9.363 \cdot 10^{-8}$

Table B.1: Parameters of 400 kV cable.

Appendix C

Radial Independent Resonance in the Small System

In Chapter 4, for the Small System, there was seen to be a resonance peak created by the ring part of the system consisting of Line 1-2, Line 1-3 and Line 2-3, as seen in Figure C.1, which is independent on the network parameters of the grid outside, in this case Line 3-4. This appendix aims to show how the frequency of the resonance peak can be calculated in the case of equal lines, modelled as nominal-PI.

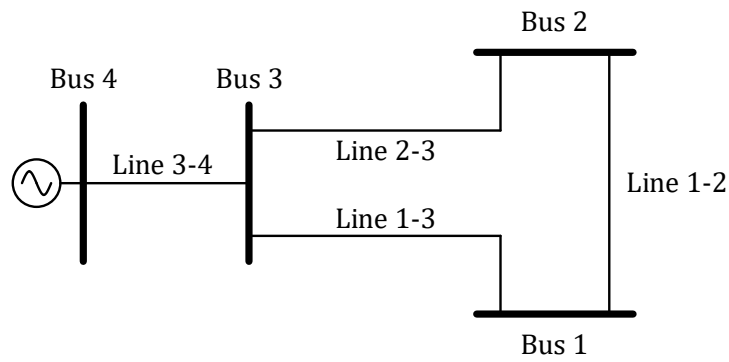


Figure C.1: Single line diagram of the Small System.

In Figure C.2 the system components are represented as series impedance and shunt admittance. The capacitances C_{12} , C_{13} , C_{23} and C_{34} account for half of the capacitance of their respective line, thus two of them account for the full capacitance of the line. It is assumed that all the capacitances in the system and the generator grounding is connected to a common neutral point, and this can be assumed as only the positive sequence impedance is of interest and the ground will mostly affect the zero sequence impedance. The lines in the system are the same length and have the same impedance and capacitance per length, which makes it possible to make a capacitance transformation, which will be shown later.

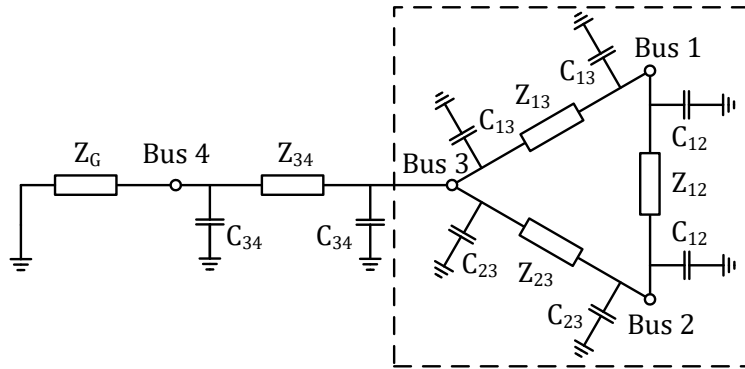


Figure C.2: The Small System represented as series impedance and capacitance.

First the focus will be on the ring system marked by the dashed box. Looking at Figure C.3 the capacitance in the dashed box is connected to a common neutral point as C_1 and since every line in the system is equal the capacitance can be given as seen in Equation C.1.

$$C_1 = 2 \cdot C_{12} = 2 \cdot C_{13} = 2 \cdot C_{23}. \tag{C.1}$$

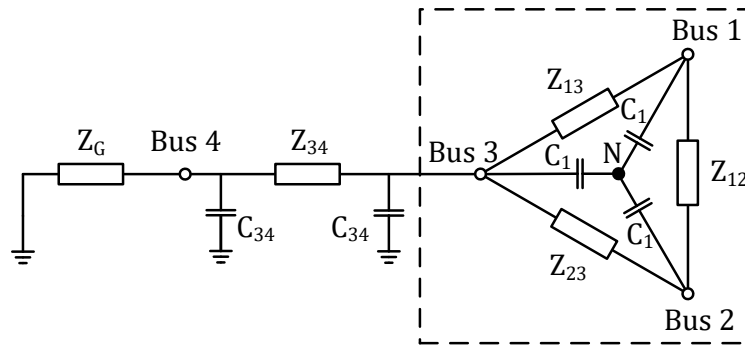


Figure C.3: The Small System after the capacitances in the dashed box are connected to a common neutral.

Next the series impedance is transformed from delta to star as seen in Equations C.2, C.3 and C.4

$$Z_1 = \frac{Z_{12}Z_{13}}{Z_{12} + Z_{13} + Z_{23}} \tag{C.2}$$

$$Z_2 = \frac{Z_{12}Z_{23}}{Z_{12} + Z_{13} + Z_{23}} \tag{C.3}$$

$$Z_3 = \frac{Z_{13}Z_{23}}{Z_{12} + Z_{13} + Z_{23}} \tag{C.4}$$

Due to the lines being equal, the impedances are equal, as seen in Equation C.5.

$$Z_1 = Z_2 = Z_3 = \frac{Z_{12}}{3} = \frac{Z_{13}}{3} = \frac{Z_{23}}{3} \tag{C.5}$$

After the transformation, the system is now as shown in Figure C.4. When the impedance is seen from Bus 1 the current will flow as given by the red arrow. The connection from the neutral point to Bus 2 is seen as an open circuit, thus the impedance and capacitance in the red box can be neglected.

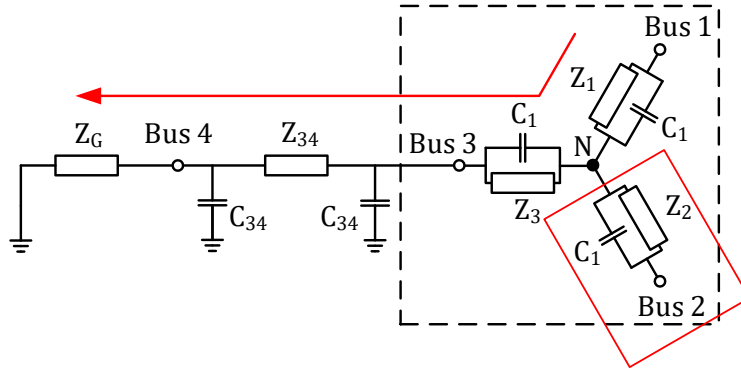


Figure C.4: The Small System after the delta to star transformation of impedances Z_{12} , Z_{13} and Z_{23} .

The rest of the system outside the dashed box is now transformed to have the same representation by connecting to the neutral point, as seen in Figure C.5.

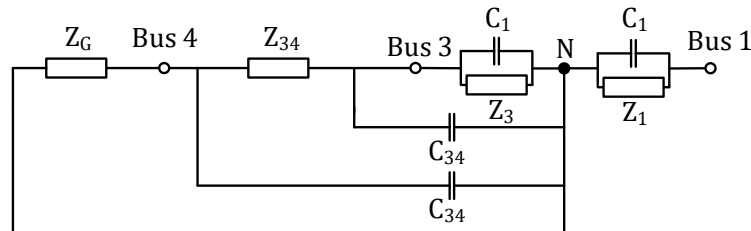


Figure C.5: The Small System after capacitance C_{34} and source grounding have been connected to the common neutral.

The part of the system consisting of the impedance and capacitance from Bus 1 to the neutral point will have a resonance point that is not affected by the rest of the system. The frequency of the resonance point due to Z_1 and C_1 , where $Z_1 = R_1 + j\omega L_1$, is given by Equation C.6.

$$f_r = \frac{1}{2\pi\sqrt{\frac{L_1}{3} \cdot C_1}} \tag{C.6}$$

Figure C.5 also shows that if Bus 3 is the observed and injected busbar the resonance peak caused by the ring circuit will not be present, because the current will not flow into the Bus 1 and Bus 2 branches, as they are open-circuited.

For non-equal lines a sensitivity analysis approach, as was shown in Chapter 4, could be used to prove that the resonance peak is independent of the radial line.

Appendix D

Additional Results from Chapter 5

This appendix shows the results of the First Order Coefficient Homotopy Method when Bus 2 and Bus 3 are the observed and injected busbars respectively. In Figure D.1 the results of $|V_{2,2}[1]|$ are shown. $|V_{2,2}[1]|$ is similar to $|V_{1,1}[1]|$ with the difference being that the value for a filter in Bus 1 or Bus 2 is switched, meaning a filter in Bus 1 in $|V_{1,1}[1]|$ has the same value as a filter in Bus 2 for $|V_{2,2}[1]|$. The value of the method indicates that for the first resonance peak a filter in Bus 1 or 2 will have more impact than a filter in Bus 3. For the second resonance peak, a filter in Bus 3 have the most impact, while a filter in Bus 1 or Bus 2 have equal magnitude at their peaks, but their peaks occur at different frequencies. For the third resonance peak the method indicates that only a filter in Bus 1 or Bus 2 will impact the peak.

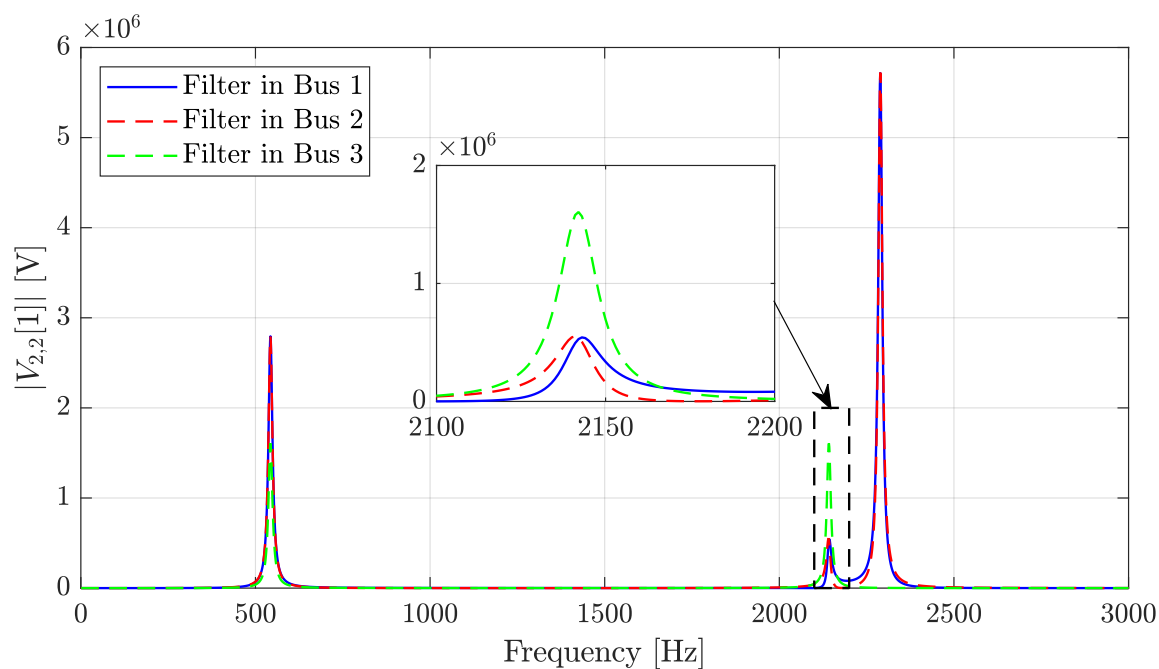


Figure D.1: $|V_{2,2}[1]|$ from the First Order Coefficient Homotopy Method, with different filter locations, with observation and injection from Bus 2.

In Figure D.2 the absolute impedance seen from Bus 2 is plotted with a C-type filter in Bus 1, Bus 2 and Bus 3 respectively. It can be seen that the First Order Coefficient Homotopy Method correctly predicted the most impactful filter position.

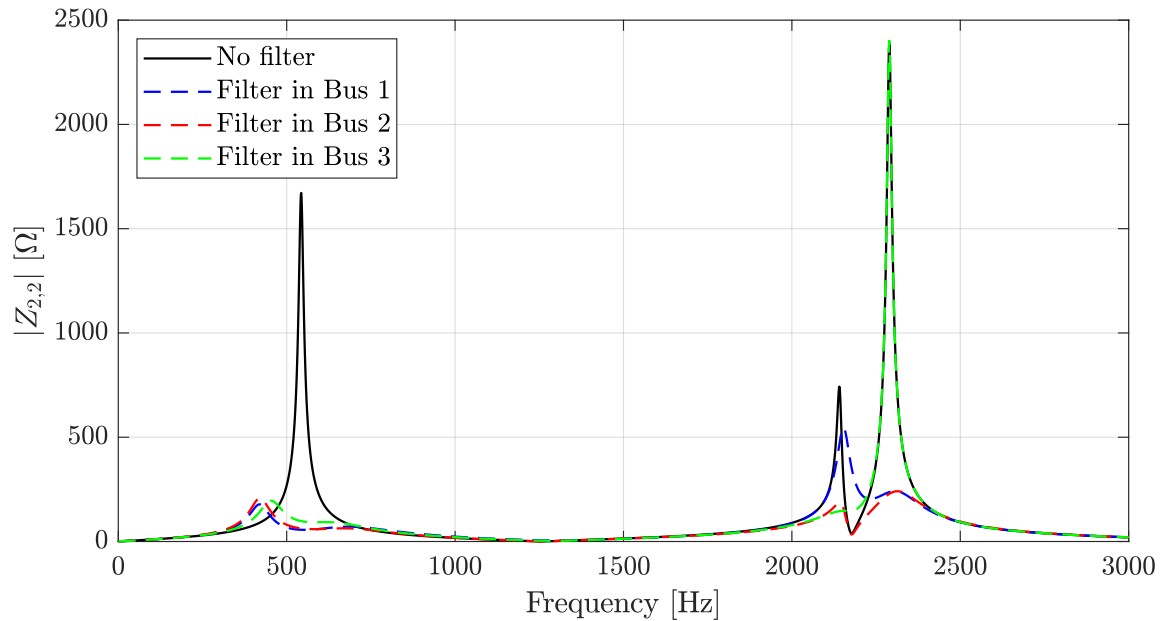


Figure D.2: Absolute impedance seen from Bus 2, when C-type filter is implemented in different positions.

In Figure D.3 the results of $|V_{3,3}[1]|$ are shown. The results of the method indicates that for the first resonance peak a filter in Bus 1 or 2 will have more impact than a filter in Bus 3. For the second resonance peak, a filter in Bus 3 have the most impact, while a filter in Bus 1 or 2 have equal impact. The third resonance, which was observed from Bus 1 and 2, is not seen when Bus 3 is the observed busbar as this resonance peak is created by the ring circuit, which is not present when observed from Bus 3.

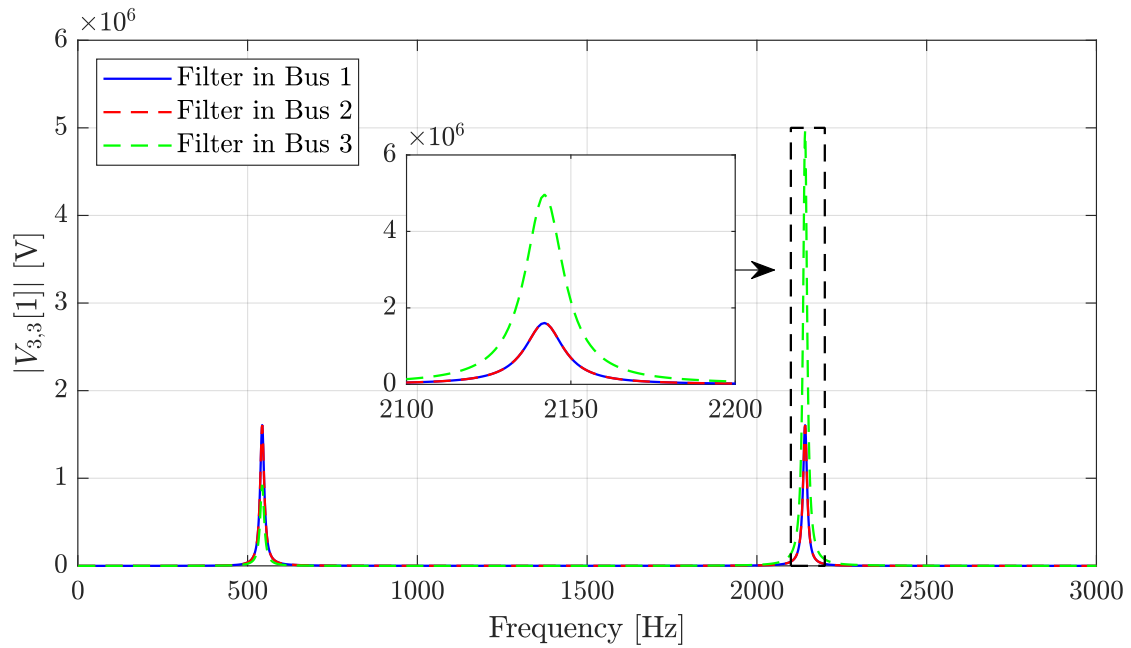


Figure D.3: $|V_{3,3}[1]|$ from the First Order Coefficient Homotopy Method, with different filter locations, with observation and injection from Bus 3.

In Figure D.4 the absolute impedance seen from Bus 3 is plotted with a C-type filter in Bus 1, Bus 2 and Bus 3 respectively. It can be seen that the First Order Coefficient Homotopy Method correctly predicted the most impactful filter position.

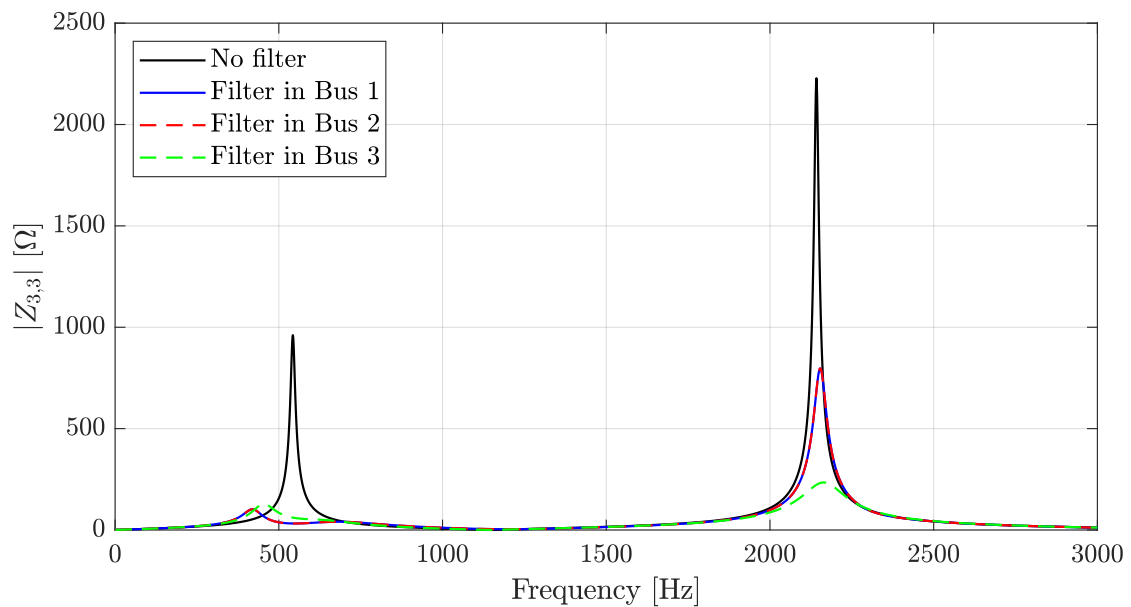


Figure D.4: Absolute impedance seen from Bus 3, when C-type filter is implemented in different positions.

Appendix E

First Order Coefficient Homotopy Method using Real and Imaginary Parts

This appendix investigates if any further knowledge can be gained from the First Order Coefficient Homotopy Method, when using the real and imaginary part compared to the absolute value. $V_{1,1}[1]$ is the first order coefficient of the power series, which means that Bus 1 is the observed and injected busbar.

First the absolute impedance of the frequency scan of the Small System presented in Chapter 4 is shown in Figure E.1 with a frequency range of 2100-2200 Hz. The reason for choosing the frequency range of 2100-2200 Hz is that in Section 5.2, which involved the First Order Coefficient Homotopy Method, this range had a difference in $V_{1,1}[1]$ between a filter in Bus 1 or Bus 2, which was not seen for the other peaks. The real and imaginary part of $V_{1,1}[1]$ are investigated as they could possibly provide more information and a better indication of the value of $|Z_{1,1}|$ after the filter implementation.

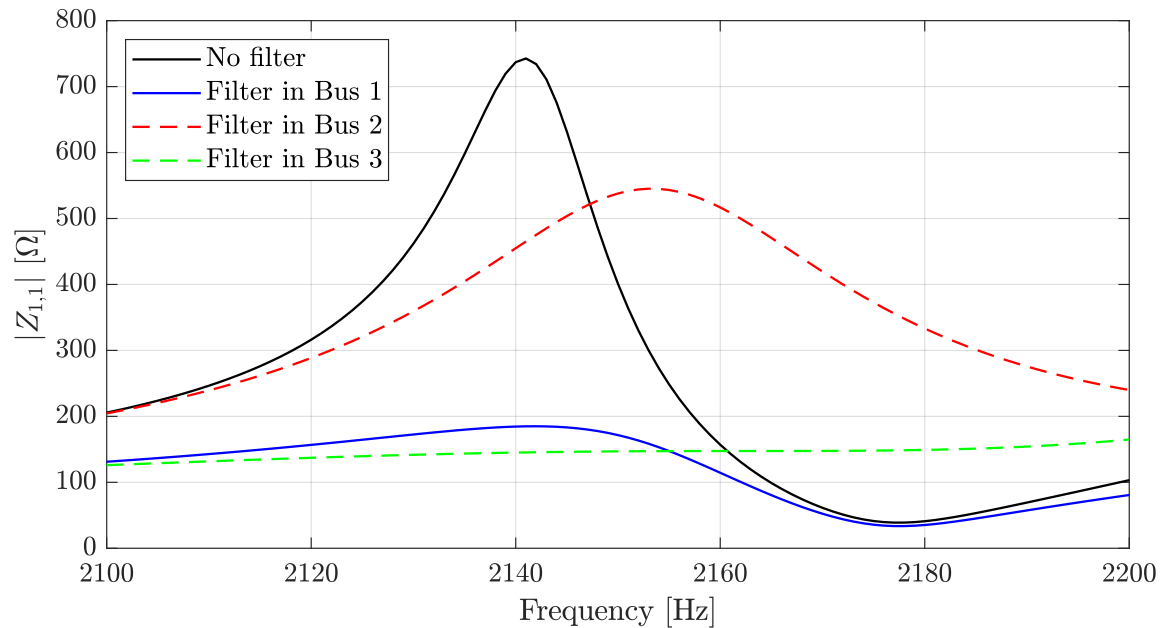


Figure E.1: Absolute impedance of the Small System, in the frequency range of 2100-2200 Hz, with filters implemented in the different busbars.

The absolute value of $V_{1,1}[1]$ does not indicate whether the impact of an actual filter

is an increase or a decrease due to the way the absolute value is calculated, for complex values, as seen in Equation E.1.

$$|\alpha + j\beta| = \sqrt{\alpha^2 + \beta^2} \quad (\text{E.1})$$

The value being squared removes the indication of a positive or negative value in the real and imaginary part of $V_{1,1}[1]$, which would otherwise indicate if $|Z_{1,1}|$ is being increased or decreased at the given frequency.

The absolute value of $V_{1,1}[1]$ from the First Order Coefficient Homotopy Method is shown in Figure E.2 for a frequency range of 2100-2200 Hz. This is the information that is available when taking the absolute value of $V_{1,1}[1]$ and will be used as a reference when comparing with the real or imaginary part of $V_{1,1}[1]$.

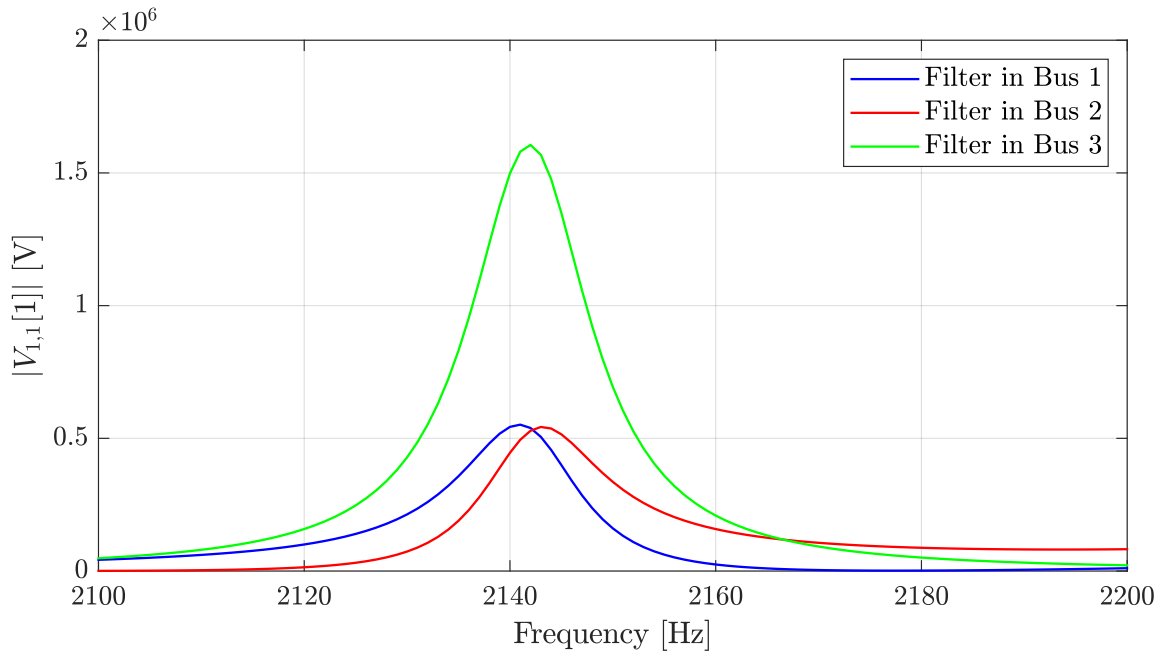


Figure E.2: The absolute value of $V_{1,1}[1]$ from the First Order Coefficient Homotopy Method in the frequency range of 2100-2200 Hz.

In Figure E.3 the real part of $V_{1,1}[1]$ is shown for the frequency range of 2100 – 2200 Hz. Comparing the real part of $V_{1,1}[1]$ in Figure E.3 with the absolute value of $V_{1,1}[1]$ in Figure E.2, the real part of $V_{1,1}[1]$ is able to show the difference between an expected increase or decrease in the magnitude of $|Z_{1,1}|$. When the real part of $V_{1,1}[1]$ is positive it indicates an increase in the $|Z_{1,1}|$, meaning an amplification at the given frequency, while a negative value indicates a decrease in $|Z_{1,1}|$, meaning a damping at the specific frequency.

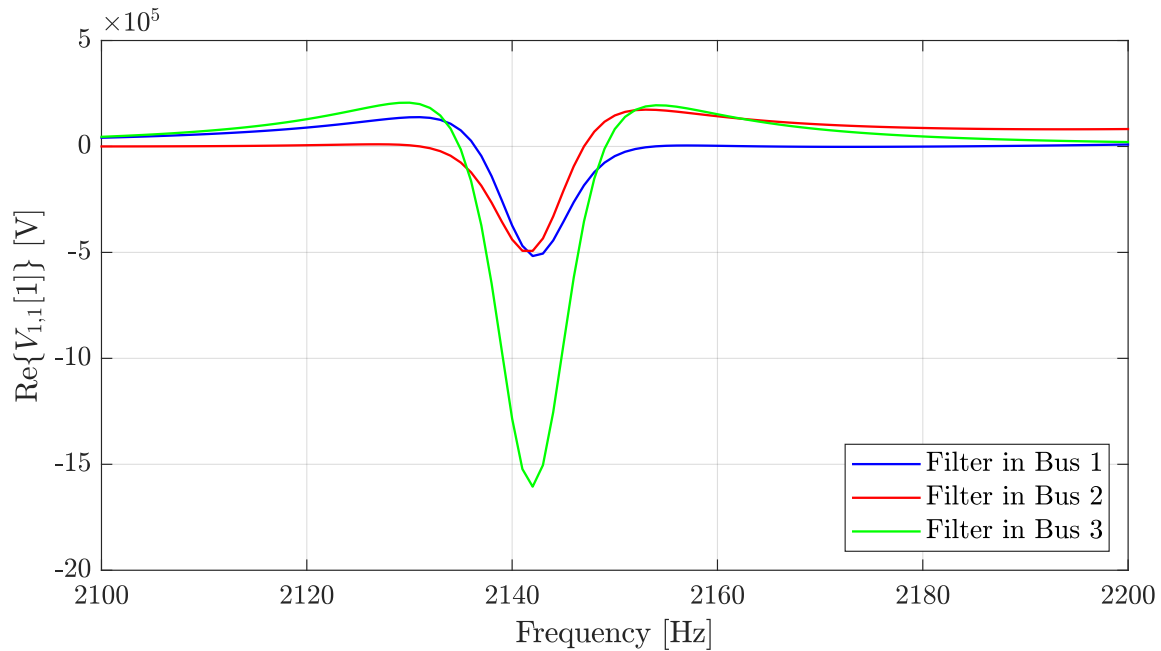


Figure E.3: The real part of the First Order Coefficient Homotopy Method in the frequency range of 2100-2200 Hz on the Small System.

At 2100 Hz in Figure E.3, for the filter in Bus 2, the real value of $V_{1,1}[1]$ is approximately 0 V which should correspond to a low effect in the impedance scan. When comparing with the impedance scan in Figure E.1 for the same frequency, it is also seen that there is not a large difference between the case with and without a filter in Bus 2 for this frequency. This could also have been predicted from the absolute value of $V_{1,1}[1]$, as seen in Figure E.2, as the absolute value of $V_{1,1}[1]$ is low, which means that a low impact is expected by inserting the filter at this location at 2100 Hz. For the filter position in Bus 1 or Bus 3 at the same frequency, the real part of $V_{1,1}[1]$ is positive which should correspond to an increase in impedance, however in the frequency scan there is a decrease in the impedance. This illustrates the fact that the real part of $V_{1,1}[1]$ can not alone describe the change when a filter is implemented, as the imaginary part of $V_{1,1}[1]$ also has an impact.

At 2160 Hz in Figure E.3, for the filter in Bus 1, the real part of $V_{1,1}[1]$ is approximately 0 V, which corresponds to no affect in the impedance scan. When comparing to Figure E.1 at the same frequency, this filter position follows the impedance when there is no filter implemented, thus fitting with the indication from the real part of $V_{1,1}[1]$. For a filter position in Bus 2 or Bus 3 at 2160 Hz, the real part of $V_{1,1}[1]$ is positive which should correspond to an increase in $|Z_{1,1}|$. This occurs for the filter in Bus 2 and to some extent for the filter in Bus 3. The difference in magnitude of the real value of $V_{1,1}[1]$ for a filter in Bus 2 compared to Bus 3 does not indicate that the difference in the impedance should

be as high as it is, as seen in Figure E.1. This means that the imaginary part of $V_{1,1}[1]$ also has an impact.

Using the real part of the First Order Coefficient Homotopy Method to predict how the impedance of the system changes when a filter is implemented is shown to not be an accurate method as the positive and negative values of the real part does not always correspond to the actual change in the impedance when an actual filter is implemented. For some frequencies and filter positions the real part of $V_{1,1}[1]$ accurately predicts whether the impedance is increased or decreased at the frequency, when a filter is implemented. However for other cases the real part of $V_{1,1}[1]$ can not be used alone to predict the change in impedance. This is partly because the imaginary part of $V_{1,1}[1]$ will also have an impact.

In Figure E.4 the imaginary part of $V_{1,1}[1]$ is shown for the frequency range of 2100-2200 Hz. The imaginary part of $V_{1,1}[1]$ is more difficult to analyse than the real part of $V_{1,1}[1]$. If the real part of $Z_{1,1}$ is observed it is always positive, which enables the possibility of the real part of $V_{1,1}[1]$ to indicate an increase or decrease in $Z_{1,1}$. However as the imaginary part of $Z_{1,1}$ is changing between positive and negative values, depending on whether the system is inductive or capacitive respectively, at that point, the imaginary part of $V_{1,1}[1]$ does not indicate an increase or decrease in the same way as the real part of $V_{1,1}[1]$. Instead the imaginary part of $Z_{1,1}$ has to be observed before the indications of the imaginary part of $V_{1,1}[1]$ can be understood. Typically the imaginary part of $V_{1,1}[1]$ is negative when the imaginary part of $Z_{1,1}$ is positive, which would indicate a decrease in $|Z_{1,1}|$ at the observed frequency. However as inductive and capacitive filters introduce a shift in the frequency of the resonance points it becomes very difficult to quantify what the final value of $|Z_{1,1}|$ is, at the given frequency, after the introduction of an actual filter.

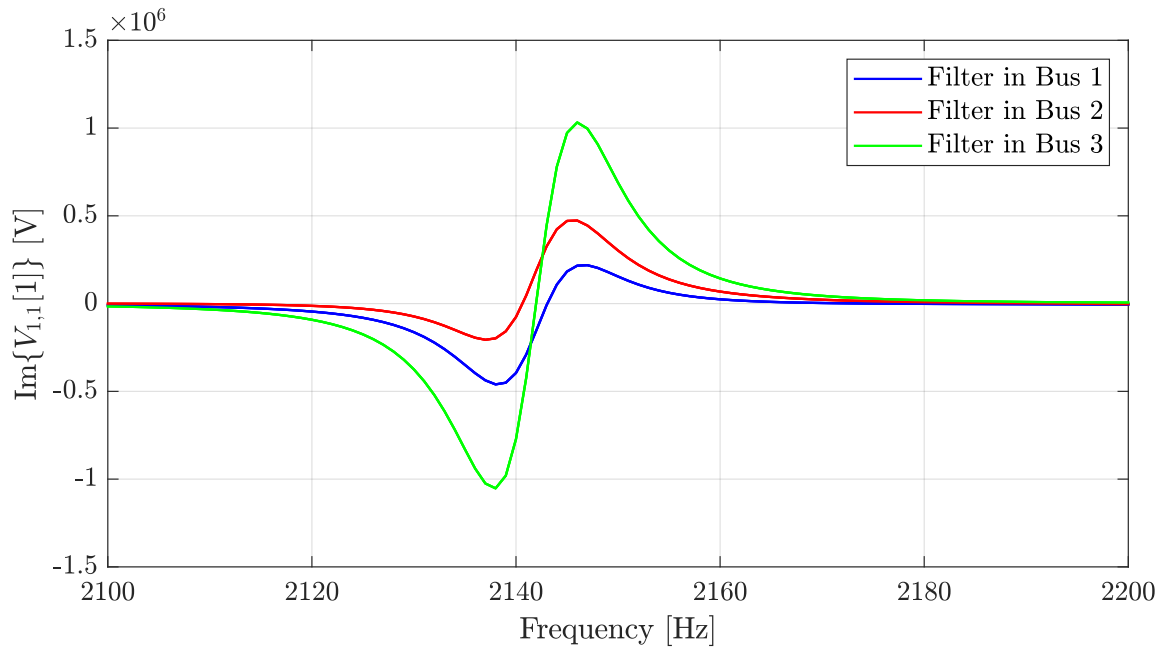


Figure E.4: The imaginary part of $V_{1,1}[1]$ in the frequency range of 2100-2200 Hz on the Small System.

Figure E.5 shows the imaginary part of $V_{1,1}[1]$ for the frequency range of 530-560 Hz, which is the first resonance peak. A filter in Bus 1 or Bus 2 is seen to have the same impact, while a filter in Bus 3 is seen to have a lower impact. Observing Figure E.6, which shows $X_{1,1}$ for different positions of a capacitive and inductive filter respectively. The figure is a zoom of Figure 4.9, and in the figure legend "Cap fil" denotes the flat admittance profile capacitive filter and "Ind fil" denotes the flat admittance profile inductive filter described in Section 4.2. It is seen that implementing the same capacitive filter in different busbars causes different shifts in the frequency of the resonance peaks, which is located at the zero crossing of $X_{1,1}$. Comparing Figure E.5 and Figure E.6 it is found that the imaginary part of $V_{1,1}[1]$ can provide information about which filter position causes the largest shift in the resonance peak frequency. The larger value of the imaginary part of $V_{1,1}[1]$ for a filter position in Bus 1 or Bus 2, compared to a filter position in Bus 3, causes a larger shift in the resonance peak frequency for Bus 1 and Bus 2, which also end up being at the approximate same frequency, which was indicated by the imaginary part of $V_{1,1}[1]$.

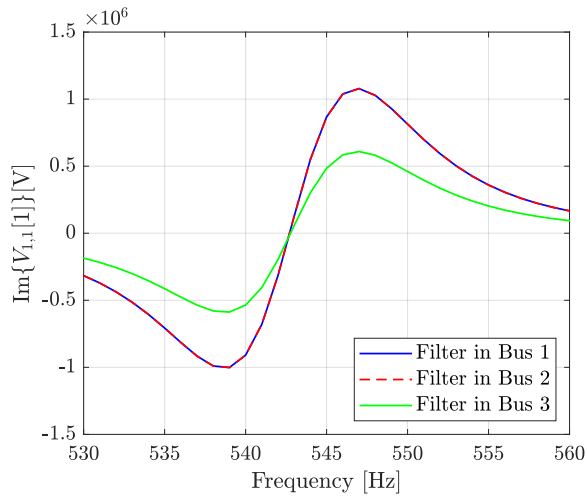


Figure E.5: The imaginary part of $V_{1,1}[1]$ in the frequency range of 530-560 Hz on the Small System.

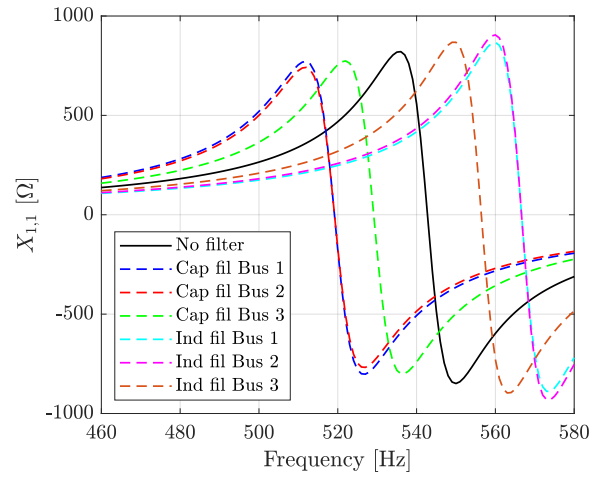


Figure E.6: Reactance scan of system seen from Bus 1, in the frequency range of 460-580 Hz, before and after a purely capacitive and inductive filter are connected at different busbars.

As shown in Section 4.2 there is interaction between the resistive and reactive parts of the filter and this is also apparent when comparing Figure E.3 and E.4, where the imaginary part is seen to be large in value at the same time as the real part. This essentially means that it is possible to investigate the impedance change by observing both the real and imaginary parts independently, however there will still be an underlying impact of the other, due to the way the real and imaginary parts follow each other. Another problem about using the imaginary part of $V_{1,1}[1]$ is that an actual filter will cause a shift in the resonance frequencies, which is mostly due to the imaginary part of the filter impedance, but can also be because of the resistive part of the filter.

Finally it can thus be stated that splitting the absolute value of $V_{1,1}[1]$ into real and imaginary values can give some knowledge about the final result of the impedance scan. The real value can indicate if the change in the impedance is increasing or decreasing. The movement of resonances, in terms of frequencies, can be indicated with the imaginary part of $V_{1,1}[1]$, however this should be understood as an indication of the relative movement between the different filter positions, if the same filter is implemented in the different positions. The idea about using $V_{1,1}[1]$ to predict the final impedance value after an actual filter is implemented is very flawed, and can not be recommended as $V_{1,1}[1]$ only provides an initial direction and the final filter values will have a large impact. Therefore the method of using $V_{1,1}[1]$ should at this point only be used for an initial screening of which filter positions have the largest impact. For this purpose the absolute value of $V_{1,1}[1]$ will suffice as the intention is not to predict the final impedance values, but rather determine the most impactful filter positions.

Appendix F

Additional Results for Large System

This appendix analyses the plots and results for the second and third resonance peak from the Large System in Chapter 6.

Results of Peak 2

Figure F.1 shows $|V_{TJE,TJE}[1]|$ for the second resonance peak before the implementation of the EDR-IDU line.

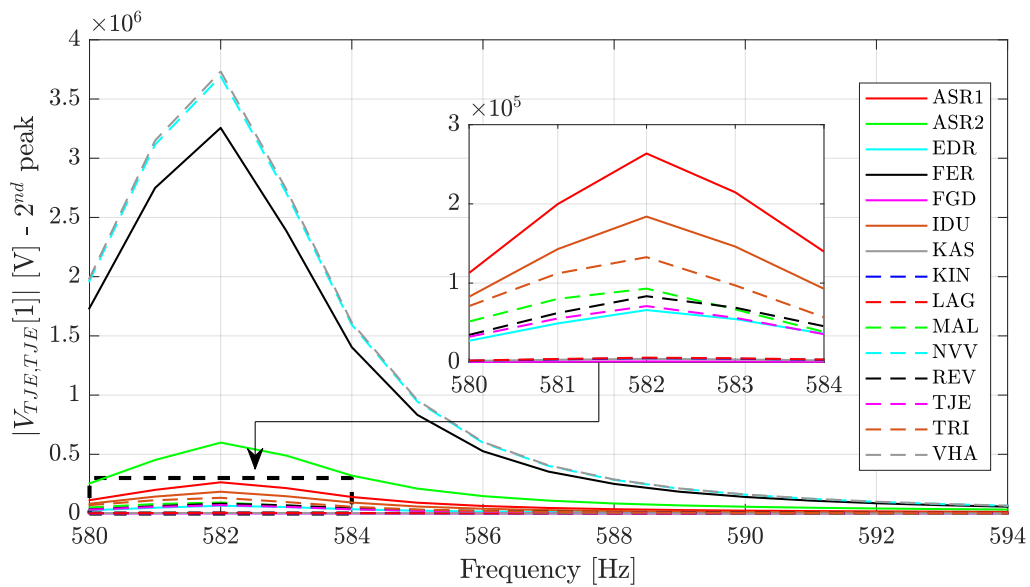


Figure F.1: $|V_{TJE,TJE}[1]|$ for the second resonance peak, before the EDR-IDU line is implemented.

Figure F.2 shows $|Z_{TJE,TJE}|$ for the second resonance peak before the implementation of the EDR-IDU line.

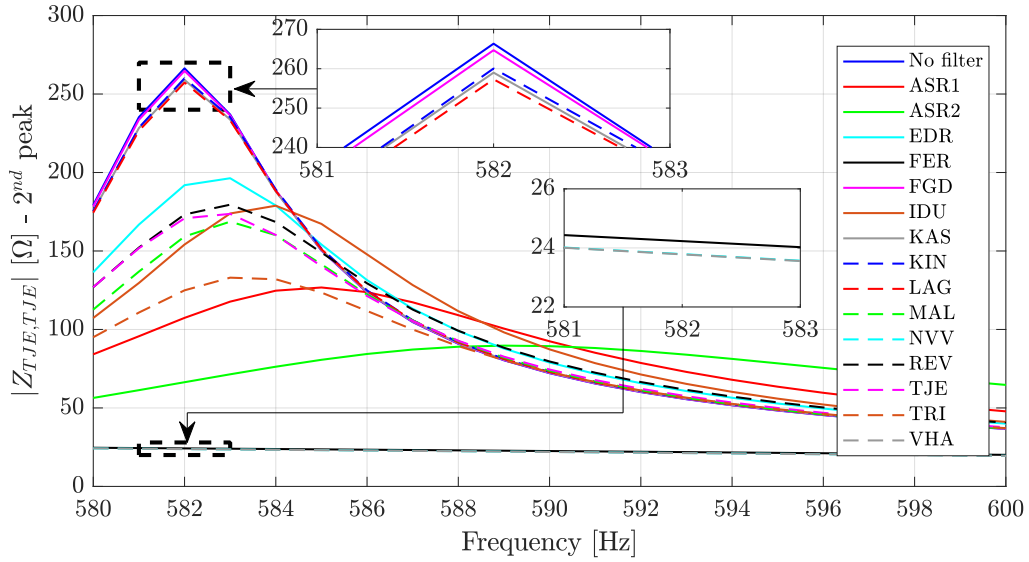


Figure F.2: $|Z_{TJE,TJE}|$ at the second resonance peak after implementation of a C-type filter tuned to the 5th harmonic order, before the EDR-IDU line is implemented.

Figure F.3 shows $|V_{TJE,TJE}[1]|$ for the second resonance peak after the implementation of the EDR-IDU line.

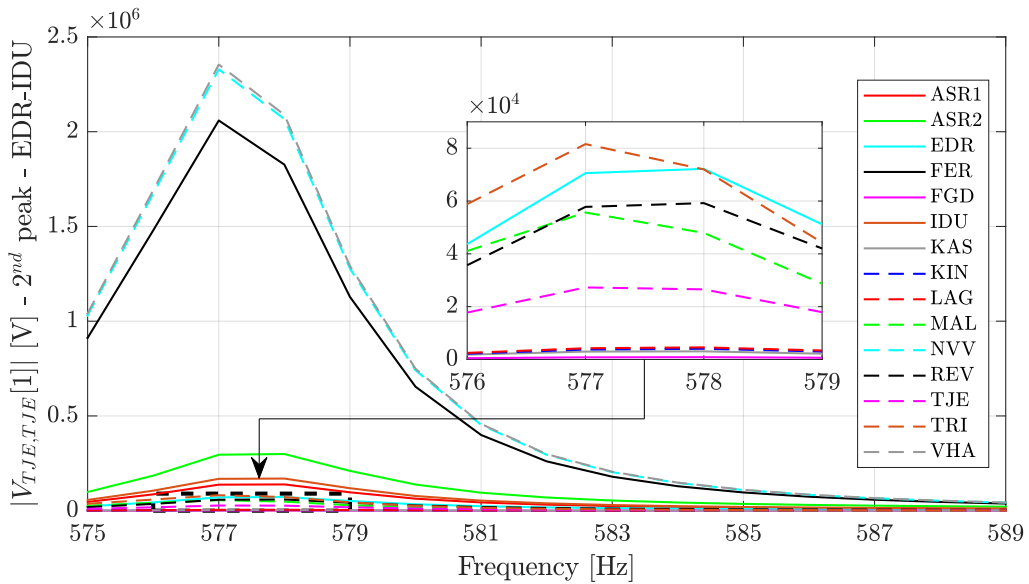


Figure F.3: $|V_{TJE,TJE}[1]|$ for the second resonance peak, after the EDR-IDU line is implemented.

Figure F.4 shows $|Z_{TJE,TJE}|$ for the second resonance peak after the implementation of the EDR-IDU line.

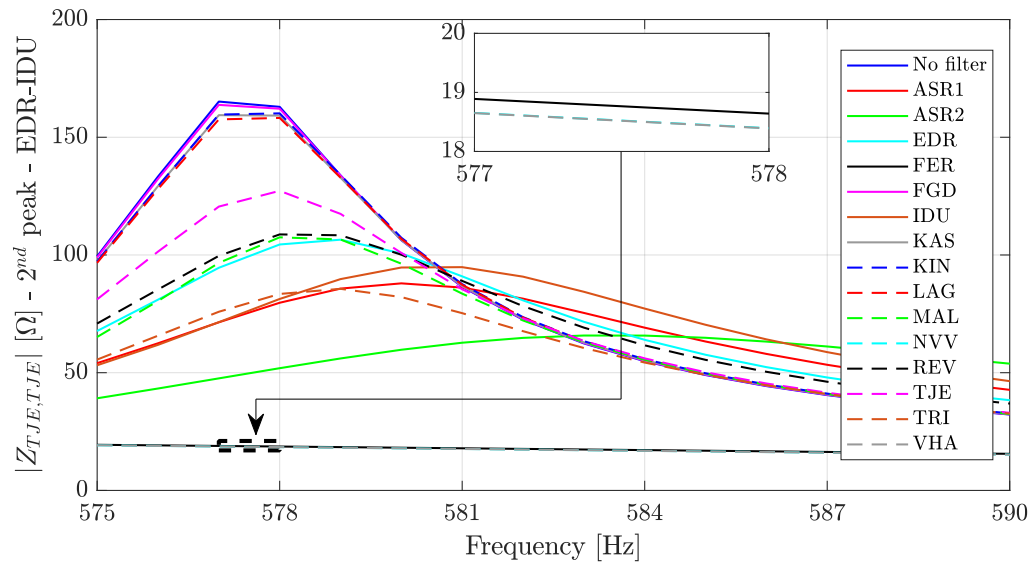


Figure F.4: $|Z_{TJE,TJE}|$ at the second resonance peak after implementation of a C-type filter tuned to the 5th harmonic order, after the EDR-IDU line is implemented.

The results of the First Order Coefficient Homotopy Method for the second resonance peak are summarised in Table F.1.

Peak 2	Before EDR-IDU				After EDR-IDU			
	$ V[1] $	Rank	$ Z $	Rank	$ V[1] $	Rank	$ Z $	Rank
No Filter	-	-	266.4	16	-	-	165.2	16
ASR1	$2.636 \cdot 10^5$	5	107.4	5	$1.373 \cdot 10^5$	6	71.41	5
ASR2	$5.987 \cdot 10^5$	4	66.39	4	$2.953 \cdot 10^5$	4	47.59	4
EDR	$6.595 \cdot 10^4$	11	191.9	11	$7.057 \cdot 10^4$	8	94.56	8
FER	$3.256 \cdot 10^6$	3	24.23	3	$2.059 \cdot 10^6$	3	18.89	3
FGD	$1.136 \cdot 10^3$	15	264.7	15	$0.808 \cdot 10^3$	15	163.8	15
IDU	$1.840 \cdot 10^5$	6	154.1	7	$1.681 \cdot 10^5$	5	71.47	6
KAS	$4.327 \cdot 10^3$	14	259.0	13	$2.978 \cdot 10^3$	14	159.4	13
KIN	$5.252 \cdot 10^3$	13	260.1	14	$3.756 \cdot 10^3$	13	159.6	14
LAG	$5.882 \cdot 10^3$	12	257.3	12	$4.254 \cdot 10^3$	12	157.6	12
MAL	$9.300 \cdot 10^4$	8	159.2	8	$5.565 \cdot 10^4$	10	96.65	9
NVV	$3.692 \cdot 10^6$	2	23.79	2	$2.329 \cdot 10^6$	2	18.65	2
REV	$8.343 \cdot 10^4$	9	173.2	10	$5.779 \cdot 10^4$	9	99.62	10
TJE	$7.095 \cdot 10^4$	10	170.8	9	$2.728 \cdot 10^4$	11	120.6	11
TRI	$1.327 \cdot 10^5$	7	124.9	6	$8.156 \cdot 10^4$	7	75.89	7
VHA	$3.732 \cdot 10^6$	1	23.78	1	$2.355 \cdot 10^6$	1	18.65	1

Table F.1: Comparison of $|V_{TJE,TJE}[1]|$ and $|Z_{TJE,TJE}|$ before and after implementation of the EDR-IDU line, for the second resonance peak.

Before Implementation of the EDR-IDU Line

Comparing the filter position ranks of $|V_{TJE,TJE}[1]|$ and $|Z_{TJE,TJE}|$, before the implementation of the EDR-IDU line, for the second resonance peak, there is a maximum difference of one ranking for the same filter position. This highlights that the method predicts which filter has the largest impact satisfactorily for each specific resonance frequency. A noticeable difference between the results of the first resonance peak and the second resonance peak is that the filter position in TJE has a relatively low impact for the second resonance peak. Instead a filter in either of the three busbars FER, NVV and VHA have the highest impacts. It is found that by disconnecting the FER-NVV and FER-VHA lines, thus effectively disconnecting the ring circuit, the second peak completely disappears, while the other two resonance peaks shift in frequency. This indicates two things, one being that the second resonance peak observed in TJE is created by the interaction with the FER, NVV and VHA ring circuit, and secondly that placing a filter in one of these busbars removes the interaction between TJE and the ring circuit. It was found

when examining $|V_{TJE,VHA}[1]|$ and $|Z_{TJE,VHA}|$, meaning observing in TJE and injecting in VHA, that the second resonance peak was at the same frequency however of much larger magnitude compared to $|V_{TJE,TJE}[1]|$ and $|Z_{TJE,TJE}|$. This again indicates that for this resonance peak there is a strong interaction between TJE and VHA. Comparing $|V_{TJE,TJE}[1]|$ and $|V_{TJE,VHA}[1]|$ for the second resonance peak the ranking of the filter positions are the same. Thus it is confirmed that placing a filter in one of the ring circuit busbars greatly impacts the second resonance peak when seen from TJE.

After Implementation of the EDR-IDU Line

Comparing the filter position ranks of $|V_{TJE,TJE}[1]|$ and $|Z_{TJE,TJE}|$, after the implementation of the EDR-IDU line, for the second resonance peak, there is a maximum difference of one ranking for the same filter position. The only major difference before and after the implementation of the line is the filter position in EDR which goes from being ranked 11th to being ranked 8th for both $|V_{TJE,TJE}[1]|$ and $|Z_{TJE,TJE}|$. The same tendency occurred for the first resonance peak. The filter position in IDU gains a rank and thus it is again found that the filter positions affected are generally close to where the change is made.

Results of Peak 3

Figure F.5 shows $|V_{TJE,TJE}[1]|$ for the third resonance peak before the implementation of the EDR-IDU line.

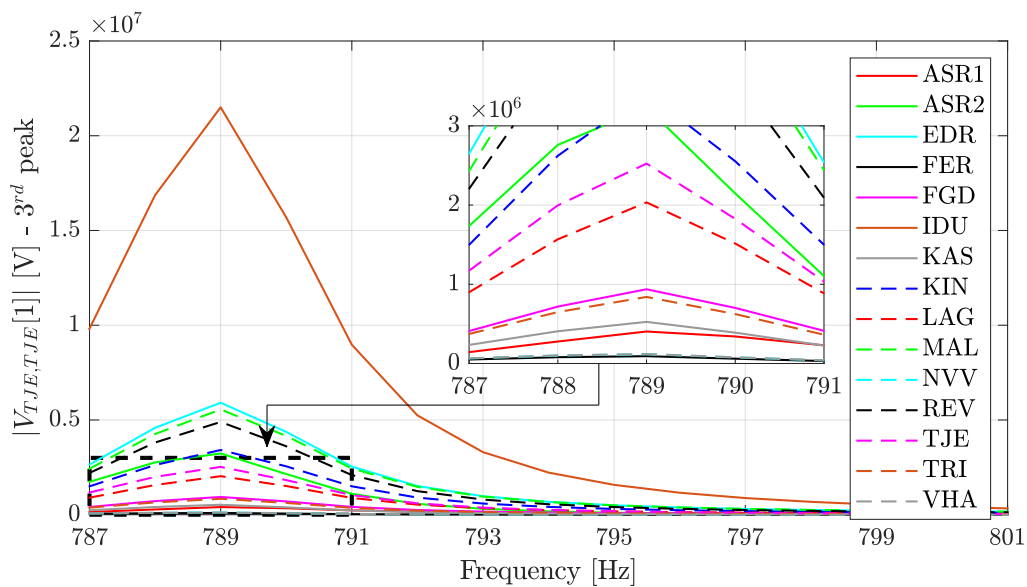


Figure F.5: $|V_{TJE,TJE}[1]|$ for the third resonance peak, before the EDR-IDU line is implemented.

Figure F.6 shows $|Z_{TJE,TJE}|$ for the third resonance peak before the implementation of the EDR-IDU line.

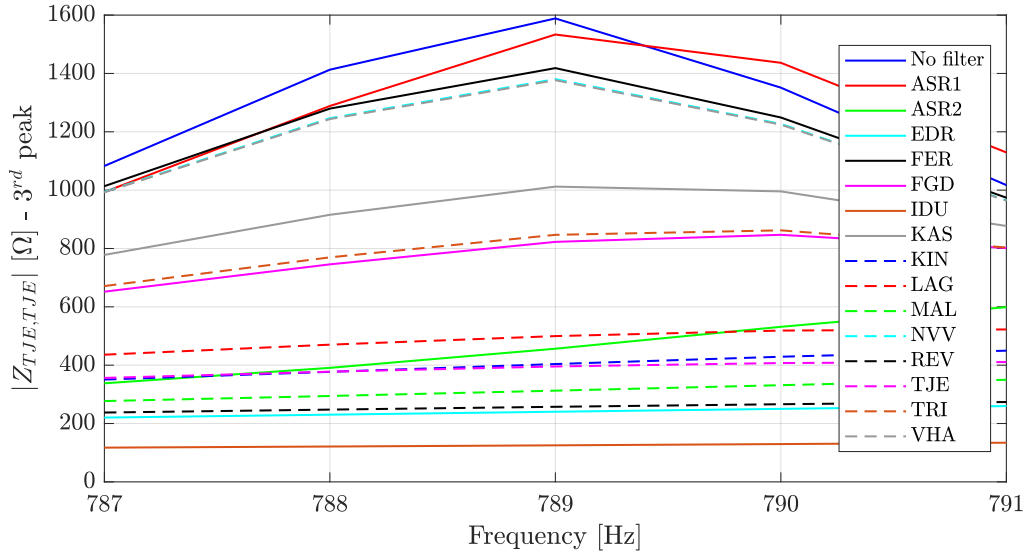


Figure F.6: $|Z_{TJE,TJE}|$ at the third resonance peak after implementation of a C-type filter tuned to the 5th harmonic order, before the EDR-IDU line is implemented.

Figure F.7 shows $|V_{TJE,TJE}[1]|$ for the third resonance peak after the implementation of the EDR-IDU line.

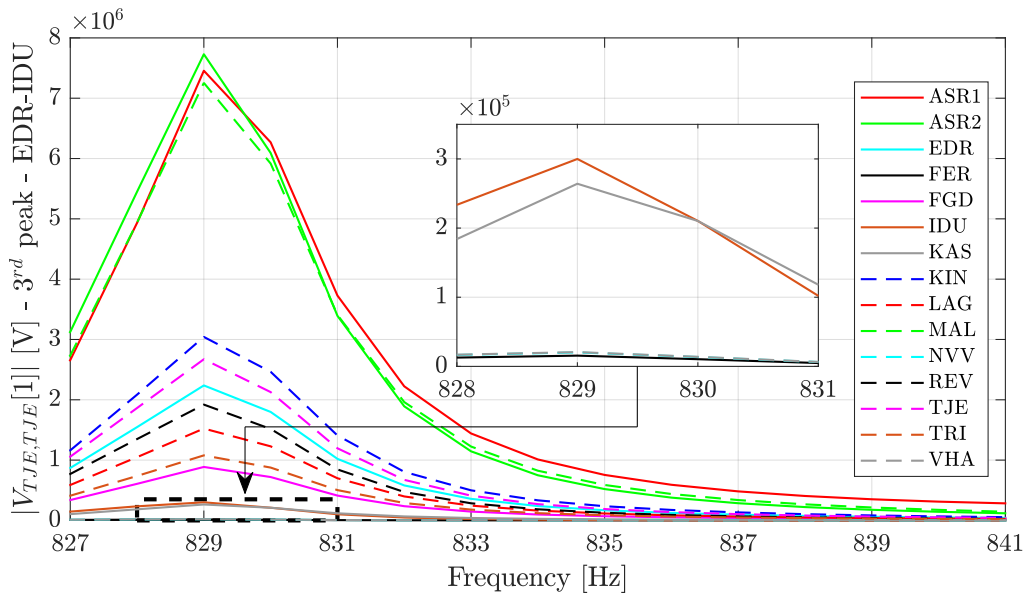


Figure F.7: $|V_{TJE,TJE}[1]|$ for the third resonance peak, after the EDR-IDU line is implemented.

Figure F.8 shows $|Z_{TJE,TJE}|$ for the third resonance peak after the implementation of the EDR-IDU line.

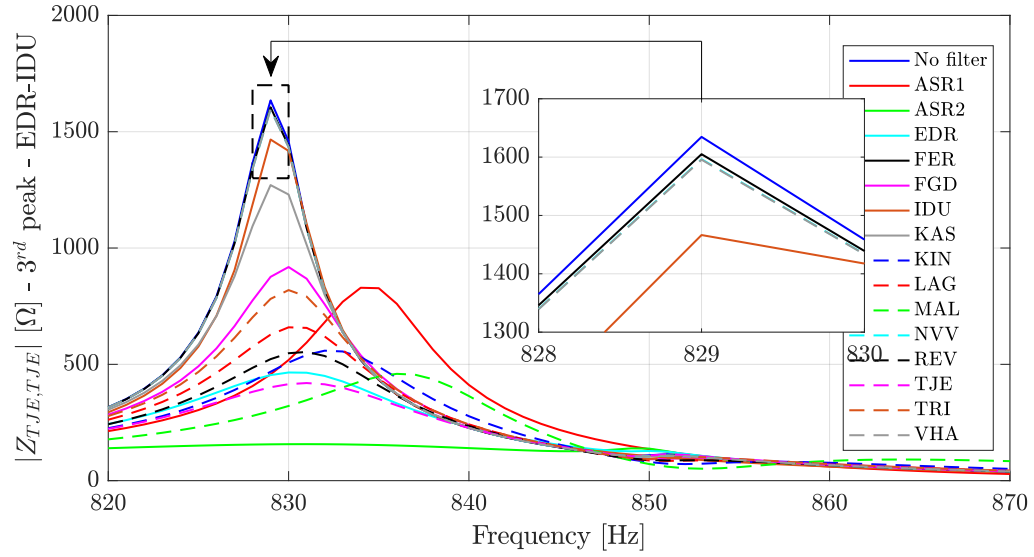


Figure F.8: $|Z_{TJE,TJE}|$ at the third resonance peak after implementation of a C-type filter tuned to the 5th harmonic order, after the EDR-IDU line is implemented.

The results of the First Order Coefficient Homotopy Method for the third resonance peak are summarised in Table F.2.

Peak 3	Before EDR-IDU				After EDR-IDU			
	$ V[1] $	Rank	$ Z $	Rank	$ V[1] $	Rank	$ Z $	Rank
No Filter	-	-	1589	16	-	-	1635	16
ASR1	$4.037 \cdot 10^5$	12	1533	15	$7.456 \cdot 10^6$	2	456.8	5
ASR2	$3.232 \cdot 10^6$	6	456.4	7	$7.729 \cdot 10^6$	1	156.2	1
EDR	$5.910 \cdot 10^6$	2	240.4	2	$2.238 \cdot 10^6$	6	453.7	4
FER	$9.223 \cdot 10^4$	15	1418	14	$1.555 \cdot 10^4$	15	1605	15
FGD	$9.371 \cdot 10^5$	9	822.7	9	$8.865 \cdot 10^5$	10	876.0	10
IDU	$2.150 \cdot 10^7$	1	125.2	1	$2.999 \cdot 10^5$	11	1466	12
KAS	$5.254 \cdot 10^5$	11	1012	11	$2.641 \cdot 10^5$	12	1271	11
KIN	$3.415 \cdot 10^6$	5	403.9	6	$3.042 \cdot 10^6$	4	468.0	6
LAG	$2.034 \cdot 10^6$	8	499.7	8	$1.523 \cdot 10^6$	8	627.7	8
MAL	$5.555 \cdot 10^6$	3	312.7	4	$7.254 \cdot 10^6$	3	298.6	2
NVV	$1.168 \cdot 10^5$	14	1380	13	$2.021 \cdot 10^4$	14	1596	14
REV	$4.895 \cdot 10^6$	4	257.3	3	$1.920 \cdot 10^6$	7	522.4	7
TJE	$2.524 \cdot 10^6$	7	395.6	5	$2.672 \cdot 10^6$	5	401.4	3
TRI	$8.402 \cdot 10^5$	10	846.8	10	$1.078 \cdot 10^6$	9	781.3	9
VHA	$1.192 \cdot 10^5$	13	1377	12	$2.067 \cdot 10^4$	13	1596	13

Table F.2: Comparison of $|V_{TJE,TJE}[1]|$ and $|Z_{TJE,TJE}|$ before and after implementation of the EDR-IDU line, for the third resonance peak.

Before Implementation of the EDR-IDU Line

Comparing the filter position ranks of $|V_{TJE,TJE}[1]|$ and $|Z_{TJE,TJE}|$, before the implementation of the EDR-IDU line, for the second resonance peak, there is a maximum difference of three rankings for the same filter position. The filter position with the largest difference in ranking is the ASR1 busbar. This can not be explained by other busbars having values close with the ASR1 busbar, so at this filter position the method is slightly inaccurate, and a potential reason for this is given in the next paragraph.

Looking at Figure F.5 which shows $|V_{TJE,TJE}[1]|$ for the third resonance peak before the implementation of the EDR-IDU line, it can be seen that for a filter position in ASR1 the value of $|V_{TJE,TJE}[1]|$ has a slightly more upward curve after the resonance frequency compared to other filter positions. Looking at Figure F.6 it can also be seen that the value of $|Z_{TJE,TJE}|$ stays higher than the other filter positions after the resonance frequency. This could be the reason for the relatively large ranking difference for the ASR1 filter position.

This shows a case where the use of real and imaginary values instead of absolute values could be beneficial. From making a further investigation into the real value of $V_{TJE,TJE}[1]$ it is found that the method correctly predicts a small value of damping at the resonance frequency, followed by an amplification at frequencies after the resonance frequency. Due to this amplification at frequencies right after the resonance point the value of $|Z_{TJE,TJE}|$ at the resonance point is affected, and this causes the difference in rankings for a filter position in ASR1.

Noticeably the ring circuit of FER, NVV and VHA have a very small effect at this resonance peak, while the group of FGD, KAS, KIN and LAG all have a larger effect, which was not seen for the earlier resonance peaks. This confirms that the use of the ideal voltage sources does not always impact nearby filter positions the same and that the system structure also has an effect.

Again a filter position in TJE is seen to not be the best solution when observing $|V_{TJE,TJE}[1]|$, but as seen with the earlier results TJE has a tendency to be better ranked in terms of $|Z_{TJE,TJE}|$, meaning that when an actual filter is implemented it performs better than expected.

After Implementation of the EDR-IDU Line

Comparing the filter position ranks of $|V_{TJE,TJE}[1]|$ and $|Z_{TJE,TJE}|$, after the implementation of the EDR-IDU line, for the third resonance peak, there is a maximum difference of three rankings for the same filter position. Again the filter position in ASR1 has the largest difference in rankings.

The implementation of the EDR-IDU line radically changes the most impactful filter positions most notably ASR1 which goes from having a low impact to being one of the most impactful, and IDU going from being the most impactful to being one of the worst. The filter position in EDR is also significantly affected as would be expected due to the busbar being directly affected by the change in the system.